The role of contraction in skeletal muscle development

Mazelet, Lise

THE ROLE OF CONTRACTION IN SKELETAL MUSCLE DEVELOPMENT

Lise Mazelet

PhD Thesis

... “ La fonction crée l’organe.” (Lamarck, 1809)

Statement of originality

I, Lise Mazelet, confirm that the research included within this thesis is my own work or that where it has been carried out in collaboration with, or supported by others, that this is duly acknowledged below and my contribution indicated. Previously published material is also acknowledged below.

I attest that I have exercised reasonable care to ensure that the work is original, and does not to the best of my knowledge break any UK law, infringe any third party's copyright or other Intellectual Property Right, or contain any confidential material.

I accept that the College has the right to use plagiarism detection software to check the electronic version of the thesis.

I confirm that this thesis has not been previously submitted for the award of a degree by this or any other university.

The copyright of this thesis rests with the author and no quotation from it or information derived from it may be published without the prior written consent of the author.

Signature: 

Date: 18th of August 2005

Details of collaboration and publications

Collaborations

The small angle X-Ray diffraction study and the mechanical analysis, presented in Chapter 3 and 5, were conducted in collaboration with Pr.Anders Arner and Dr.Mei Li, during a 6 weeks visit at Pr.Arner Laboratory (Karolinska Instituet, Stockholm). Funded by the Physiological Society and EuFishBioMed.

The Src study, presented in Chapter 4, was conducted with Jugraj Singh Bassi an undergraduate BSc student I supervised in Dr.Ashworth laboratory (QMUL, London).

Publications

Mazelet, L., Li, M., Arner, A., Ashworth, R. "Myofilament lattice spacing and skeletal muscle active contraction." Manuscript in preparation.

Mazelet, L., Parker, M.O., Li, M., Arner, A., Ashworth, R. "Rescue of thin filament length in paralysed zebrafish embryos: the role of tropomodulin." Manuscript in preparation.

Singh Bassi, J., Mazelet, L., Karunarathna, U., Ashworth, R. "A novel role for Src kinase in zebrafish somite development." Manuscript in preparation.

Doel, C., Zhang, Z., Mazelet, L., Waters, R., Bashiruddin, J. "Dynamics of foot-and-mouth disease virus replication in cells at different phases of the cell-division cycle." Frontiers of Agricultural Science Engineering, 2014, 1(3): 250-257.

Wright, C. F., Gloster, J. Mazelet, L., Paton, D.J., Ryan, E.D. "Short-lived carriage of foot-and-mouth disease virus in human nasal cavities after exposure to infected animals." Veterinary Record, 2010, 167(24): 928-31.

Mazelet, L., Dietrich J., Roland, J.L. "New RT-qPCR assay for viral nervous necrosis virus detection in sea bass, Dicentrarchus labrax (L.): application and limits for hatcheries sanitary control." Fish and Shellfish Immunology, 2010, 30 (1):27-32.

Abstracts

Mazelet, L., Parker, M.O., Brennan, C., Huq, N., Ashworth, R. “Recovery from skeletal muscle paralysis: studies using embryonic zebrafish”. Journal of Muscle Research and Cell Motility 2013

Mazelet, L., Teh, M.T., Ashworth, R. “The role of contraction in skeletal muscle development: a study of focal adhesion kinase *in vivo*”. New Directions in Biology and Disease of Skeletal Muscle Conference, 2012, New Orleans USA. http://www.med.upenn.edu/muscle

Mazelet, L., Audebert, F. “La leishmaniose canine dans le bassin mediterranéen français“. [Canine leishmaniasis in the French mediterranean basin] Université Pierre et Marie Curie, PARIS VI, 2003.
http://tipi.free.fr/savsite/divers/Lise_Mazelet.pdf

Abstract

The aim of this project was to determine the role of contraction in skeletal muscle development. The role of the initial spontaneous contractions observed in zebrafish embryos from 17 to 24 hours post fertilisation was examined. Genetic and pharmacologic approaches were used to study paralysis-induced disruption of skeletal muscle structure and function and subsequently determine the role of contraction. The structural and functional characteristics of developing skeletal muscles were found to be regulated by a dual mechanism of both movement-dependent and independent processes, *in vivo*.

Novel data demonstrates that contraction controls sarcomere remodelling, namely regulation of actin length, via movement driven localisation of the actin capping protein, Tropmodulin1. Myofibril length was also shown to be linked to the mechanical passive property, stretch, with lengthening leading to an increase of the muscle's ability to stretch. In addition, myofibril bundling and the myofilament lattice spacing, responsible for active tension generation via cross-bridge formation, were shown to be unaffected by paralysis and thus, movement-independent processes. Furthermore, the mechanism of the contraction-driven myofibril organisation pathway at the focal adhesion complexes (FAC), was shown to be different in zebrafish compared to mammals, with mechanosensing revolving around the Src protein rather than Fak.

In summary, the role of contraction was established as a critical driver of myofibril organisation and passive tension in the developing zebrafish skeletal muscle. Passive tension regulates muscle function by determining its operational range ensuring that the needs of locomotion are met. Furthermore, investigation of FAC's role in the contraction-driven myofibril organisation pathway led to the discovery of a novel function for Src in zebrafish somitogenesis. These two findings (i) that contraction is a driver of myofibril organisation and (ii) that Src is a key protein of the skeletal muscle development provides the potential for new therapeutic approaches in humans.

Word count: 297

Table of Contents

List of Figures

List of Tables

CHAPTER 1

INTRODUCTION

1. Introduction

1.1 Skeletal muscle

1.1.1 A striated structure

Muscle fibres are composed of myofibrils which contain myofilament proteins (mainly actin and myosin) that act as the building blocks of the sarcomere, the basic contractile unit. Myofibrils are composed of repeating sarcomeres that run both in series and parallel. The characteristic myofibril striated appearance of light and dark bands, readily observable by light microscopy, is the direct result of the precise alignment of the filament systems of the sarcomeres. The principal components of the striated muscle sarcomeres are the actin thin filaments that span the isotropic I band and overlap with the myosin thick filaments in the anisotropic A band. The actin thin filaments are anchored at the Z-disc, which are the mechanosensitive lateral boundaries of the sarcomere. The thin filaments extend towards the middle of the sarcomere and act as spring linking the region of active force generation (A band) with the bordering Z-discs, allowing the reversible mechanical stretch response required for efficient contractile activity. Towards the centre of the sarcomere, the pointed ends of actin filaments interdigitate with the myosin filaments within the A band, forming the cross-bridges and allowing actin and myosin filaments to slide alongside (Huxley et al., 1954). In the middle of the sarcomere, the M-band is the anchoring site of myosin filaments, where they cross link with electron-dense M-bridges and M-filaments (Luther et al., 1978; Obermann et al., 1996). The appearance of defined M-bands is considered to be the final step of myofibril assembly (Markwald 1973; Clark et al., 2002) (Figure 1.1).

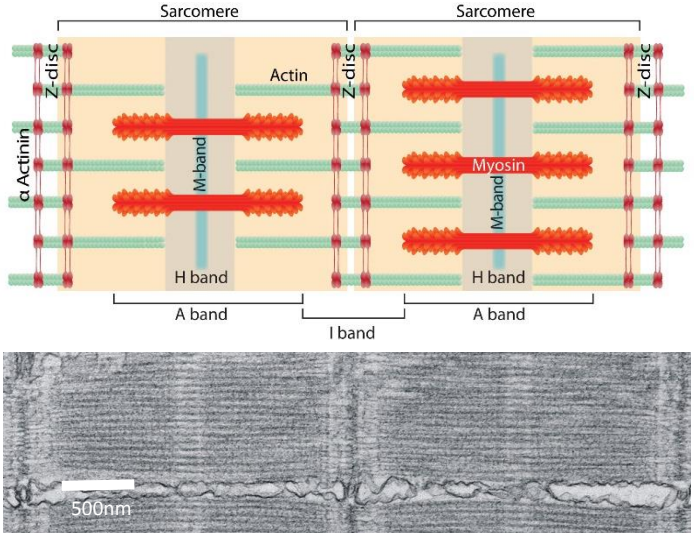

Figure 1.1: Skeletal muscle striated structure. [A] Schematic representation of the serial and parallel structural arrangement of sarcomeres in skeletal muscle myofibril. **[B]** Electron micrograph of a longitudinal section through zebrafish myotomal muscle showing the typical sarcomere striations of vertebrate striated muscle (Adapted from Squire et al., 2008).

1.1.2 Myofibril Assembly

The regular array of identical sarcomeres observed in skeletal muscles is conserved across the animal kingdom, which implies that the mechanism of myofibril assembly is also likely to be conserved. Indeed, the 'premyofibril model of myofibrillogenesis' was established in cultured avian muscle cells and later *in vivo* in zebrafish, suggesting that myofibrillogenesis is a fundamentally conserved process (Sanger et al., 2009; Sanger et al., 2010). During skeletal muscle development sarcomere structure is established in a series of steps, starting with the initiation of actin polymerisation at the protocostameres (Sparrow and Schöck, 2009) and ending with the formation of the M-band (Markwald, 1973). The later stages, which include the determination of sarcomere length, are regulated by muscle contraction (Figure 1.2).

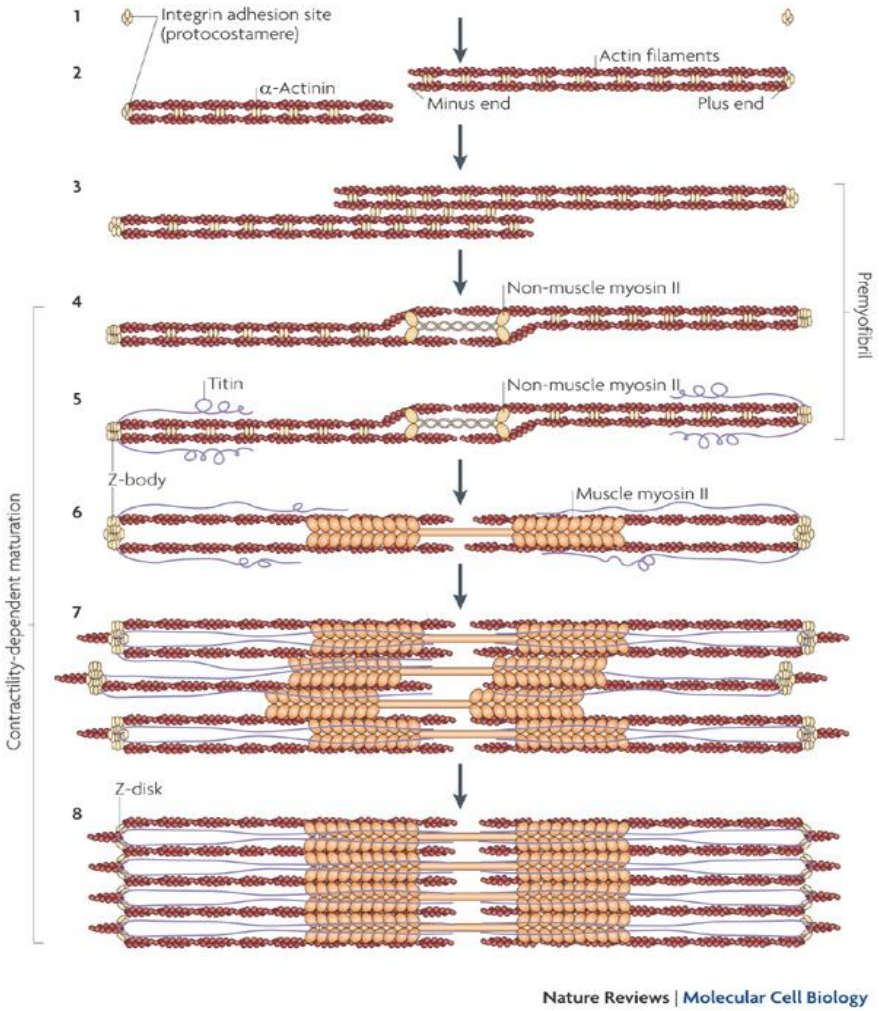

Figure 1.2: Sparrow and Schöck model of myofibril assembly. [steps 1, 2] Integrin adhesion sites (protocostameres) that form at random positions along the muscle cell polymerize actin filaments. For simplicity, only two actin filaments per adhesion site are shown. **[step 3]** Overlapping actin filaments of opposing polarity fuse through α-actinin-mediated crosslinking. **[step 4]** Laterally fused antiparallel actin filaments incorporate non-muscle myosin II, which displaces α-actinin. Note that several non-muscle myosin II bipolar filaments can be incorporated, depending on the number of actin filaments in the stress fibre. **[step 5]** Protocostameres recruit titin and more α-actinin, thereby giving rise to electron-dense Z-bodies. **[step 6]** Muscle myosin II bipolar filaments are then incorporated, perhaps with the help of titin. **[step 7]** Correct spacing

is mediated by both titin and further length maturation of thin filaments. Z-bodies that are now connected to Z-bodies on the other side align longitudinally in the future Z-disk plane through contractility-dependent maturation. **[step 8]** Z-bodies then coalesce laterally into Z-disks. Although not depicted, the distance between two protocostameres in steps 1–5 probably varies substantially. The final sarcomere length is mostly set from step 6 onwards, although subtle modulations might occur, such as thin filament elongation. Adapted from Sparrow and Schöck, 2009.

Studies have revealed that inhibition of contraction causes myofibril and sarcomere disassembly, whereas stimulation accelerates reassembly (De Deyne, 2000). Nonetheless the contribution of contraction to sarcomere assembly *in vivo* is not well understood (Sparrow and Schöck, 2009). It is this later step, contraction-dependent maturation and the organisation of the myofibrils and of their myofilaments that is a critical determinant of mature skeletal muscle contractile function. Myofibril organisation and mechanotransduction are critical for the maintenance of structure and function in mature skeletal muscle and ultimately for co-ordinated movement, as reviewed by Boonyarom and Inui (2006). Initial muscle immobilisation and subsequent muscle adaptation studies (Williams and Goldspink, 1978; Goldspink, 1998), established that it is both the spatial arrangement of the sarcomeres relative to the axis of force generation and their size that are critically important in muscle function (Bian et al., 2012).

1.1.3 Muscle activation: excitation-contraction coupling

The sarcomere Z-discs are the initial biomechanical sensors conducting force through the myofibrils via the excitation-contraction (E-C) coupling. Muscle contraction is the result of this signal transduction process connecting membrane depolarisation and the contractile event itself. The neurotransmitter acetylcholine (ACh) is released at the neuromuscular junction following voltage dependent Ca^{2+} influx in the nerve cell. The process of E-C coupling begins with the binding of ACh to its receptor, which induces the local depolarisation of the sarcolemma as positively charged sodium ions (Na^{+}) enter the muscle cell via the ACh receptor, triggering an action potential. This transmembrane voltage depolarisation spreads through the sarcolemma and T-tubules, where it is sensed by a Ca^{2+} channel plasmalemmal voltage gated dihydropyridine receptor (DHPR) which triggers the opening of a second Ca^{2+} channel, the sarcoplasmic reticulum (SR) ryanodine receptor (RyR), allowing Ca^{2+} release from the SR. Those two channels present a coordinated spatial arrangement in order to achieve this physical coupling. DHPR complexes are formed of four subunits organized in tetrads, α_{1S} voltage sensing and pore forming and β_{1a}, $\alpha 2\delta$ and γ, auxiliaries. RyR are six-transmembrane ion channels presenting a cytosolic four-fold symmetric ‘mushroom-like’ superstructure and a SR transmembrane ‘stalk’ (Zalk et al., 2015). As the RyR open, Ca^{2+} is released from the SR into the sarcoplasm, where it diffuses and binds with the troponin complex, which

in turn initiates a tropomyosin conformational change, uncovering the myosin binding sites of the actin strands. Myosin heads then bind on these exposed binding sites on actin, forming the cross-bridges (Figure 1.3). Myosin heads also bind ATP, whose hydrolysis provides the energy necessary to the myofilaments 'power stroke' movement. ATP also drives the activity of SR Ca^{2+} ATPase which actively pumps Ca^{2+} back into the SR, resulting in tropomyosin shielding myosin-actin binding sites and ultimately inducing muscle relaxation.

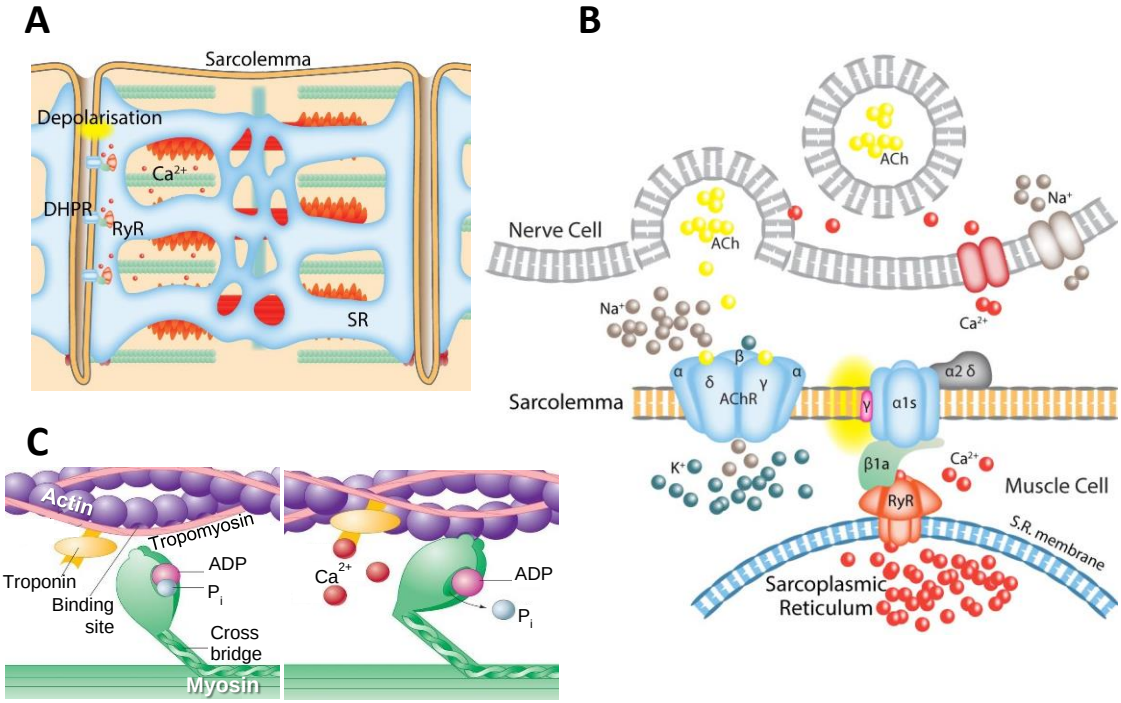

Figure 1.3: Excitation-contraction coupling and cross-bridges. [A] Z-discs localisation of DHPR and RyR on the sarcolemma and the SR membrane respectively. **[B]** E-C coupling starts with the release of ACh and the activation of ACh receptors (AChR), followed by the entry of Na^+ in the muscle cell and sarcolemma depolarisation. Voltage gated DHPR are then activated and allosterically activate RyR, which allow Ca^{2+} release in the sarcoplasm. **[C]** Ca^{2+} ions bind to troponin, which induced a conformational change of the troponin-tropomyosin complex and reveals the actin binding sites, otherwise blocked by tropomyosin. Myosin heads attach to the actin binding sites and to ATP, which hydrolysis into ADP and Pi generate the 'power stroke' and results in the actin and myosin filaments slide movement giving rise to the muscle contraction.

Evidence from studies in isolated cultures has shown that contraction itself is an important regulator in the later stages of myofibril assembly, alignment and sarcomere spacing (Sparrow and Schöck, 2009; Sanger et al., 2010; Sanger et al., 2005; Fujita et al., 2007). In addition, in vivo studies, have also shown that contraction regulates myofibril development. In *C elegans*, there are 4 stages of muscle development, in which the structural sarcomeric components initially accumulate and localised to membranes (Hresko et al., 1994). The final stage involves sarcomeric organisation and coincides with the onset of muscle twitching. These movements appear necessary for the maintenance of muscle structure, specifically events such as the spatial arrangement of cell attachments. Furthermore, actin-myosin interaction during assembly is important for

sarcomeric order in *Drosophila* (Reedy and Beall, 1993) and the excitation-contraction pathway controls sarcomere length during zebrafish development (Brennan et al., 2005). Therefore, evidence supports the fact that contraction is key for both mature and developing skeletal muscle structure. This project is focused on the role of contraction during skeletal muscle development in zebrafish.

1.2 Zebrafish, an *in vivo* model

1.2.1 Background

Zebrafish, *Danio rerio*, from the order of the Cypriniformes and the Cyprinidae family, is a freshwater tropical teleost fish from the Indian subcontinent. Zebrafish is an emerging model for biomedical research, it's use increased in the last decade following on initial studies performed by George Streisinger and his team at the University of Oregon, where zebrafish was the first vertebrate to be cloned (homozygous diploid clones) (Streisinger et al., 1981). Zebrafish have many advantages as a model for studying vertebrate development *in vivo*. Its development ex-utero is rapid, at 28.5°C cell division occurs every 15 minutes during the cleavage period (0-3 hours post fertilisation [hpf]), later on during the segmentation (10-24hpf) somites are added every 30min, by 24hpf the body plan is established and by 48hpf the larvae are swimming freely (Figure 1.4). This set sequence of events gives a very useful staging tool that provides accuracy in developmental studies (Kimmel et al., 1995) and the optical transparency of the embryos during the early stages of development allow the visualisation and imaging of the tissue morphogenesis. Generation time is relatively short, 2-3 month depending on the rearing conditions, namely density, as in an identical fish tank, fish from a smaller shoal will grow and mature faster than in a larger one. Spawning is easily induced in a controlled environment, as it is determined by the fish circadian rhythm. Furthermore, their reproductive rate is high, a female can lay up to 500 eggs per clutch every other day and they are very easy to maintain. Besides, zebrafish low economical costs and less problematical ethical constrains when compared to other vertebrate models, also make it an advantageous model organism (Ablain and Zon, 2013; Dooley and Zon, 2000). Additionally, teleosts make up half of the vertebrate species, they exhibit a high level of biodiversity which is thought to be due to the tetrapoidisation/rediploidisation that took place 400Myr ago (Jaillon et al., 2004). This high level of variability makes fish an interesting model for the study of many biological questions, specifically in evolution studies but also in physiology research. Hundreds of duplicate gene pairs generated during this genomic event have been maintained throughout evolution. Differential loss or subfunction partitioning of such gene duplicates might have been involved in the

generation of fish variability. Comparison of data generated by genome projects as well as complementary studies in other species will significantly contribute to our understanding of gene evolution and function in humans and other vertebrates (Volff, 2005).

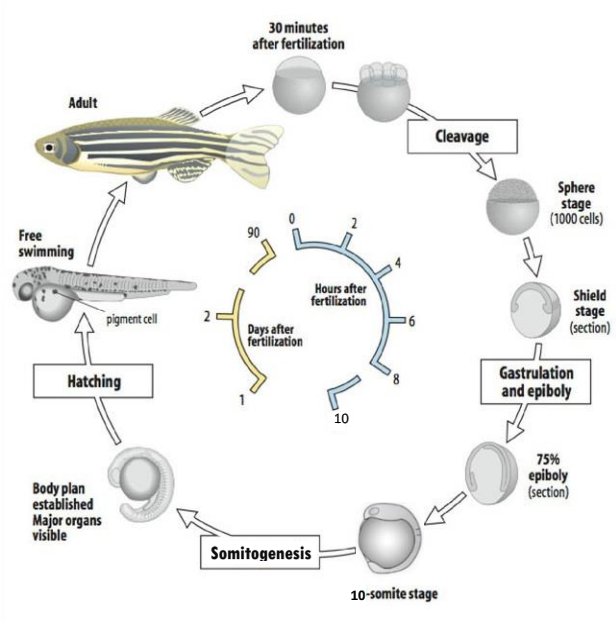

Figure 1.4: Zebrafish, *Danio rerio*, life cycle. The zebrafish embryo develops as a mound-shaped blastoderm sitting on top of a large yolk cell. It develops rapidly and by 2dpf the fish, still attached to the remains of its yolk, hatches, by 3 month the adults are fertile. Adapted from Wolpert et al. (2015).

Therefore, zebrafish offers powerful possibilities to study the vertebrate gene function, notably involved in muscle development and diseases, even more so since genetic manipulations, with knockdown or over-expression, can be performed and mutagenesis screening and transgenic lines are accessible (Lieschke and Currie, 2007). Zebrafish have 25 chromosomes, the whole genome size is about half of that in humans (15 billion vs. 30 billion of base-pairs). Recent genome sequencing has shown that ~26000 protein coding genes exist in zebrafish, and that they share large conservative features with the mammalian genome. Specifically, ~70% of human genes have corresponding orthologs in zebrafish (Howe et al., 2013). The identification of zebrafish ortholog genes that match human developmental regulatory genes has already made it a useful model to study various forms of skeletal muscle dystrophy and several cardiomyopathies (Dou et al., 2008).

In summary, the distinctiveness of this project rests on the versatility of the zebrafish model. This vertebrate *in vivo* model enables the study of complex interactions between tissues. It allowed the study of myofibrils in an environment in which they are capable of differentiating into full range of definitive muscle-types. Further, it allowed the use of a wide array of techniques (genetic, imaging, molecular, mechanical, behavioural), which taken together give an accurate account of the physiological event considered.

1.2.2 Zebrafish muscle specificities

1.2.2.1 Structure

Supported by the buoyancy of water and their swim bladder, zebrafish require large muscles to locomote through their viscous environment. In zebrafish, skeletal muscle display some particularities distinguishing them from mammals. As with other vertebrates, two types of muscle fibres are found in the developing fish, slow and fast muscle fibres. However, in teleosts the slow muscle fibres derive from adaxial cells that elongate to span the length of the somite and then migrate radially (Figure 1.5 A-F). Following migration, they form a monolayer of superficial muscle cells that differentiate into slow muscle fibres and form a wedge-shape triangle on the lateral surface of the somite that specialise in maintaining a slow swimming movement (Devoto et al., 1996) (Figure 1.5 G). In contrast, the teleost's fast muscle fibres arise from the lateral presomitic muscle cells, which remain within the deep portion of the myotome. They will provide the burst of rapid swimming necessary to escape or hunt (Stickney et al., 2000). Another unique feature of zebrafish skeletal muscle is that myofilaments bundles are more densely packed than in mammals. Furthermore, their optimal sarcomeric length is 2.15μm, compared to 1.85μm in mammal skeletal muscle (Figure 1.5 H, I, J). Finally, fish skeletal muscle structure is quasi-crystalline, which is a real advantage for ultrastructural studies and imaging. This is the result of a structural difference of the fish A-bands, which are arranged in a 'simple lattice'. This organisation reveals the identical rotation of myosin filaments around their long axis ensuring a simple regular structure and a long rotational range. This is in contrast with the higher vertebrate muscles 'superlattice', reflecting the complex irregular arrangement of their myosin filaments along their long axis, which are pointing in two different directions (Figure 1.5 K, L) (Squire et al., 2008; Dou et al., 2008).

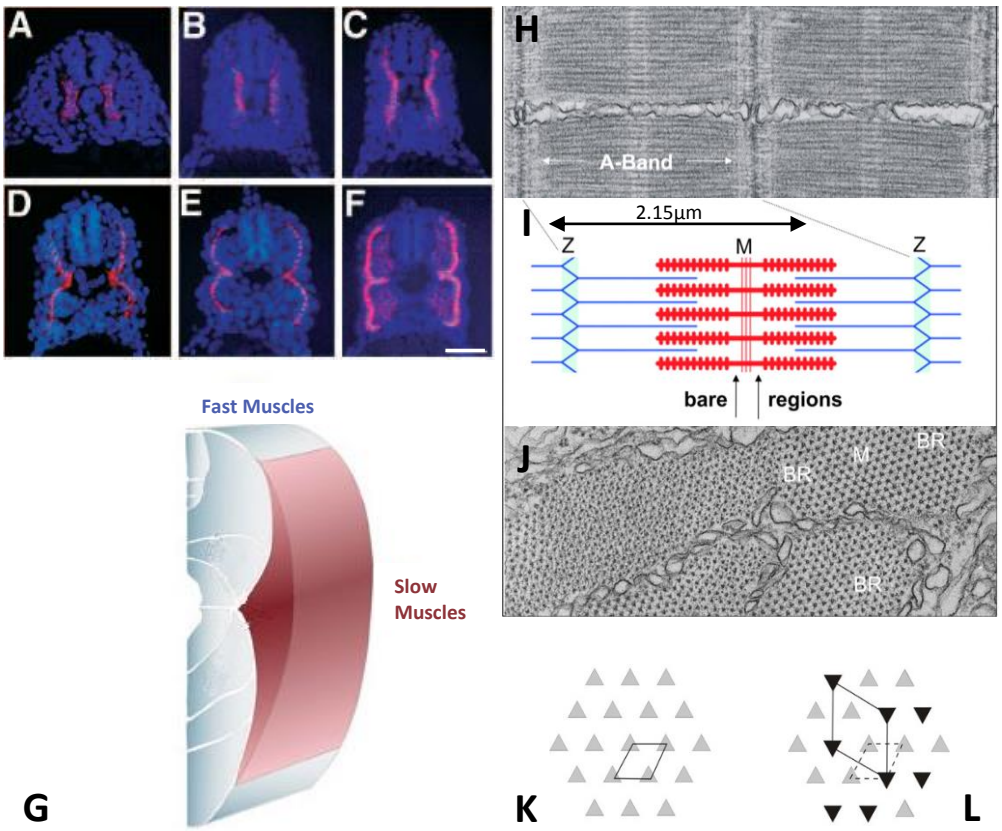

Figure 1.5: Zebrafish skeletal muscle particularities. [A-F] Adaxial cells migrate radially away from the notochord, between other somitic cells. In the caudal trunk, migration occurs over approximately 7 hours. Transverse sections through the caudal trunk (somites 14-17) were immunolabeled with F59 to mark adaxial cells myosin and counter stained with Hoechst to reveal the nuclei. **[A]** 17hpf (16 somites) embryo. F59 immunoreactivity is present only in adaxial cells, the labeling is perinuclear. **[B]** 18.5hpf (19 somites) embryo. The adaxial cells have begun to move dorsally and ventrally; this is approximately the time at which these cells are elongating in the anterior posterior dimension. **[C]** 20.5hpf (23 somites) embryo. The adaxial cell population now extends almost the full dorso-ventral extent of the myotome. **[D]** 21.5hpf (25 somites) embryo. Radial migration of the adaxial cells has begun. **[E]** 23hpf (28 somites) embryo. Most of the adaxial cells have reached the lateral surface. **[F]** 24hpf embryo. The adaxial cells are now lateral. A subset of adaxial cells remains adjacent to the notochord, generating an hourglass shape to the layer of superficial muscle cells. The deep cells of the myotome are now beginning to express the F59 epitope weakly. In these transverse sections, dorsal is up. Scale bar, 50 mm. **[G] Fast and slow muscle distribution in teleosts mature skeletal muscle. [H-J] Structural organisation of the zebrafish skeletal muscle. [H]** Electron micrograph of a longitudinal section through zebrafish myotomal muscle showing the typical sarcomere striations of vertebrate striated muscle. The sarcomere **[I]**, which extends between Z-bands (Z) and is ~2.15µm long, consists of the centrally placed A-bands and the less densely packed I-bands, which extend between successive A-bands. The A-band are formed by an array of myosin filaments carrying myosin head projections and cross-link halfway along their length at the M-band (M). Each side of the M-band are the bare regions where the myosin filament backbones appear triangular. **[J]** Electron micrograph of zebrafish myotomal muscle in cross section showing myosin filament profiles near to the M-band (M) and in the adjacent bare regions (BR). The triangular profiles in one bare region all point in the same direction indicating the presence of a simple and tight lattice arrangement. **[K,L] Illustrations of the bare region arrangements of myosin filaments profiles in a simple lattice and a superlattice. [K]** The simple lattice has identically oriented triangular profiles throughout. **[L]** The superlattice has two filament orientations with an irregular, statistical arrangement. Adapted from Devoto et al., 1996 and Squire et al., 2008.

1.2.2.2 The initial contractile event

Zebrafish have proved useful as a model to study the development of vertebrate skeletal muscle, including myofibril organisation and alignment. Contractile movements in zebrafish embryos are initiated at 17hpf, as functional neuromuscular connections within the body of the fish start to form and the slow muscle fibres begin their lateral migration. The axons of primary motor neurons exit the spinal cord and contact the skeletal muscle, in the somites of the embryo. Prior to 24hpf, the primary motor neurons make contact with the skeletal muscle, initially with the slow muscle before spreading out through the somite, into the fast muscle (Figure 1.6 A). The initial movements have a very characteristic pattern (Figure 1.6 B), the frequency of the spontaneous body contractions peaks at 19hpf before tailing off by 24hpf.

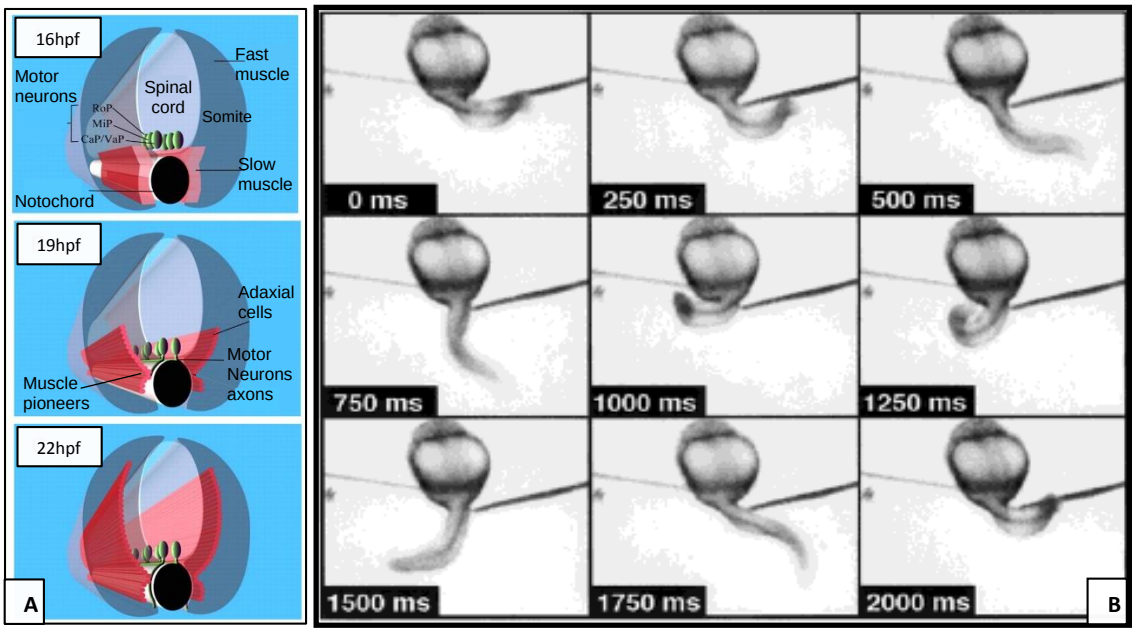

Figure 1.6: 17-24hpf: A contractile developmental event. [A] Functional neuromuscular junctions form between 17 and 24hpf, and coincide with the slow muscle fibres lateral migration and the onset of spontaneous body movements. **[B]** Example of one cycle of spontaneous contractions of an agarose-restrained embryo at 19hpf. Images were captured every 15 frames (250 ms). The embryo was dorsal side up with the head facing the top of the image. The behaviour consisted of a contraction to the left followed by a contraction to the right. The length of the embryo was 1.4 mm. Adapted from: Brennan et al., 2005 ; Devoto et al., 1996 ; Eisen et al., 1986 ; Saint-Amant and Drapeau, 1998.

The role of these initial movements is currently unclear. There is evidence to suggest that these movements are important in the initiation and refinement of nerve-muscle connections (Brennan et al., 2005; Devoto et al., 1996; Eisen et al., 1986; Saint-Amant and Drapeau, 1998). Furthermore, previous work investigated the hypothesis that this contractile development event is necessary for myofibril organisation using both an irreversible paralysing pharmacological agent, Blebbistatin, (Lahne et al., 2009) and immotile mutant lines (*nic1* and *cacnb1*^{ts25}) (Brennan et al., 2005) to disrupt the E-C coupling pathway.

1.2.3 Zebrafish motility mutants

Motility mutants, such as *Nic1*^{b107} (Brennan et al., 2005; van der Meulen et al., 2005), *sop*^{fixe} (Etard et al., 2005) or *cacnb1*^{ts25} *relaxed* (Schredelseker et al., 2005) , lack key components of the E-C coupling pathway and their skeletal muscle is unable to contract. Evidence from several laboratories show that a lack of E-C coupling leads to disruption of their muscle fibre development, myofibrils are thin and wavy and lack bundling and alignment (Behra et al., 2002; Brennan et al., 2005; van der Meulen et al., 2005). At the sarcomere level this translates into a number increase and a disruption of their spacing (Etard et al., 2005). At an ultrastructural level, their sarcomeres are shorter, with a shorter A band and prominent H band, these changes in dimension suggests that the actin and myosin filaments length themselves are altered in immotile mutants, as observed in the ACh receptor mutant, *sop*^{fixe} (Etard et al., 2005) (Figure 1.7). These observations support the hypothesis that contraction is necessary for the organisation of myofibrils during early vertebrate muscle development *in vivo* (Brennan et al., 2005).

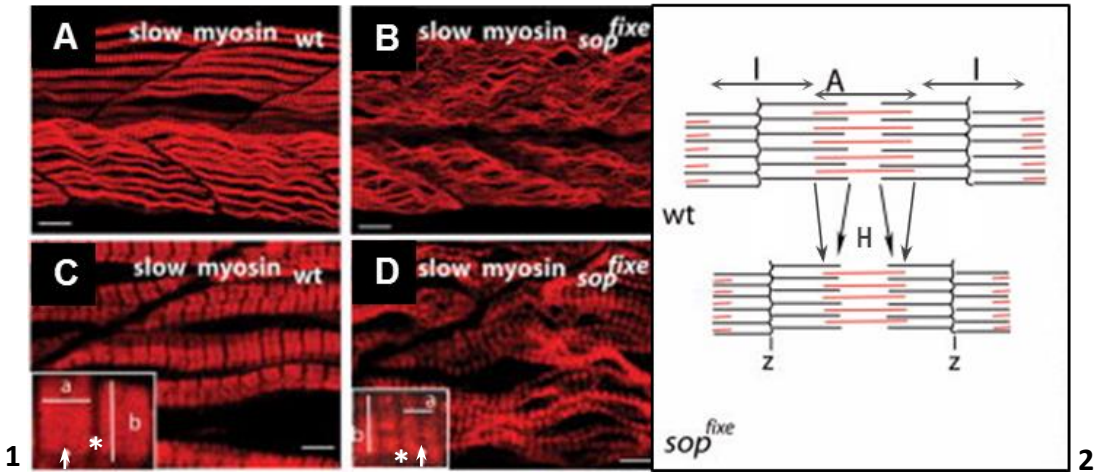

Figure 1.7: Structure of myofibrils in immotile *sop*^{fixe} mutants. [1] Wild-type (A,C) and *sop*^{fixe} (B,D) embryos were stained with antibodies against slow muscle myosin at 26hpf. Immunoreactivity of slow muscle myosin highlights the A band (C,D). The H band and M band are indicated by an asterisk and arrow, respectively. C,D: The length of the A band, (a = 1.63µm for wild-type [wt] C, and 1.3µm for *sop*^{fixe} D) and the width of the myofibril (b = 2.3µm for wt C, and 1.9µm for *sop*^{fixe} D) are reduced in the mutant. **[2]** Schematic representation of the sarcomere structure in wild-type and *sop*^{fixe} embryos. Note the enlargement of the H band and the shortening of the A band. Lateral views, anterior to the left. Scale bars = 10µm in A,C ; 2.5µm in C,D. Adapted from Etard et al., 2005.

1.2.3.1 *Relaxed* mutants

In this study, the c*acnb1*^{ts25}, *relaxed* mutant line was used to determine the effect of paralysis and explore the role of contraction during skeletal muscle development *in vivo*. This mutant line carries a G-A non-sense point mutation in exon 13 of the gene *CACNB1* encoding the DHPRβ_{1a} subunit leading to premature termination at the position Trp454.

It is a monogenetic heredity, therefore 25% of the offspring would be homozygotes. These homozygotes *relaxed* mutants lack the DHPRβ_{1a} subunit protein, preventing the correct targeting of DHPR to the sarcolemma and tetrad formation, disrupting the DHPR-RyR physical interactions and the E-C coupling, therefore inducing total skeletal muscle paralysis (Figure 1.8). However, whether DHPRβ_{1a} subunit function exclusively lies in the physical coupling of these two Ca^{2+} channels (DHPR-RyR) enabling E-C coupling or whether it participates in the signal transduction between voltage-sensor and Ca^{2+} release remains to be shown (Schredelseker et al., 2005).

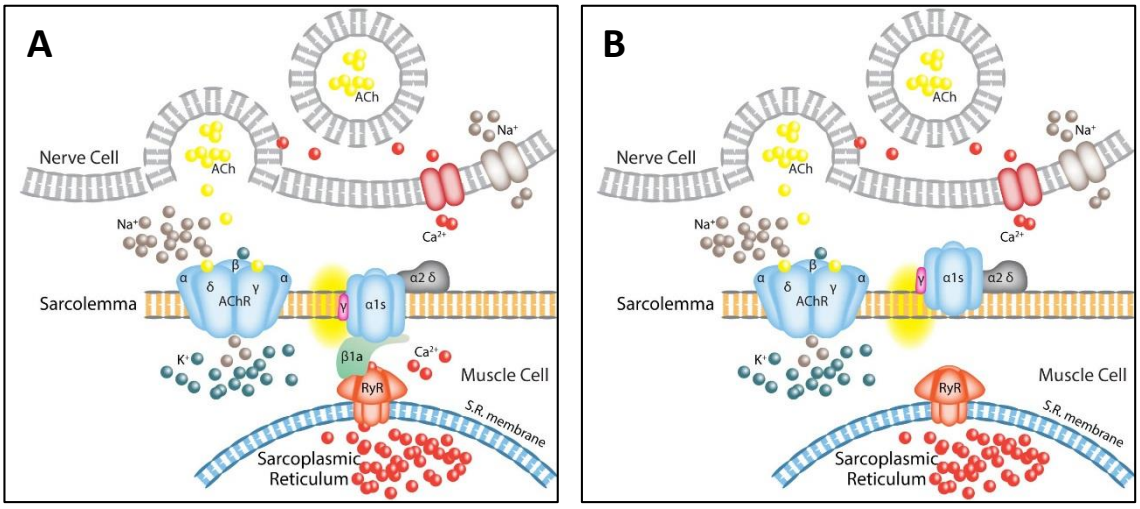

Figure 1.8: *Relaxed*, immotile mutant cacnb1^{ts25-}/cacnb1^{ts25-} (rr). [A] DHPR-RyR physical coupling. **[B]** In *relaxed,* a G-A non-sense point mutation in exon 13 of the gene *CACNB1* encoding DHPRβ_{1a} subunit, results in its lack of expression, and DHPR is mistargeted to the sarcolemma. The tetrads formation is hampered and the voltage-gated Ca^{2+} channels cannot link the action potentials to Ca^{2+} release within the muscle fibres. This disruption to the E-C coupling pathway induces total skeletal muscle paralysis (Schredelseker et al., 2009).

These immotile mutants display a disrupted myofibril phenotype. Their myofibrils are 'wavy' with an obvious lack of bundling and alignment, whilst their cell boundaries are not affected (Figure 1.9 A-E). Evidence suggests that it is an increase in serial sarcomere addition rather than cell shape changes that disrupts the myofibril arrangement (Figure 1.9 F), as no disruption of the cell boundaries nor of the myotendinous junction were observed when staining for β-catenin, strongly expressed in zebrafish sarcolemma (Lahne et al., 2009).

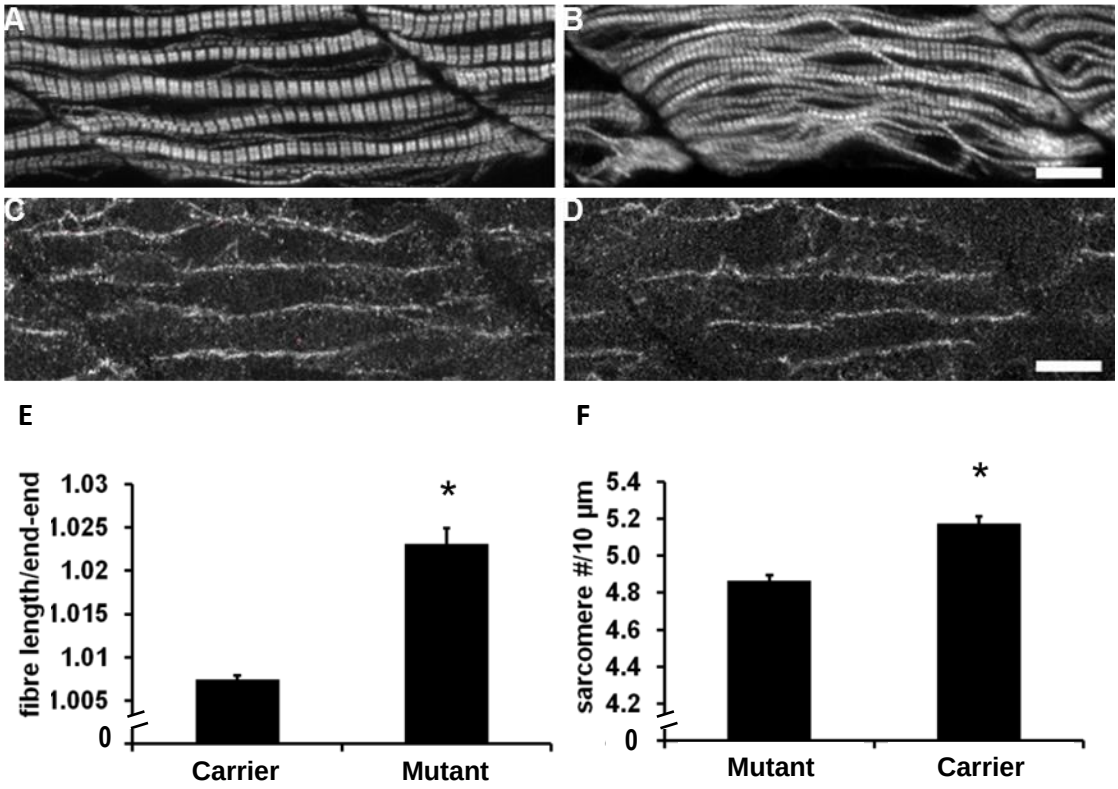

Figure 1.9: Myofibril alignment is disrupted in the *relaxed* mutant skeletal muscle. Immunostaining of myosin with F59 and confocal projections reveal myofibril organisation in **(A)** control heterozygous carriers and **(B)** homozygous *relaxed* mutants, at 24hpf. Confocal images of embryos labelled with a β-catenin antibody in **(C)** control heterozygous carriers and **(D)** homozygous *relaxed* mutants at 24hpf. **(E)** The myofibril organisation index (myofibril length / somite length) is significantly increased in the homozygous *relaxed* mutants embryos compared to controls (n=6 embryos) **(F)** Sarcomere number/10 µm was significantly increased in homozygous *relaxed* mutants compared to heterozygous carriers. Mean ± S.E.M, P* < 0.05, Student's *t*-test. Scale bar 25µm. (Lahne et al., 2009).

1.2.4 Pharmacological treatments

1.2.4.1 Irreversible paralysis treatment

Immotility mutants support the hypothesis that contraction is necessary for the organisation of myofibrils during early vertebrate muscle development *in vivo.* However, the mutant approach has several drawbacks: (i) a lack of mutant lines that carry mutations in the E-C coupling signaling proteins and (ii) it is not possible to manipulate the timing of the paralysis. An alternative method of exploring the effect of paralysis and the role of contraction in skeletal muscle development, is to induce paralysis in wildtype embryos using pharmacological agents. This method allows control of the time at which paralysis occurs and enables assessment of the contribution of the multiple E-C coupling components to myofibril organisation. Previous work used Blebbistatin (BBST) to block the E-C coupling, this pharmacological agent binds irreversibly to muscle and non-muscle myosin II and prevents acto-myosin interaction. It was established that when paralysis coincided with neuromuscular junctions formation and the onset of embryonic

movement (17-24hpf), myofibril organisation was most disrupted (Lahne et al., 2009). This suggests that myofibril organisation is driven by the initial contractile event itself (Figure 1.10). This finding is in contrast to cell culture studies that support a role for spontaneous and activity-generated intracellular Ca^{2+} signals in myofibril construction, in particular during sarcomere formation (De Deyne, 2000). Ca^{2+} driven actin-myosin interaction (cross bridge cycling) was thought to be necessary for myofibril bundling rather than sarcomeric construction (Ramachandran et al., 2003).

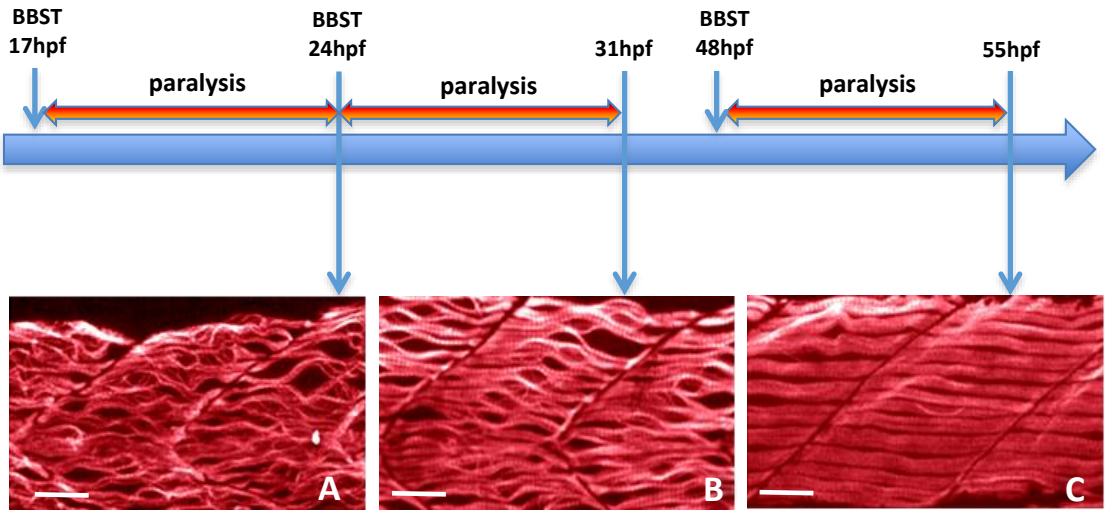

Figure 1.10: 17-24hpf paralysis is most disruptive to myofibril organisation. Confocal projections of immunohistochemically labelled slow muscle fibres in 50µM Blebbistatin treated zebrafish embryos. Zebrafish embryos were exposed to Blebbistatin for 7 hours from either 17-24hpf **[A]**, 24-31hpf **[B]** or 48-55hpf **[C]** (Anti-myosin antibody F59, scale bar 25 µm). The severity of myofibril misalignment of slow muscle fibres as a result of Blebbistatin exposure is correlated with the developmental time point at which it is applied. Myofibril disruption is most pronounced in A and diminishes progressively when applied later (B, C). (Lahne et al., 2009).

Taken together, the observations made in the immotile mutant lines (*nic1* and *cacnb1*^{ts25}) and in pharmacological experiments, showed that when the E-C coupling pathway was blocked at the level of membrane depolarisation (*nic1*, lacking ACh receptors), at the DHPR-RyR physical coupling (*cacnb1*^{ts25}, lacking the DHPRβ_{1a} subunit), or at the actin myosin cross-bridges (using Blebbistatin), myofibril disruption was observed (Figure 1.11). This establishes that during the 17-24hpf contractile event it is the actin-myosin interaction and the contraction itself, rather than Ca^{2+} alone as previously thought, that drives myofibril organisation (Lahne et al., 2009).

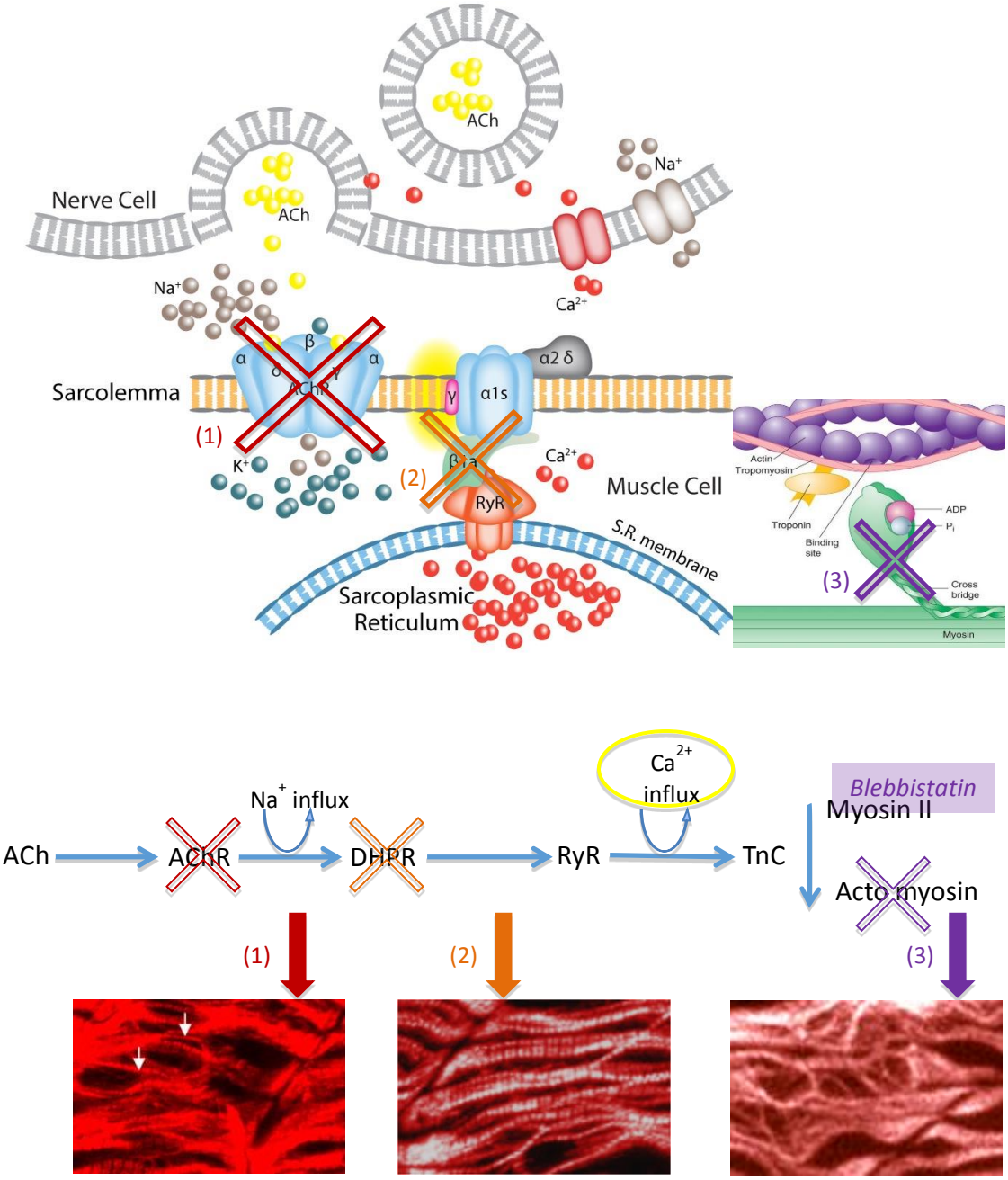

Figure 1.11: Exploring the excitation-contraction coupling pathway. (1) The red crosses represents the blockage of membrane depolarisation at the sarcolemma, resulting from the lack of ACh receptors of the *nic1* mutants. **(2)** The orange crosses represents the suppression of the DHPR-RyR physical interaction, due to the lack of DHPRβ_{1a} subunit of the *relaxed* mutants. **(3)** The purple crosses represents the inhibition of the acto-myosin interaction, due to the pharmacological agent Blebbistatin binding to myosin II (purple box). All three disruptions of the E-C coupling pathway, resulted in comparable myofibril disruption. The third treatment does not impair the Ca^{2+} influx within the muscle cell, and confirms that it is the contractile event that drives myofibril organisation. (Anti-myosin antibody F59 ; picture 1 from Brennan et al., 2005 ; pictures 2&3 from Lahne et al., 2009)

1.2.4.2 Reversible paralysis treatment: a novel approach

Genetic and pharmacological studies have suggested the importance of the initial contractile event in regards with myofibril organisation. This hypothesis was tested, in this study using a reversible Na^+ channel blocking anaesthetic, Tricaine (methanesulfonate (MS222) 0.03% w/v), which temporarily induced paralysis during the onset of movement (17-24hpf), before allowing contractile recovery. This experimental design allowed the assessment of the restoration of contractile activity on paralysis-induced disorganised myofibrils (Figure 1.12).

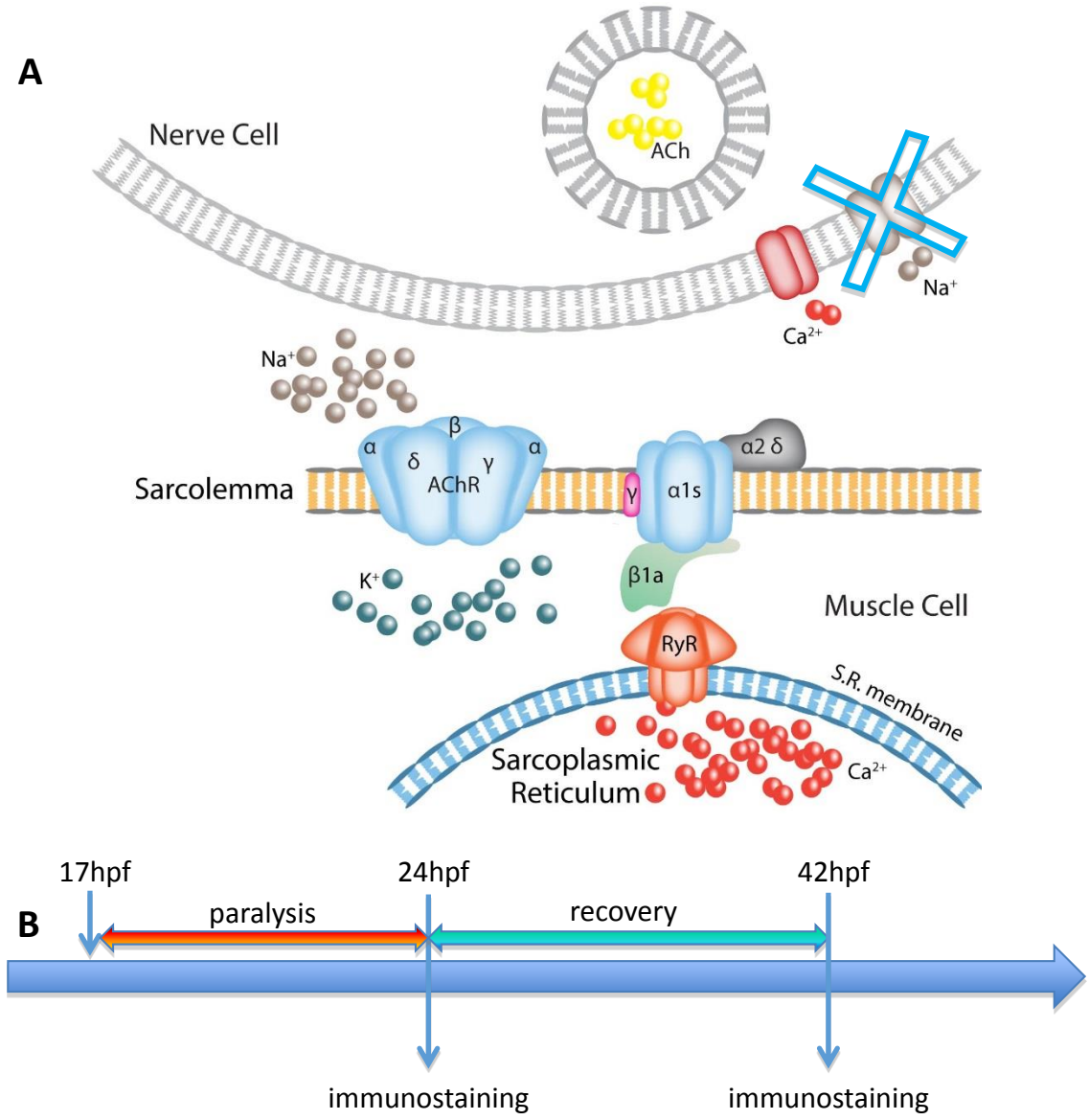

Figure 1.12: Experimental design. [A] Excitation–contraction pathway. The blue cross represents the action of Tricaine which temporary blocks the Na^+ channels and therefore blocks the E-C coupling pathway. **[B] Experimental time course.** Embryos were incubated in Tricaine (0.03% w/v) for 7 hours starting at 17hpf. At 24hpf embryos were removed, fixed and stained immediately or put into recovery in embryo medium and fixed and stained at 42hpf or functionally assessed later in development.

1.2.5 Mechanosensitive structure within myotendinous junctions and costameres: the Focal Adhesion Complex (FAC)

Contraction may regulate myofibril organisation in the developing skeletal muscle, but the signalling system of the mechanotransduction that enables this process to occur remains to be described. In skeletal muscle fibres force can be transmitted laterally via costameres or serially via myotendinous junctions (Huijing, 1999; Monti et al., 1999; Ervasti, 2003). Costameres physically connect with the actin cytoskeleton at the sarcomere Z-disc and have been implicated as a link between mechanical stimulus and downstream cell signalling (Ervasti, 2003); mediating migration and adhesion in many cells, as reviewed in Turner (2000) and Schwartz (2001). Therefore disruption of the contractile-dependent myofibril organisation in the zebrafish embryo skeletal muscle may arise via the disruption of costameric proteins, as previously shown in γ-actin knockout mice which develop progressive myopathy with defects in the connectivity between muscle fibers and/or myofibrils or at the myotendinous junctions (Sonnemann et al., 2006). Costameres and myotendinous junctions are specialist transmembrane linkages and share a couple of protein complexes, the dystroglycan and the focal adhesion complex (FAC) (Figure 1.13).

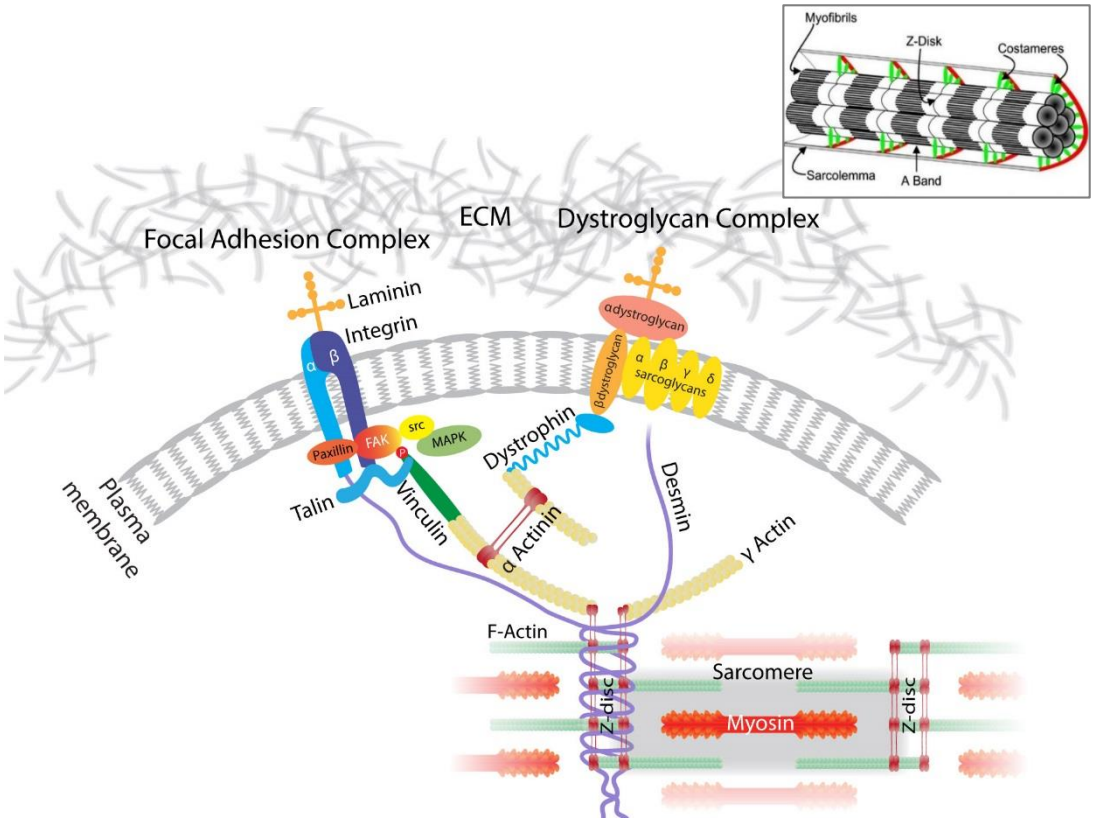

Figure 1.13: Cellular localisation and ultrastructure of costameres and myotendinous junctions in striated muscle. Costameres and myotendinous junctions share dystroglycan and focal adhesion complexes which link them to the sarcomeres Z-disc. Costameres are circumferential elements that physically couple peripheral myofibrils to the sarcolemma and the extracellular matrix (ECM) in periodic register with Z-discs (Ervasti 2003) (top insert). Myotendinous junctions are the distal site of connection between tendon and muscle.

There is evidence that the non-receptor tyrosine kinase, focal adhesion kinase (Fak), a major protein of the FAC, is involved in sensing and transducing mechanical forces within both costameres and myotendinous junction in avian and mammalian mature skeletal muscles (Flück et al., 1999). It was shown in mammalian cells (mouse) that Fak becomes activated when Tyr^{397} is phosphorylated, after cells have been submitted to mechanical loads (Durieux et al., 2009). Furthermore, Fak knockout mice embryos die with a mesodermal defect at a very early developmental stage (E8.5, 14-16 pairs of somites) illustrating the importance of Fak in early development (Furuta et al., 1995). As well as its scaffolding properties, Fak is involved in integrin mediated phosphorylation signalling cascades of many FAC proteins and most of its domains are highly conserved in between species. Integrin-mediated Fak autophosphorylation of its Tyr^{397} site generates a binding site for Src, which in turn phosphorylates a number of other tyrosine residues on Fak. Consequently, the phosphorylation state of Tyr^{397} is considered indicative of Fak's activity and Src is another key protein of the FAC. Furthermore, Fak has been localised at sites of strong cell-ECM adhesion in embryos. In *Xenopus* and mouse embryos, Fak was shown to be prominent at somite borders and in the brain (Hens and DeSimone, 1995; Polte et al., 1994). In zebrafish embryos it was shown to be prominent in somite boundaries mediating their stabilisation, and in a ring like pattern connecting the notochord to its peripheral sheath (Henry et al., 2001; Crawford et al., 2003). Fak is an important component of the focal adhesion complex, it is involved in signalling between the extracellular matrix and the cytoskeleton and is expressed in early zebrafish development. These three facts make it an obvious candidate for the signalling system of the mechanotransduction pathway that regulates myofibril organization *in vivo*. As for Src, it is strongly associated with Fak autophosphorylation and its expression has not been described in zebrafish.

1.2.6 Functional consequences of paralysis in zebrafish

Finally, to fully explore the positive feedback loop that establishes the link between skeletal muscle structure and function, the functional consequences of paralysis were examined. This part of the project was done in collaboration with Professor Arner (Karolinska Institutet, Stockholm, Sweden), during a 6 weeks visit in his laboratory. Techniques that he pioneered to study the physiological mechanical properties of developing muscle in zebrafish larvae were used to examine both *relaxed* mutants and chemically treated larvae (Dou et al., 2008). In addition, the motor behaviour of fish that had been subjected to a period of paralysis was assessed in collaboration with Doctor Brennan (QMUL, London). This work informs the disruption of skeletal muscle force production and subsequent swimming behaviour in response to paralysis in zebrafish.

Hypothesis: Contraction and its signalling pathway drives myofibril organisation during embryonic muscle development. This will be explored using both immotile mutant and pharmacologically paralysed zebrafish embryos.

CHAPTER 2

MATERIALS AND METHODS

2. Materials and methods

2.1 Zebrafish maintenance

Wildtype zebrafish (*Danio rerio*) were maintained on a 14 hours light, 10 hours dark cycle at 28°C in UK Home Office approved facilities in the QMUL fish facility as described previously (Ashworth et al., 2001). The mutant zebrafish line, *cacnb1*^{ts25} (*relaxed*) were obtained from the Max Planck Institute in Tübingen, Germany. Heterozygote adults, motile *relaxed* carriers *cacnb1*$^{ts25+}$/*cacnb1*$^{ts25-}$ (Rr) were crossed to obtain homozygous immotile *relaxed* mutant *cacnb1*$^{ts25-}$/*cacnb1*$^{ts25-}$ (rr) embryos, identified by lack of movement and inability to respond to touch from 17hpf. Homozygous immotile *relaxed* mutant *cacnb1*$^{ts25-}$/*cacnb1*$^{ts25-}$ (rr) *and* heterozygote motile *relaxed carriers* *cacnb1*$^{ts25+}$/*cacnb1*$^{ts25-}$ (Rr) sibling embryos with a normal phenotype from the same batch of eggs were assessed, wildtype (TU) were used as controls. Embryos were collected and raised at 28.5°C according to standard procedures, they were staged according to standard references and are given in the text as standard developmental time, i.e. hours post fertilisation (hpf) (Kimmel et al., 1995). Live embryos were manually dechorionated with #5 watchmaker's forceps at 24hpf in order to identify the homozygous immotile *relaxed* mutant *cacnb1*$^{ts25-}$/*cacnb1*$^{ts25-}$ (rr) embryos. Embryos were touched with a fine pipette tip to elicit a touch-evoked swimming response, homozygous *relaxed* mutant embryos were identified by their lack of response. Aged matched sibling embryos were collected from adult zebrafish separated by dividers overnight and paired at a set time each morning (Gonsar et al., 2012).

2.2 Pharmacological treatments

2.2.1 Tricaine treatment

Dechorionated wildtype (TU) embryos were transferred into embryo medium, EM, (13.7mM NaCl, 0.54mM KCl, 25.2μM Na2HPO4, 44.1μM KH2 PO4, 1.3mM CaCl2, 1mM MgSO4.7H2O, 10nM HEPES and 1L ddH2O) supplemented with 0.03% Tricaine (MS222), a reversible Na^+ channel blocking anaesthetic at 17hpf, incubated for 7 hours at 28.5^{o}C after which they were transferred in embryo medium. After 1 hour of treatment embryos were examined for their ability to move, i.e. occurrence of spontaneous contractions. Lack of movement was taken as the indicator that the treatment was successful. Control embryos were raised simultaneously. At 24hpf control and treated embryos were fixed and stained immediately or put into recovery (EM without Tricaine) and control and recovered embryos were either fixed and stained at 42hpf or mounted

for X-ray diffraction at 6 days post fertilisation (dpf), or mechanically assessed at 5-7dpf or used to assess their swimming behaviour (at 3, 5, 7 and 30dpf) (Figure 2.1).

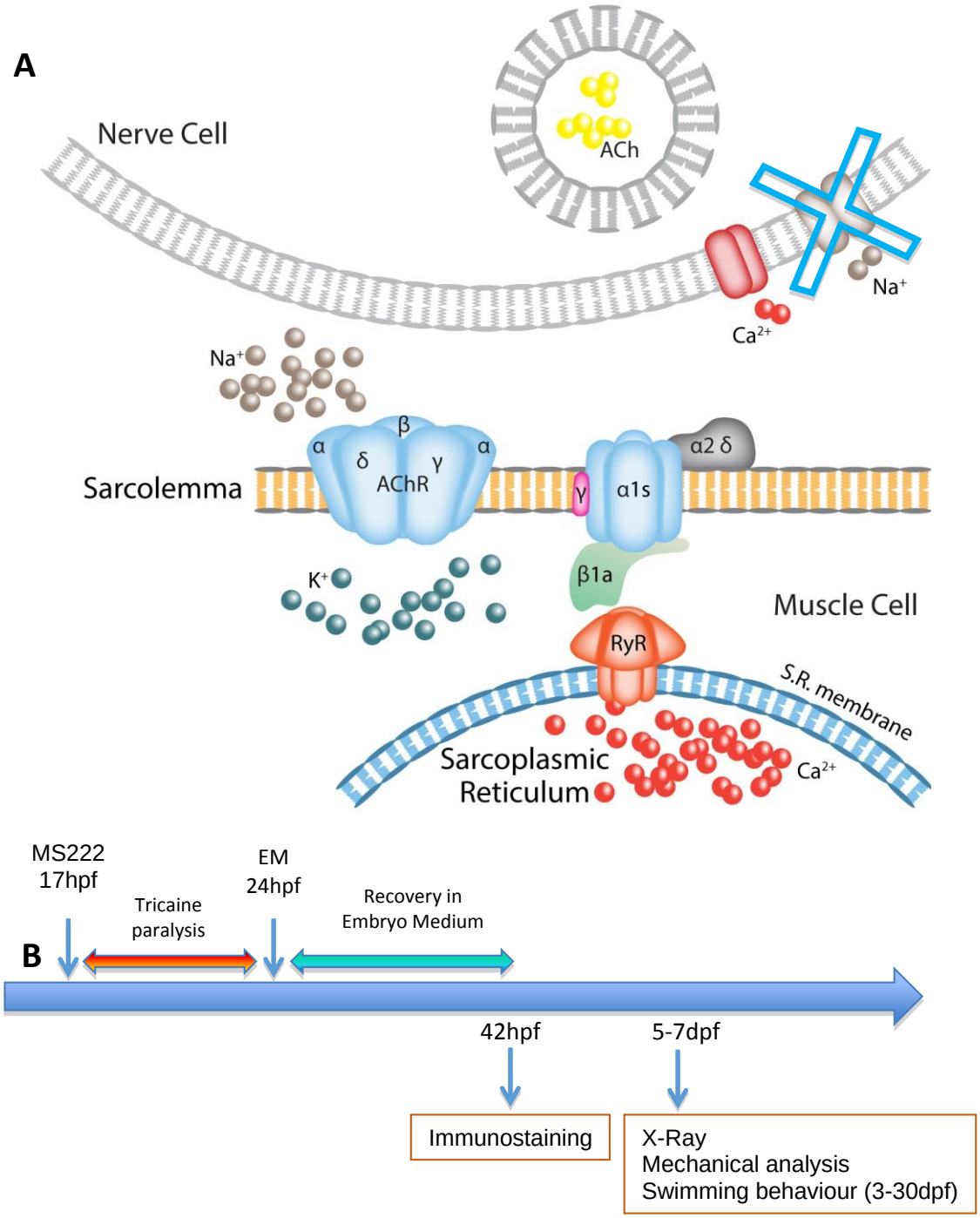

Figure 2.1: Tricaine treatment experimental protocol. [A] Tricaine, is a reversible Na^+ channel blocking anaesthetic **[B]** Embryos were incubated in 0.03% Tricaine, at 17hpf for 7 hours at 28.5°C, after which immunostaining was performed, or they were transferred in Embryo Medium for recovery, immunostaining was performed at 42hpf, X-ray diffraction at 6dpf, mechanical assessed at 5-7dpf and their swimming behaviour was recorded at 3, 5, 7 and 30dpf.

2.2.2 Tricaine-BTS treatment

Dechorionated wildtype embryos were transferred into Embryo Medium supplemented with 0.03% Tricaine at 17hpf, incubated for 12 hours at 28.5ºC after which they were transferred at 29hpf into a 50µM N-Benzyl-P-Tuloenesulfonamide, BTS (Sigma) (Cheung et al., 2002), a specific reversible inhibitor of fast myosin ATPase, and incubated at 28.5ºC up to 5 days post fertilization. BTS, was dissolved in DMSO at stock concentrations of 50mM and subsequently diluted to 50µM in embryo medium. After 1 hour of treatment, embryos were examined for their ability to move, i.e. occurrence of spontaneous contractions in embryos before 24hpf and touch response for embryos thereafter. Lack of movement was taken as the indicator that the treatment was successful. Control embryos were transferred into DMSO (1:1000) at 29hpf. Recovered embryos and control embryos kept in DMSO were transferred from the BTS solution into Embryo Medium at 5dpf. Recovered fish were assessed in X-ray experiments at 6dpf in mechanical studies at 5 and 7dpf, and their swimming was assessed at 3 months (Figure 2.2).

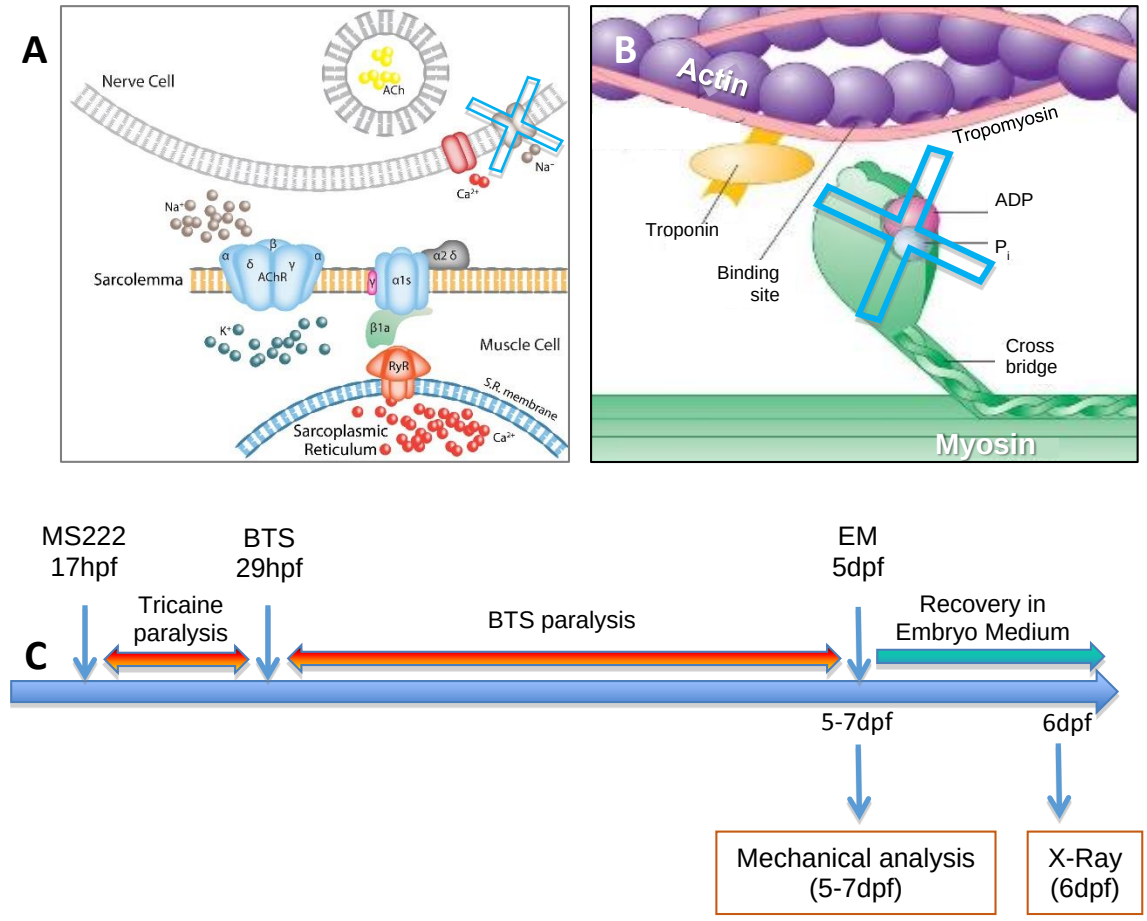

Figure 2.2: Tricaine-BTS treatment experimental protocol. [A] Tricaine, a reversible Na^+ channel blocking anaesthetic. **[B]** BTS (N-Benzyl-P-Tuloenesulfonamide) specific reversible inhibitor of fast myosin ATPase. **[C]** Embryos were incubated in 0.03% Tricaine, channel blocking anaesthetic at 17hpf for 7 hours at 28.5ºC, after which they were transferred in BTS up to 5 days post fertilization, before to be transferred in Embryo Medium for recovery and further assessment.

2.2.3 PP2 treatment

Dechorionated wildtype embryos were transferred into Embryo Medium supplemented with a DMSO solvent and PP2 (1-tert-Buty;-3-(4chlorophenyl)-1H-pyrazolo [3,4-d]pyrimidin-4-amine), tyrosine kinase inhibitor (Abcam Biochemicals) at 17hpf and incubated at 28.5°C. For the experiments five PP2 concentrations were used: 100uM, 50uM, 25uM, 12.5uM, 6.25uM. Mobility was assessed at 24, 42 and 48hpf, by touching each embryo with a fine pipette tip to elicit a touch-evoked response. Lack of movement was taken as the indicator that the treatment was successful. The embryonic phenotype was recorded by photography using a microscope equipped with a Thorlabs DCC1645C High resolution CMOS camera connected to a PC equipped with Thorlabs DCx camera software (Figure 2.3).

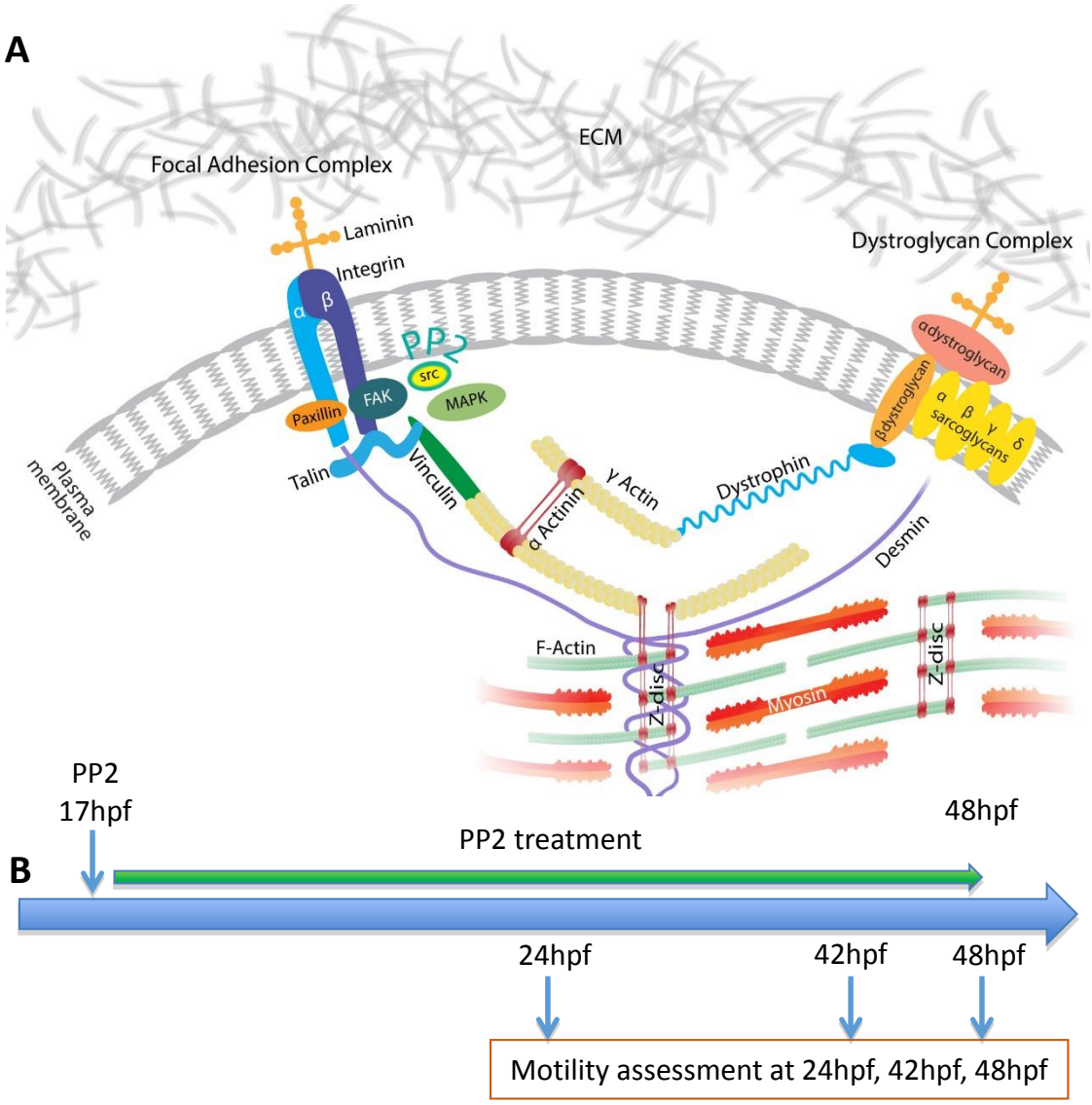

Figure 2.3: PP2 treatment experimental protocol. [A] PP2, tyrosine kinase inhibitor binds to Src, **[B]** Embryos were incubated in 50uM, 25uM, 12.5uM, 6.25uM PP2 respectively at 17hpf for 21 hours at 28.5ºC, touch-evoked response was assessed at 24, 42 and 48hpf.

2.3 Immunohistochemistry

Zebrafish embryos were collected and dechorionated before being fixed overnight at 4°C in 500µL BT fix (4% para-formaldehyde, 0.15mM CaCl2, 4%sucrose in 0.1 M PO4 buffer), as described previously (Ashworth et al., 2001; Westerfield, 1993). The following day, three 10 minutes washes in 500µL phosphate buffer (PB) were performed to remove any excess PFA, followed by a 5 minute acetone permeabilisation at -20°C and a further two 5 minute washes in 500µL PB. A block was then performed using 10% goat serum (GS) in 500µL phosphate buffer with 0.8% triton (PBT) samples were incubated on the shaker for 1 hour. Primary antibody was then added as well as PBT with 1% GS saline solution (PBST) and incubated at room temperature on the shaker overnight. The following day, five 30 minutes washes in 500µL PBT were performed to remove any remnants of the primary antibody. The embryos were then incubated overnight on the shaker (in darkness) with their respective secondary antibody (anti-mouse or anti-rabbit), diluted at 1:1000 in PBT with 1% GS. The following day, phalloidin actin labelling was performed, by incubating the samples in either Alexa Fluor 488 phalloidin (Invitrogen) diluted at 1:40 in PBT, or Rhodamine phalloidin, for 1 hour on the shaker. Following on Alexa Fluor 488 phalloidin labelling, four 30 minutes washes were then performed in PBT on the shaker. After Rhodamine phalloidin labelling, three 15 minutes washes were performed. Embryos were then either stored in a 50% glycerol - 50% PBS solution ready for mounting to view in a lateral position on glass slides in 100 % glycerol, or directly mounted in Dako (Dako Sweden AB, Stockholm Sweden). The details of primary antibodies and respective secondary antibodies used in this study are found in the tables below (Table 2.1 & 2.2).

Primary Antibody	Species raised in	Concentration (in PBST 1%GS)	From	Chapter
F59	Mouse	1:100	DSHB by Stockdale, Frank E. (DSHB Hybridoma Product)	3 & 4
Tropomodulin 1	Rabbit	1:100	Gift from Pr.Fowler Laboratory	3
Tropomodulin 4	Rabbit	1:25	Gift from Pr.Fowler Laboratory	3
Phospho-Src (Tyr^{416})	Rabbit	1:250	Cell Signaling	4
β-sarcoglycan	Mouse	1:250	Novo Castra Laboratories	4

Table 2.1: Details of Primary Antibodies.

Secondary Antibody	Species raised in	Concentration (in PBST 1%GS)	From	Associated Primary Ab
goat anti rabbit IgG Alexa Fluor 488	Goat	1:1000	Invitrogen	Tropomodulin 1 Tropmodulin 4 Phospho-Src
goat anti mouse Cy™5-linked	Goat	1:1000	GE HealthCare Uk Ltd.	F59 β-sarcoglycan

Table 2.2: Details of Secondary Antibodies.

2.4 Confocal imaging

Images from whole mount embryos were acquired using a Zeiss META 510 confocal microscope (excitation 543nm, emission 560-615 band pass filter, using 20 or 40 x lenses) at 5dpf and z-stack images up to 2dpf were acquired using a Leica (Leica SP5). Alexa 488 labelled specimens were excited with 488nm laser line and emitted light was collected at 500-550nm band pass filter using 60x lens. Secondary Cy5 labelled antibodies were excited with 633nm HeNe laser. For a comparative approach images were acquired from somites that were positioned in a region aligning with the yolk extension, immediately below the point of attachment with the yolk ball.

2.4.1 Standardisation of somite length measurements

In Chapter 4, the measurements of somite length was standardised to compare between experiments. This was achieved by measuring between the boundaries at the level of the horizontal myoseptum, between the two apexes of the chevron shaped somite boundaries. A 30μm line was drawn perpendicular to the horizontal myoseptum measurement both ventrally and dorsally, this was followed by another perpendicular line from the 30μm readings to give rise to three parallel measurements equally spaced along the somite. For embryos that lacked a clear horizontal myoseptum, a line was drawn as best fit, but was not recorded as a measurement, from this line of best fit two parallel readings were taken if the somite boundaries were clear. Final measurements (Figure 4.13) are a mean of the three measurements taken from the somite length shown in Figure 2.4.

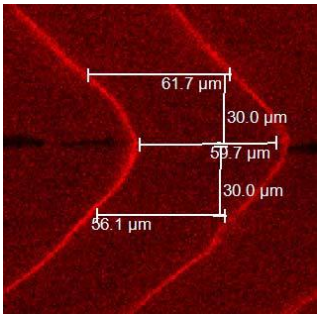

Figure 2.4: Measurement of somite length of 48hpf PP2 treated embryo. Somite boundaries stained with a β-sarcoglycan antibody.

2.4.2 Standardisation of myofibril length measurements

In Chapter 3, myofibrils waviness was obtained by tracing lines using the “open free shape curve drawing mode” in the Imaris software (Bitplane). In addition end-end length measurements (i.e. between myosepta in the trunk muscles) were taken from a straight line that connected the starting and end points of the curved line. The myofibril length was normalised to the end-end length as an index for myofibril alignment (Figure 2.5).

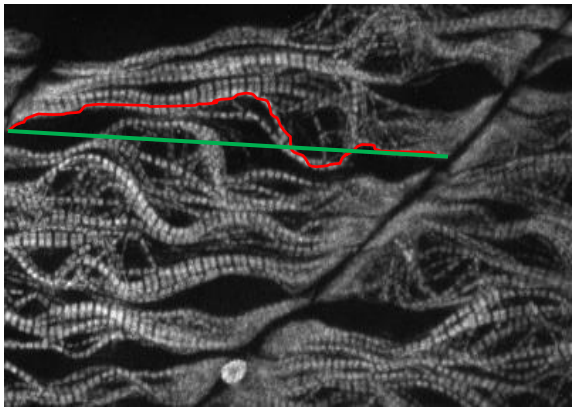

Figure 2.5: Measurement of myofibril length on 24hpf *relaxed* mutant. Immunostaining of myosin with F59 and confocal projections reveal myofibril organisation.

2.4.3 Standardisation of myofibril width measurements

The width of the myofibrils was taken perpendicularly to the median plan of the somite which was first established by measuring the width of the somite (as described in 2.5.1) and joining the centre of these measurements, using the Leica LAS AF software (Figure 2.6).

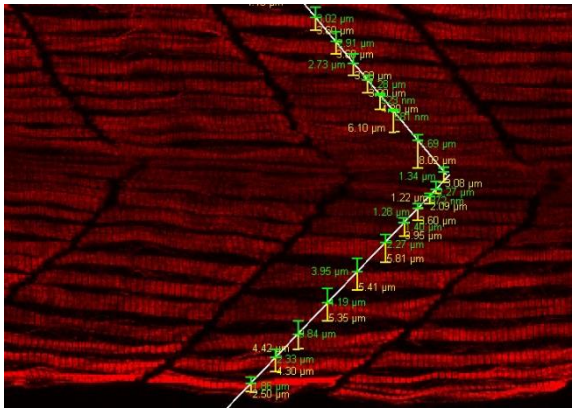

Figure 2.6: Measurement of myofibril width on wildtype 24hpf embryo. Immunostaining of myosin with F59 and confocal projections reveal myofibril organisation.

2.4.4 Standardisation of actin length measurements

The length of the actin myofilaments was estimated by measuring phalloidin stained actin filaments between the boundaries of adjacent H zones, H-H measurement, five measurements were taken per fish, using the Leica LAS AF software (Figure 2.7).

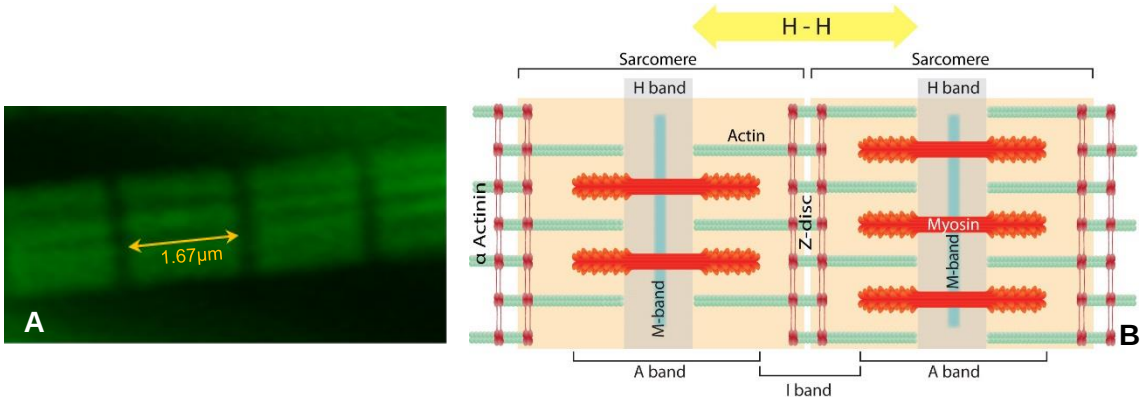

Figure 2.7: H-H measurement. [A] Confocal image of actin filaments stained with phalloidin (1/40) **[B]** Measurement were made in between H bands, across Z-discs and sarcomeres.

2.4.5 Standardisation of cross-sectional area measurements

Cross-sectional area of transversal sections through dorsal region of the somite of phalloidin stained embryos was estimated by multiplying transversal and longitudinal measurements, using the Leica LAS AF software, as depicted in Figure 2.8.

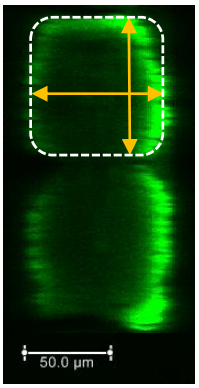

Figure 2.8: Cross-sectional measurement in 5dpf wildtype embryo. Confocal image of actin filaments stained with phalloidin (1/40).

2.5 Molecular analysis

2.5.1 RNA Extraction

A Micro-Fast track 2.0 Invitrogen kit was used for the mRNA extraction. mRNA was extracted from several batches of wildtype frozen embryos varying in size, ie. 100, 92, 45, 25 and 20 embryos. 'Twin' batches of embryos, one of homozygotes *relaxed* mutants, the other of their sibling's heterozygotes and wildtypes controls, were assessed. The mRNA concentration was determined by spectrophotometry using the Nanoview GE Healthcare.

2.5.2 PCR and electrophoresis

RTPCR was conducted following the protocol of the Access RT-PCR kit and DNase I obtained from Promega UK (#282071), in order to perform both cDNA synthesis and PCR in one step to reduce possible inaccuracies due to manual handling, as pipetting errors. Three pairs of primers were used to amplify respectively *fak1a, fak1b* and *βactin* (Table 3). *βactin* was chosen as a positive control in order to check the presence of RNA. The wildtype total RNA was used as a primer positive control for the three pairs of primers. Furthermore, DEPC water was run as a negative control for each set of primer, and the kit's positive control (RNA/primer) was also run. A gel electrophoresis was then performed, 5µL aliquot of the PCR products were mixed to 1µL of Loading Buffer and run on a 1% agarose/TAE gel for 35min. at 80V, along with a 100bp ladder (Biolabs), to determine *fak1a, fak1b* and *βactin* weight, which is respectively 353bp, 346bp and 238bp.

2.5.3 qRTPCR

2.5.3.1 Embryo collection for qRTPCR

Zebrafish embryos were collected and pooled at different developmental stages, 10 embryos at 24hpf, 3 embryos at 48hpf, 2 embryos at 72hpf and 2 embryos at 96hpf respectively. Embryos were pooled in that way after optimisation of the qRTPCR technique, to ensure that there was a similar amount of mRNA in each sample. They were immersed in 200µL of Lysis Buffer (Invitrogen Dynabeads mRNA Direct Kit) in 1.5mL eppendorf tubes and immediately frozen on dry ice. They were then kept at -80C prior to mRNA extraction.

2.5.3.2 mRNA extraction and oligonucleotides

Poly-A^+ mRNA was extracted directly from embryos using the Dynabeads® mRNA Direct™ kit (Invitrogen), and purified mRNA was then reverse transcribed into cDNA using the Reverse Transcription System kit (Promega). Oligonucleotide pairs for use as qRTPCR primers were designed for *fak1a* (GenBank ID: AF348085.1), *fak1b* (GenBank ID: AT196213.1), *foxm1* (Uniprot: HFH11b mRNA (U74613), GAPDH (NCBI Reference Sequence: NM_001115114.1), βActin (GenBank: AF057040.1), using the Roche primer design webtool (Table 2.3).

Gene of interest ID	Primer sense	Primer Sequence
fak1a AF348085.1	Forward	GGC GAG CGT CTG GCT ATG CC
	Reverse	GAG AGC AGG CCA TGT GGG CC
fak1b AT196213.1	Forward	CCA CCG ACA GGA GCC TCC CA
	Reverse	ATA GCT GTC GGC CGG GCT CA
foxm1 HFH11b mRNA (U74613)	Forward	CCT CAG ATC CCA CAA GTT GC
	Reverse	GCT TCA TCT TCC TCT CTG TGC
GAPDH NM_001115114.1	Forward	GTG GAG TCT ACT GGT GTC TT
	Reverse	GTG CAG GAG GCA TTG CTT ACA
βactin AF057040.1	Forward	AAG CAG GAG TAC GAT GAG TC
	Reverse	TGG AGT CCT CAG ATG CAT TG

Table 2.3: *fak1a*, *fak1b*, *foxm1*, GAPDH, βActin sequences designed using the Roche primer design webtool.

2.5.3.3 qRTPCR

For quantification of *fak1a, fak1b* and *foxm1* mRNA transcripts, the pairs of primers *fak1aF/R, fak1bF/R* and *foxm1F/R* were used for PCR amplification (Hybaid MultiBlock System) from a pooled cDNA sample of zebrafish embryos, this confirmed that each primer pair produced a single PCR band. The PCR product was purified after gel electrophoresis and quantified using a spectrophotometer. A serial dilution of *fak1a, fak1b* and *foxm1* cDNA was used to generate a standard curve (10^9 to 10^2 copies of *fak1a*, *fak1b* and *foxm1* mRNA per 2μL) using the LightCycler. The mRNA copy number of *fak1a, fak1b* and *foxm1* in each sample was determined from the standard curve using the LightCycler quantification software. The zebrafish *GAPDH* and *βActin* were used as a reference housekeeping genes for all quantification of *fak1a, fak1b* and *foxm1* mRNA levels. The *GAPDH* and *βActin* primers were used to PCR amplify a fragment of 173bp and 238bp respectively from a cDNA sample of zebrafish embryos. Similarly, a standard titration curve for *GAPDH* and *βActin* was performed, and the mRNA copy number of *GAPDH* and *βActin* in each sample was determined as described above. The amount of *fak1a, fak1b* and *foxm1* mRNA in each sample was normalized against the combined

amount of *GAPDH* and *βActin* mRNA in the same sample and subsequently expressed as the mRNA copy number of *fak1a, fak1b* or *foxm1* per 1000 copies of *GAPDH* and *βActin* mRNA.

Real-time quantitative PCR was performed using a LightCycler 480 (Roche Diagnostics) in which PCR reactions were performed in a 10μL volume of FastStart DNA Master SYBR Green I mix (Roche Diagnostics Ltd.), containing 5μM primers, dH_2O and *Taq* DNA polymerase, DNA double-strand specific SYBR Green I dye, nucleotides, and buffer. A typical protocol comprised an initial denaturation at 95°C for 5 min, followed by 45 cycles of 95°C for 10 s, 65°C annealing for 6 s, and 72°C elongation for 7s, fluorescence was measured at 2/3°C below specific melting peak of each product. At the end of the 45 cycles, samples were subjected to a melting analysis to confirm amplification specificity of the PCR products. During this step, samples were heated from 72 to 95°C at a steady rate of 4.4°C/s, and fluorescence was measured continuously throughout this period (Teh et al., 2002). Melting analysis of *fak1a, fak1b, foxm1*, *GAPDH* and *βActin* of all cDNA samples amplified, consistently (both intra- and inter-experiment) gave single melting peaks of 88.8 ±0.07°C (mean ± SE of n = 12, randomly chosen samples from three independent experiments), 90.8 ±0.07°C, 83.9 ±0.07°C, 84.7 ±0.06°C and 85.4 ±0.06°C respectively. PCR products were further confirmed by gel electrophoresis.

2.6 Mounting for mechanical experiments and X-ray diffraction analysis

The larvae were held in Embryo Medium, at pH 6.8–6.9. Prior to the experiment, a 5-7dpf larva was transferred to Embryo Medium containing 0.017% Tricaine (3-amino benzoic acid ethylester). When the larva was anaesthetised, the head was crushed and the preparation mounted using aluminium clips (Dou et al., 2008; Li et al., 2013). These were folded around the head and tail portions of the larvae, providing a defined and stable attachment. Small holes were made in the aluminium foil for attaching the preparation between the extended arm of an AE801 force transducer (SensoNor, a.s., Horten Norway) and a fixed pin for length adjustment using a micrometer screw (Figure 2.9). For mechanical experiments the preparation held horizontally in a 0.5mL Perspex organ bath at room temperature (22°C). For X-ray diffraction experiments the preparation was mounted between a fixed hook and a hook on a micrometer screw, for length adjustment. The experiments were performed at 22°C in MOPS buffered physiological solution (in mM: 118 NaCl, 24 MOPS, 5 KCl, 1.2 $MgCl_2$, 1.2 Na_2HPO_4, 1.6 $CaCl_2$, and 10 glucose) at 22°C, pH 7.4.

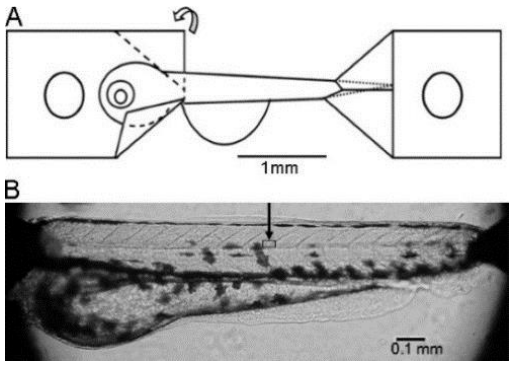

Figure 2.9: Zebrafish larvae preparation. [A] Schematic illustration of preparation attachment using aluminium foil clips at both ends of the larvae. The aluminium foil is folded along the dashed lines as shown on the left clip. A small hole is made in each clip for mounting. **[B]** Photograph of the preparation mounted on the microscope stage (Dou et al., 2008).

2.7 Small angle X-Ray diffraction

Small angle X-ray diffraction was used to determine the interfilament distances in the zebrafish larvae, as described previously (Dou et al., 2008), at beamline I911-SAXS at the MAX II ring of the MAX IV Laboratory in Lund, Sweden (Li et al., 2013; Labrador et al., 2013). The larvae were euthanised and mounted horizontally as described above between two hooks in a Kapton cuvette in the MOPS buffered physiological solution and stretched to different lengths (L) relative to slack (Ls). In a few experiments the MOPS buffered solution was supplemented with 5mM NaCN to induce metabolic inhibition and a rigor state. The camera length was 230cm and calibrations of the X-ray patterns were made using diffraction from rat tail collagen. The diffraction patterns were recorded using a PILATUS 1M detector (DECTRIS Ltd.) with exposure times between 5 and 10s. For analysis of diffraction patterns in living and non-stretched preparations, the larvae were anesthetised with Tricaine and kept in Embryo Medium in a cuvette. Equatorial patterns were recorded and the spacing and intensities of the 1.0 and 1.1 reflections were evaluated using background subtraction by fitting a polynomial function, determining the centre position (lattice spacing) and the integrated the area (intensity) under the peaks (Figure 2.10).

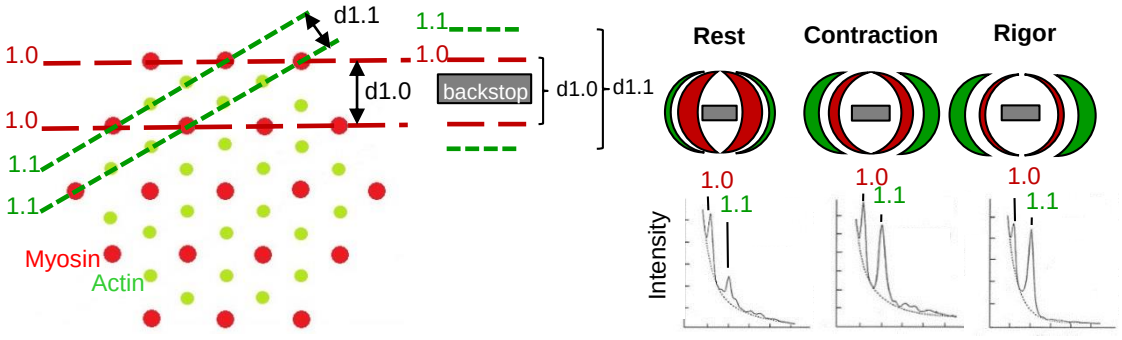

Figure 2.10: Skeletal muscle lattice and small-angle X-ray diffraction patterns. Left: Transverse view of thick and thin filament lattice and equatorial reflections in X-ray diffraction of skeletal muscles. **Right:** Graphical representation of the reflection pattern of skeletal muscle at rest, during contraction and in rigor and their densitometer traces. Modified from Millman, 1998.

2.8 Mechanical analysis

The larval preparations were mounted as described above at slack length and then stimulated (single twitches) with 0.5ms electrical pulses (supramaximal voltage) at 2 min intervals via two platinum electrodes placed on both sides of the preparation. Length (L) was increased in steps between the contractions, from the slack length (Ls) to a length above the maximal for active force (Lopt). At each length, active and passive force were recorded. Force signals were recorded and analysed using LabChart® (ADInstruments Ltd, Oxford, UK). Using this procedure the Lopt, as well as the shape of the passive and active length-force relationships, were determined.

2.9 Sarcomere length measurements and volume calculation

In one series of experiments we mounted muscle preparations in a cuvette with a glass window enabling analysis of sarcomere length using a 40x objective on an inverted microscope. Muscles were stretched in a similar manner as in the force and X-ray diffraction experiments to different lengths relative to slack. This data enabled us to relate the extent of stretch to sarcomere length. Using the sarcomere length data, the sarcomere volume was estimated. The cross-sectional area of one sarcomere is composed of 6 equal sided triangles, where $2/3*d_{10}$ is the side (Figure 11). $(d_{10})^2 * 2 / \sqrt{3}$ is the area of the sarcomere cross section and Volume = Area * sarcomere length, i.e. $(D_{10})^2 * 2/\sqrt{3}$ * Sarcomere length (SL). If we plot $1/ (D_{10})^2$ vs. SL and get the slope, the volume can be calculated as Volume = (1/slope) * 2 / √3, as described by (Millman, 1998) (Figure 2.11).

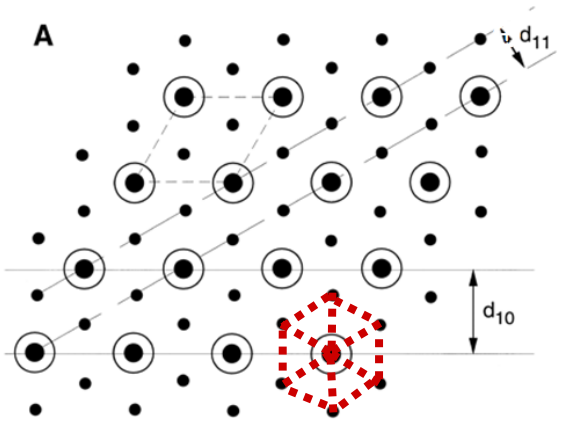

Figure 2.11: Filament lattice with the d10 and d11 spacings. The cross-sectional area of one sarcomere, composed of 6 equidistant triangles, is indicated with the red dotted line (Millman, 1998).

2.10 Behavioural analysis

Optical analysis of larval swimming behaviour can be used as a semi-quantitative method to identify major motility problems (Granato et al., 1996). Swimming basal behaviour was assessed by recording the distance travelled and number of rotations of both control and drug treated embryos over 2 min trials at 3, 5, 7, 30 days and 3 months post fertilisation using an automated behavioural analysis system, an Image Source DMK camera linked to the tracking software Ethovision™. The Ethovision™ tracking software presented the results as a numerical value based on displacement from the initial start point, there were 120 data points from the 2 minute experiment (Figure 2.12).

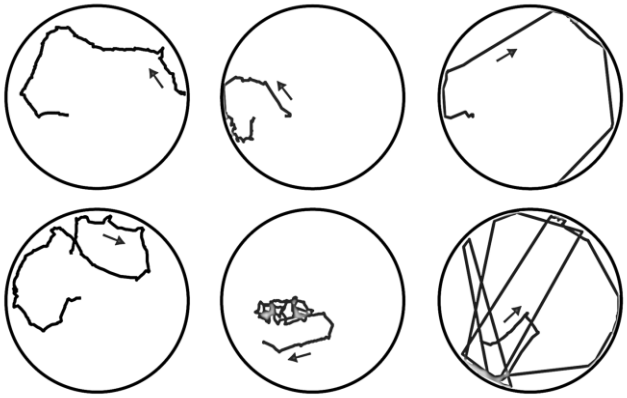

Figure 2.12: Schematic representation of swimming basal behaviour recordings. The embryos were tested during 2 minutes in a 6 well plate, with each of the wells forming an arena for the zebrafish embryos to be tested in. Swimming variables distance travelled and number of rotation were recorded using an Image Source DMK camera linked to the Ethovision™ tracking software on a PC.

2.11 Statistical analysis

Statistical analysis in this study were performed with the Graphpad Prism, SPSS and R softwares.

2.11.1 Statistical analysis of the swimming behaviours recorded with Ethovision™

Larvae were filmed from above for 2 minutes, allocated into 1 second bins. Distance travelled (mm/sec) and rotations (n/sec) were assessed as a function of age (4 levels: 72hpf, 120hpf, 168hpf and 732hpf) and Tricaine treatment (2-levels: Tricaine treated vs. control). Distance travelled data were entered into a random intercept linear mixed effects model, with individual ID nested in batch as a random effect. Denominator degrees of freedom were estimated using the Satterthwaite approximation. Initial null

model fits indicated that the errors were non-normal, but this was corrected by a log (base-10) transformation. Rotations data were overdispersed (zero-inflated) and fitted to a mixed effects model with a negative-binomial (generalised linear mixed effects model). As before, individual ID nested in batch was added as a random effect. The contribution of 'time' to the variance was assessed by likelihood ratio test from the null models, but this was omitted from final models. This analysis was performed using the R 'lme4' package.

2.11.2 Statistical analysis of the PP2 study

Using the SPSS software, one-way and two-way ANOVA were used to reject the null hypothesis, then a post hoc LSD (least significant difference) test was used to test for a dose effect. Dose effect was calculated by comparison of the LSD between the concentrations of treatment. For the staining analysis the different experiments were used as a random factor, to see if there was any variation of somite length between the experiments.

CHAPTER 3

EFFECT OF PARALYSIS ON MYOFIBRIL STRUCTURE AND ORGANISATION

3. Effect of paralysis on myofibril structure and organisation

3.1. Introduction

Skeletal muscle fibres are composed of myofibril bundles, which contain the contractile machinery (i.e. the sarcomeres). The correct formation of myobrils, myofibrillogenesis, is therefore critical for skeletal muscle function. Striated skeletal muscle structure is conserved across the animal kingdom implying that myofibrillogenesis and the mechanism of myofibril assembly is a fundamental process (as reviewed by Sanger et al., 2010). Contraction is key for myofibril differentiation and assembly (Chapter 1 Figure 1.2); however, the underlying mechanism of this process is not well defined. The internal structure of the skeletal muscle fibres is maintained in part by their own intrinsic contractile activity (Boonyarom and Inui, 2006). Evidence from studies in isolated cultures has shown that contraction is an important regulator in the later stages of myofibril assembly, alignment and sarcomere spacing (Sparrow and Schöck, 2009; Sanger et al., 2005; De Deyne, 2000; Fujita et al., 2007). In addition, *in vivo* studies, in *C elegans* (Hresko et al., 1994; Moerman and Williams, 2006) and *Drosophila* (Reedy and Beall, 1993), have also shown that contraction regulates myofibril development. In zebrafish, the excitation-contraction pathway was shown to control sarcomere length (Brennan et al., 2005).

Zebrafish have proved useful as an *in vivo* model to study the development of vertebrate skeletal muscle, including myofibril organisation and alignment. Contractile movement in zebrafish embryos is initiated at 17hpf, as functional neuromuscular connections within the body of the fish start to form (Chapter 1 Figure 1.6). Zebrafish motility mutants (which lack components of the excitation-contraction coupling pathway) contain skeletal muscle that is unable to contract and development of the muscle fibres is disrupted (Behra et al., 2002; Brennan et al., 2005; van der Meulen et al., 2005). Evidence from several laboratories show that, a lack of E-C coupling in the skeletal muscle of immotile zebrafish embryos disrupts (i) myofibril alignment (thin wavy myofibrils) and (ii) sarcomere width and filament length (in the A and possibly M band). These studies show that contraction is necessary for the organisation and refinement of myofibril structure during early vertebrate muscle development.

There is evidence that it is the contractile event itself rather than upstream signalling events, such calcium release that is important for myofibril alignment (Lahne et al., 2009) (Chapter 1 Figure1.11). This has led to the hypothesis that contractile activity is driving myofibril organisation; however, this has not been tested directly *in vivo*. Furthermore, the severity of myofibril misalignment in paralysed embryos was shown to correlate with

specific developmental time points. The most pronounced effect being observed when embryos were paralysed from 17-24hpf rather than later on (24-41hpf and 48-55hpf) (Chapter 1 Figure 1.10) (Lahne et al., 2009). This time window (17-24hpf) coincides with the initiation of the spontaneous contractile activity (Chapter 1 Figure 1.6). These initial spontaneous contractions are proposed to be an endogenous developmental event that play a key role in the organisation of myofibrils during early skeletal muscle development.

Actin filaments are the most abundant protein in myofibrils, they anchor at the Z disc, span the I band and extend towards the middle of the sarcomere (Chapter 1 Figure 1.1). The I band, as well as containing structures, notably actin, has several essential functions, including linking the region of active force generation (the A band, where the myosin cross links) with the Z-discs ensuring sarcomere linkage, and acting as a spring for the reversible mechanical stretch response required for efficient contractile activity. To ensure the spring like action and maintenance of tension through the sarcomeres, myofibril and ultimately the skeletal muscle, the length of thin filaments is very precise. Actin length is proposed to be regulated via several remodelling mechanisms, mainly through interactions with the template protein nebulin and capping proteins (tropomodulins and CapZ), that sequester monomeric actin, sever actin filaments, and/or promote actin polymerization and depolymerisation, as reviewed by Clark and Trinick (Clark et al., 2002; Trinick, 1994; Gokhin and Fowler, 2013). While the classic nebulin ruler model that determines actin length was appealing in its simplicity, recent studies have shown that this model was incorrect. Thin filaments are more accurately modeled as bipartite structures with the following concatenated segments: (i) a constant-length, nebulin-coated thin filament core region (‘proximal segment’) starting at the Z-line and continuing to a distance of ~0.95 μm away from the Z-line; (ii) a variable-length, nebulin-free, thin filament extension (‘distal segment’) starting at ~0.95 μm away from the Z-line and continuing to the thin filament pointed end, which is capped by Tmod. The constant length of the nebulin-coated proximal segment excludes the possibility of a ruler function for nebulin, since thin filament lengths vary across different muscles (Gokhin et al., 2012; Gokhin et al., 2010; Castillo et al., 2009; Littlefield et al., 2002; Ochala et al., 2012; Ringkob et al., 2004). While the variable length of the distal segment implicates Tmod-mediated pointed-end actin dynamics as the chief determiner of skeletal muscle-specific thin filament lengths in vivo (Gokhin and Fowler, 2013).

Actin filaments have distinct polarity and, in the sarcomere are orientated so that the positive or barbed ends are anchored to the Z-bands, whereas the negative or pointed ends are not attached to any structure but capped by capping proteins, notably tropomodulins (Tmod) and Leiomodins (Lmod). These capping proteins, which control actin polymerisation at the actin pointed ends, have a critical role in regulating thin

filament length (Littlefield and Fowler, 2008) sarcomeric structure and organisation (Chereau et al., 2008). The importance of Tmod is highlighted by their presence in all metazoans, with four isoforms of Tropomodulins expressed in mammalian cells (Gokhin and Fowler, 2011), the isoforms that regulate actin filaments in skeletal muscle are Tmod1 and Tmod4 (Gokhin et al., 2010). Lmods are evolutionarily related to Tmods and display tissue-specific patterns of expression distinct from, but overlapping with, the expression of Tmod isoforms (Conley, 2001). By capping the pointed ends of actin filaments, Tmods and Lmods control actin filament assembly, length, and stability. Studies have shown that overexpression of Tmods shortens thin filaments, whereas knockdown or inhibition of the capping activity of Tmods results in the elongation of thin filaments (Gokhin and Fowler, 2011; Gregorio et al., 1995; Littlefield et al., 2001; Mardahl-Dumesnil and Fowler, 2001; Ono, 2010). Furthermore Lmod2 and 3 are expressed in skeletal muscle and their interaction with Tmods appears to modulate actin nucleation activity and localisation (Skwarek-Maruszewska et al., 2010).

Studies have shown that during muscle paralysis in zebrafish embryos, disruption to the myofibril structure is accompanied by rearrangements at the ultrastructural level, within the filaments of the sarcomeres themselves, namely changes in length (Brennan et al., 2005). Furthermore, evidence from mammalian work suggests that actin filament remodeling, specifically lengthening, may have a direct impact on myofibril organisation (as reviewed by Ono, 2010) (Gokhin et al., 2010) and function, as thin filaments determine the optimal sarcomere length for force generation (Littlefield and Fowler, 2008). This has led to the hypothesis that contraction may regulate actin length and associated capping protein distribution during zebrafish myofibril organization.

In order to study the importance of contraction in skeletal muscle development, namely myofibril organisation, a combination of genetic and pharmacological approaches were established. An immotile mutant line (*cacnb1^{ts25}, relaxed*), which lacks functional voltage-gated calcium channels (dihydropyridine receptors) in skeletal muscle, and treatment of embryos with a reversible anaesthetic (Tricaine and BTS) allowed the study of paralysis (in mutants and anaesthetised fish) and recovery of movement (reversal of anaesthetic treatments). The effect of paralysis on skeletal muscle structure at both myofibril and myofilament level in early embryos (aged between 17-24hpf) was determined using immunostaining and confocal microscopy, as well as small angle X-ray diffraction. Furthermore, the consequences of paralysis and recovery on the localisation of the actin capping proteins Tropomodulin 1 and 4 was also assessed to establish if contractility was necessary to their correct positioning and actin regulatory activity.

Hypothesis: Myofibril elongation has been observed in immotile mutant zebrafish embryos leading to the hypothesis that contraction is necessary for the regulation of myofibril length (Brennan et al., 2005). This hypothesis was tested in this chapter by determining whether paralysis-induced lengthening of myofibrils can be rescued by reimposing movements in living zebrafish embryos using a reversible anaesthetic. In addition, once the process of myofibril regulation was established, the underlying mechanisms were investigated. Sarcomere and myosin shortening occur as a result of paralysis, however the effect on actin myofilament length is unknown. Thus, it was proposed that contraction drives actin length, this hypothesis was tested in this chapter using the same technique as described above for myofibrils.

3.2 Results

An experimental paradigm was developed to investigate whether reinstalling contraction would lead to a recovery of myofibril organisation. Myofibril organisation has been shown to be most disrupted when paralysis occurs between 17 and 24hpf, a time coinciding with the formation of neuromuscular junctions and the onset of initial embryonic movement (Lahne et al., 2009). This suggests that the initial 17-24hpf contractile event itself, drives myofibril organisation during early development and is therefore important for the establishment of skeletal muscle structure and function in the zebrafish embryo. Wildtype embryos were treated with a reversible anaesthetic (Tricaine) to induce paralysis between 17-24hpf (as described in Chapter 2 Figure 2.1). Staining at 24hpf demonstrated that the wavy phenotype observed in *relaxed* mutant embryos could be reproduced in chemically paralysed embryos. Subsequently, at 24hpf, embryos were removed from anaesthetic to enable recovery of movement and staining at 42hpf (18 hours after paralysis) revealed that the myofibril recovery was possible (Figure 3.1).

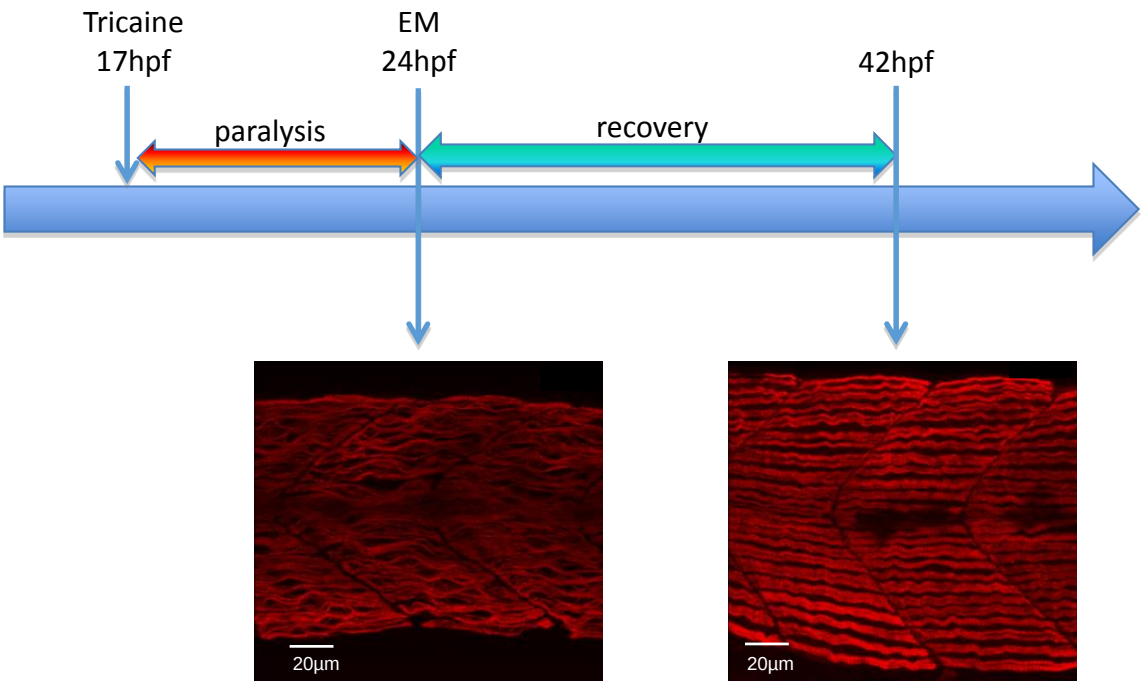

Figure 3.1: 17-24hpf paralysis disrupts myofibril organisation, movement recovery restores it. Confocal projections of immunohistochemically labelled slow muscle fibres anti-myosin antibody F59. Zebrafish embryos were exposed to Tricaine for 7 hours from 17-24hpf, before recovery was allowed in Embryo Medium up to 42hpf (Scale bar 25 µm). Movement restoration after paralysis leads to skeletal muscle structure recovery.

3.2.1 Early paralysis-induced myofibril organisation disruption is partially restored by the recovery of contractile movement

Paralysis between 17 and 24hpf in either chemically treated or immotile mutants lead to the development of a 'wavy' myofibril phenotype in paralysed embryos (Figure 3.2 G, J) when compared to controls at 24hpf (Figure 3.2 A, D). Staining at 42hpf, after 18 hours of recovery and movement, revealed a partial structural recovery of myofibril organisation in chemically paralysed embryos (Figure 3.2 H), as compared to controls (Figure 3.2 B). Further, structural recovery appeared to be sustained at 5 days post fertilisation (Figure 3.2 I), whereas the myofibrils in immotile *relaxed* mutants remained wavy throughout the experimental period (Figure 3.2 K, L).

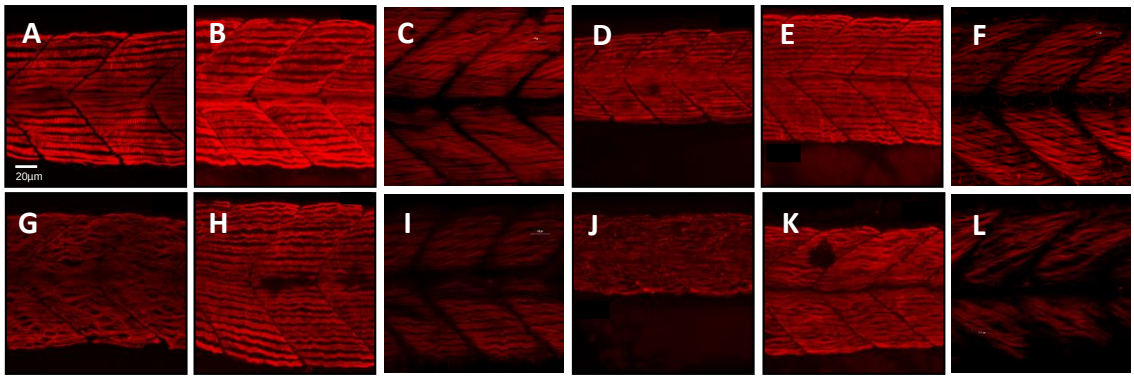

Figure 3.2: Paralysis-induced disruption of myofibril organisation is partially reversed by restoring movement in developing skeletal muscle. Control embryos (Embryo Medium alone) and treated embryos (Embryo Medium with Tricaine) were incubated for 7 hours starting at 17hpf. At 24hpf embryos were removed and control **(A)** and treated embryos **(G)** were fixed and stained immediately or put into recovery (Embryo Medium without Tricaine) and **(B)** control and **(H)** recovered embryos fixed and stained at 42hpf. Some embryos were kept in recovery from 24hpf up to 5 days before fixation and staining of both control **(C)** and recovered larvae **(I)**. *Relaxed* immotile mutants were fixed and stained at 24hpf **(J)**, at 42hpf **(K)** and 5 days **(L)** as well as motile carriers controls at 24hpf **(D)**, 42hpf **(E)** and 5 days **(F)**. Anti-myosin antibody (F59) in A,B,D,E,G,H,J,K, and Rhodamine phalloidin actin labelling in C,I,F,L reveals slow muscle fibres, scale bars corresponds to 20µm. For consistency, the somite imaged were taken at the level where the yolk sac and the yolk sac extension join.

Structural recovery of myofibrils, as observed by imaging, was evaluated in more detail using a method to quantify myofibril length and width in both chemically paralysed wildtype zebrafish embryos and paralysed *relaxed* mutants at 24 and 42hpf. At 24hpf, Tricaine treated embryos showed a significant increase in myofibril length and a decrease in myofibril width compared to control embryos (Figure 3.3 A). At 42hpf, motile recovered Tricaine treated embryos, placed into Embryo Medium from 24hpf, showed no significant difference in myofibril length and a small but significant difference in myofibril width compared to controls (Figure 3.3 A). In summary, the Tricaine-induced paralysis lead to a decrease in myofibril width and an increase in length, the later being restored after recovery of movement at 42hpf, when compared to controls. At 24hpf the myofibrils in *relaxed* immotile mutant showed a very significant increase in myofibril length and a decrease in width compared to motile carriers, in a similar manner to the Tricaine treated embryos (Figure 3.3 B). However, at 42hpf, the myofibrils in *relaxed* embryos remained significantly elongated compared to motile carriers, whereas their width had recovered to control values (Figure 3.3 B).

In summary, these results show that inhibition of contraction between 17 and 24hpf causes a significant increase in length and decrease in width of the myofibrils. The restoration of contractile movement leads to a full recovery of myofibril length but not width. Furthermore, it is noticeable that in the complete absence of movement myofibril width but not length fully recovers. These observations show that regulation of myofibril length depends on contractile activity whereas myofibril width does not.

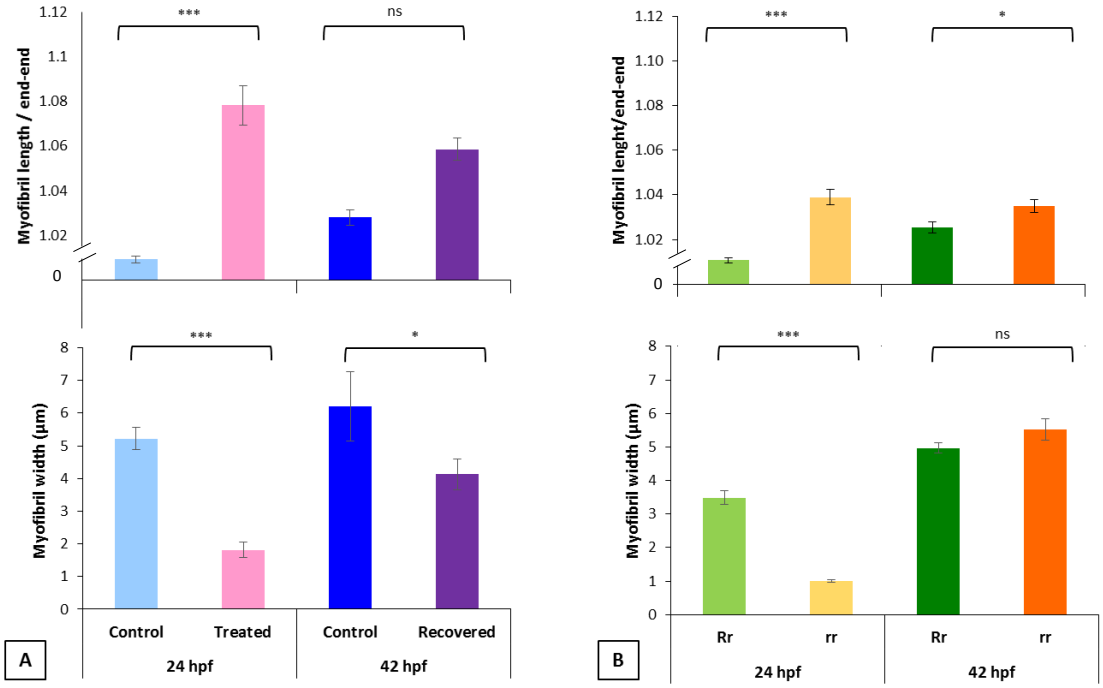

Figure 3.3: Disruption of myofibril organisation during paralysis is reversed by restoring movement in developing skeletal muscle. [A] Immediately after treatment at 24hpf, a very significant increase in myofibril length/end-end (***p<0.001) and decrease in myofibril width (***p<0.001) in Tricaine treated compared to control embryos was observed (length: controls n=6, treated n=6 and width: controls n=17, treated n=36, ANOVA, Kruskal-Wallis). After recovery by 42hpf, no significant difference (ns) in the myofibril length/end-end and a small but slightly significant difference in myofibril width (*p<0.05) in control versus recovered embryos was observed (length: controls n=18, treated n=6, width: controls n=57, treated n=23, ANOVA, Kruskal-Wallis). **[B]** At 24hpf immotile *relaxed* mutants (rr) showed a very significant increase in myofibril length/end-end (***p<0.001) and decrease in myofobril width (***p<0.001) compared to motile carriers (Rr) (length: Rr n=5, rr n=5 and width: Rr n=10, rr n=10, ANOVA, Kruskal-Wallis). At 42hpf immotile *relaxed* mutants (rr) myofibril length/end-end was still slightly significantly elongated (*p<0.05) but there was no significant difference in the myofibril width (ns) compared to motile carriers (Rr) (length: Rr n=5, rr n=5 and width: Rr n=13, rr n=13, ANOVA, Kruskal-Wallis).

3.2.2 Filament lattice spacing is not affected by paralysis

In the previous section, the regulation of myofibril width was found to be independent of movement. As myofibrils are composed of myofilaments (actin and myosin), it is likely that the lateral spacing of the myofilament within the lattice is also a movement independent process. Furthermore, in mice, motility mutants (*Myh4*^{arl}) were shown to have similar lattice pattern to wildtypes (Lindqvist et al., 2013). Taken together, these evidences suggests that myofilament spacing will be unaffected by paralysis *in vivo*.

Myofibril architecture, namely myofilament bundling, was assessed in immotile embryos at 6dpf using small angle-X-ray diffraction. This technique, has proved effective in exploring the zebrafish myofilament lattice in wildtype fish (Dou et al., 2008), but has never been used to assess immotile zebrafish muscle. Interfilament spacing was measured in 6dpf muscle preparations of the immotile *relaxed* mutants and their control

siblings, to explore if the complete lack of contractile activity during development, and the disrupted thin filament lengths (as determined at 2dpf, see 3.2.3) affect the lateral arrangement of myofilaments in the sarcomere. We also examined the filament structure in larvae recovered after Tricaine immobilisation between 17 and 24hpf, in comparison with their control at 6dpf. For these experiments, we used small-angle X-ray diffraction and determined (i) the lattice spacing from the 1.0 and 1.1 equatorial reflections (Figure 3.4) and (ii) sarcomere volume using the sarcomere length data examined in detail in Chapter 5 (Figure 5.7).

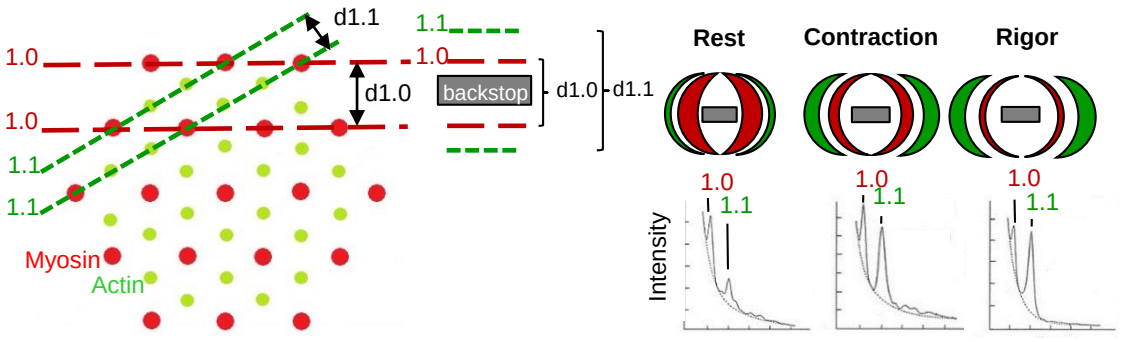

Figure 3.4: Skeletal muscle lattice and small-angle X-ray diffraction patterns. Left: Transverse view of thick and thin filament lattice and equatorial reflections in X-ray diffraction of skeletal muscles. **Right:** Graphical representation of the reflection pattern of skeletal muscle at rest, during contraction and in rigor and their densitometer traces (Modified from (Millman, 1998).

The equatorial 1.0 and 1.1 reflections were clearly visible in all groups (Figure 3.5 A-E) demonstrating that even in the completely immotile *relaxed* larvae a regular filament lattice is assembled. X-ray patterns were recorded at different degrees of stretch and the spacing of the equatorial reflections evaluated (Figure 3.5 F, G). Stretch of the muscles resulted in an outward movement of the reflections reflecting shrinkage of the filament lattice suggesting a constant sarcomere volume is maintained in all groups. The spacing of the 1.0 reflection was similar in the four groups at all degrees of stretch. Similar data was found for the spacing of the 1.1 reflection (Appendix A). The inner 1.0 reflection was strong with a low 1.1/1.0 intensity ratio of about 0.2-0.4 in all groups (Figure 3.5 G), reflecting that cross-bridges are positioned close to the thick filament backbone with no major differences between the examined groups, even in the *relaxed* immotile mutants. In a separate series we measured the sarcomere length at different degrees of stretch in immotile *relaxed* mutants and their siblings, and found a linear relationship between stretch and sarcomere length, although the sarcomere length values were markedly shorter in the *relaxed* mutants (Figure 3.5 H). In Panel I, $1/(d_{10})^2$ is plotted against sarcomere length, a straight line through the origin would reflect a constant-volume behaviour. Using this equation on our data we then estimated the sarcomere volume as described by Milman 1998 (Millman, 1998) (See 2.9). The value of the sarcomere lattice volume in siblings (3.36×10^{-3} μm^3) is close to that found in other muscles studies

(Millman, 1998). At shorter and longer lengths, the sarcomere volume value of the *relaxed* mutated muscles showed deviations from a constant volume behaviour. The best fit to the data gave a 15% lower volume of approximately 2.89 x 10^{-3} μm^3. Immotile *relaxed* larvae cannot develop an active contraction, an event that is dependent on actin myosin cross-linking. Therefore, myosin cross bridges attachment to actin was tested by introducing a rigor state in the *relaxed* mutants. A larva was anesthetised and examined after 2.5 hours in Embryo Medium in the presence of 5mM NaCN. As seen in Figure 3.5 E, this resulted in a significant change in the intensity ratio with an increase in the 1.1 intensity and a relative weakening of the 1.0, demonstrating for the first time that actin and myosin myofilament were capable of cross linking in 6dpf immotile *relaxed* mutants. A result supported by the fact that contraction can be elicited in skinned *relaxed* mutants using caffeine (Zhou et al., 2006). The data suggest that the *relaxed* mutants have a smaller sarcomere volume, associated with shorter sarcomere length, but with essentially unaltered inter filament spacing.

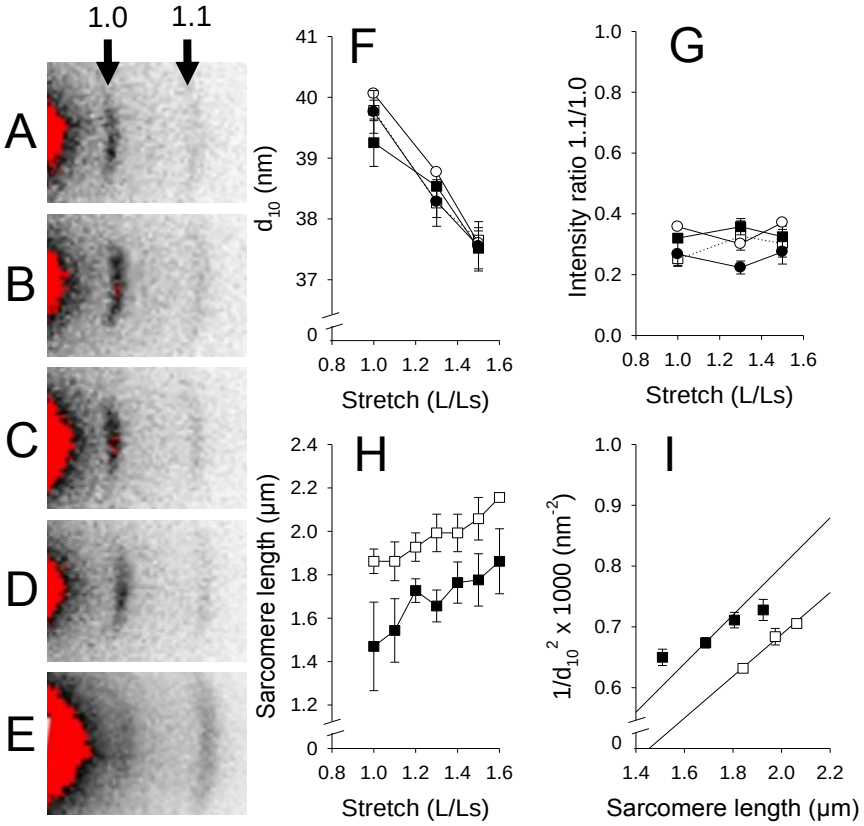

Figure 3.5: **Small angle X-ray diffraction of Tricaine treated and *relaxed* mutant larvae.** Tricaine treated larvae 17-24hpf, recovered until 6dpf (**B**, black circles), controls kept in EM until 6dpf (**A**, white circles), immotile *relaxed* mutants (**D** and **E**, black squares), and their motile siblings (**C**, white squares) at 6dpf, **A-E** show the equatorial X-ray patterns, 1.0 and 1.1 reflections are indicated. **F** shows the spacing of the 1.0 reflection (d_{10}) at different degrees stretch, expressed as length (L) relative to slack length (Ls). **G** shows the intensity ratio of the 1.1 and 1.0 reflections at different degrees of stretch. In **H** sarcomere length is determined at different degrees of stretch and in **I** $1/(d_{10})^2$ is plotted as a function of sarcomere length (predicted from data in Panel **H** and degree of stretch). The line through the data of the motile siblings corresponds to a constant volume of 3.36 x 10^{-3} μm^3. The data from the *relaxed* mutants did not fully follow constant-volume behaviour and the line indicates a volume of 2.89 x 10^{-3} μm^3. n= 4-6 except in

the controls kept in EM until 6dpf, where n=1. **E** shows a *relaxed* immotile mutant sample in rigor, displaying an increase in the outer 1.1 reflection; the 1.1/1.0 intensity ratio was 3.67 compared to about 0.4 in samples under normal conditions (**D**, **G**).

One limitation of the small angle X-ray diffraction technique is that it only allows for testing of zebrafish larvae from 4dpf. We therefore redesigned our paralysis protocol in order to test the chemically paralysed embryos at later stages, during paralysis at 5dpf and after recovery at 6dpf. We used Tricaine (reversible Na^+ channel blocking anaesthetic) and BTS (specific reversible inhibitor of fast myosin ATPase) to inhibit contraction in wildtype embryos up to 5 days. Movements in zebrafish embryos prior to 24hpf are driven primarily by slow muscle, therefore Tricaine, rather than BTS, was found to be most effective at inhibiting the initial embryonic movements up to 29hpf. BTS was then used from 29hpf until 5dpf to inhibit active contractions (Dou et al. 2008), before drug washout allowed the larvae to recover. During this long-term chemical paralysis BTS is a more effective reversible paralysing agent than Tricaine (supplementary data in Appendix F). The Tricaine-BTS treated larvae muscles lattice was found to be significantly compressed (Figure 3.6 A-D). This compression was maintained in both treated and recovered larvae up to 6dpf despite the fact that the latter group moved and had begun to swim. In addition, plotting the square of the spacing d^2 against the reverse of the sarcomere length revealed that sarcomere volume (figure 3.6 D) was smaller in Tricaine-BTS treated fish. Long term chemical paralysis with BTS resulted in myofilament lattice compression from 5dpf, these results are discussed further in Chapter 5.

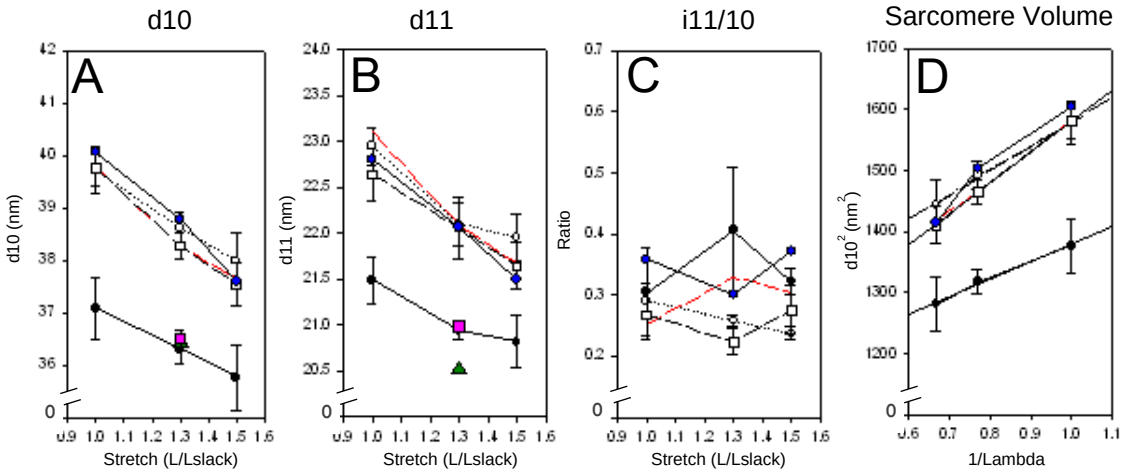

Figure 3.6: Small angle X-ray diffraction of Tricaine-BTS treated larvae. [A&B] Spacing between myofilaments is shown by the two equatorial reflections d10 and d11. Spacing data is plotted against stretch (L/Lslack= Lamda), i.e. 100, 110 ad 130% of the slack length. Tricaine-BTS treated larvae (black circles) showed a significantly compressed lattice (i.e spacing) compared to DMSO controls (white circles), those held in EM (blue squares) and the recovered group (i.e 17-24hpf Tricaine treated larvae, followed by EM, white squares). The lower spacing of Tricaine-BTS treated larvae was maintained when larvae were held in BTS for 6dpf (green triangle) and did not recover when larvae were held 24h in EM after BTS treatment and recovered swimming (pink square).

In summary, these results show that the lattice spacing is unaffected by paralysis (*relaxed* mutants) and paralysis followed by recovery (Tricaine treatment) and is therefore regulated independently of movement. Results also revealed that prolonged paralysis (Tricaine-BTS treatment) caused irreversible compression of the lattice, even after the restoration of movement.

3.2.3 Paralysis leads to actin lengthening

Paralysis is known to alter myofibril arrangement in developing skeletal muscle, this is dependent on myofilament structure, specifically actin length (Clark et al., 2002). The effects of paralysis and the subsequent recovery of movement on actin length was examined using immunohistochemistry and confocal scanning microscopy. Actin remodeling was assessed by measuring actin myofilament length during paralysis at 24 and 42hpf and after movement recovery at 42hpf, in both Tricaine treated and immotile *relaxed* mutant embryos. Immotile *relaxed* mutants showed a very significant lengthening of actin filaments at 24hpf and 42hpf in comparison to motile carriers (Figure 3.7 D). Tricaine paralysis also caused a significant lengthening of actin filaments at 24hpf and 42hpf (17-42hpf paralysis), in comparison to motile controls (Figure 3.7 C). This implies that inhibition of movement causes significant lengthening of actin filaments in the developing skeletal muscle. Furthermore, 42hpf recovered embryos (17-24hpf paralysis followed by movement recovery) showed a complete rescue of actin length (Figure 3.7 C). This suggests that movement contributes to the regulation of actin filament length. However, it is also interesting to note that in embryos that remained paralysed throughout the experiment (17-42hpf), both mutant and paralysed embryos, showed a significant shortening in actin filament length between 24 and 42hpf. This indicates that an additional component of the mechanism regulating actin length is independent of movement.

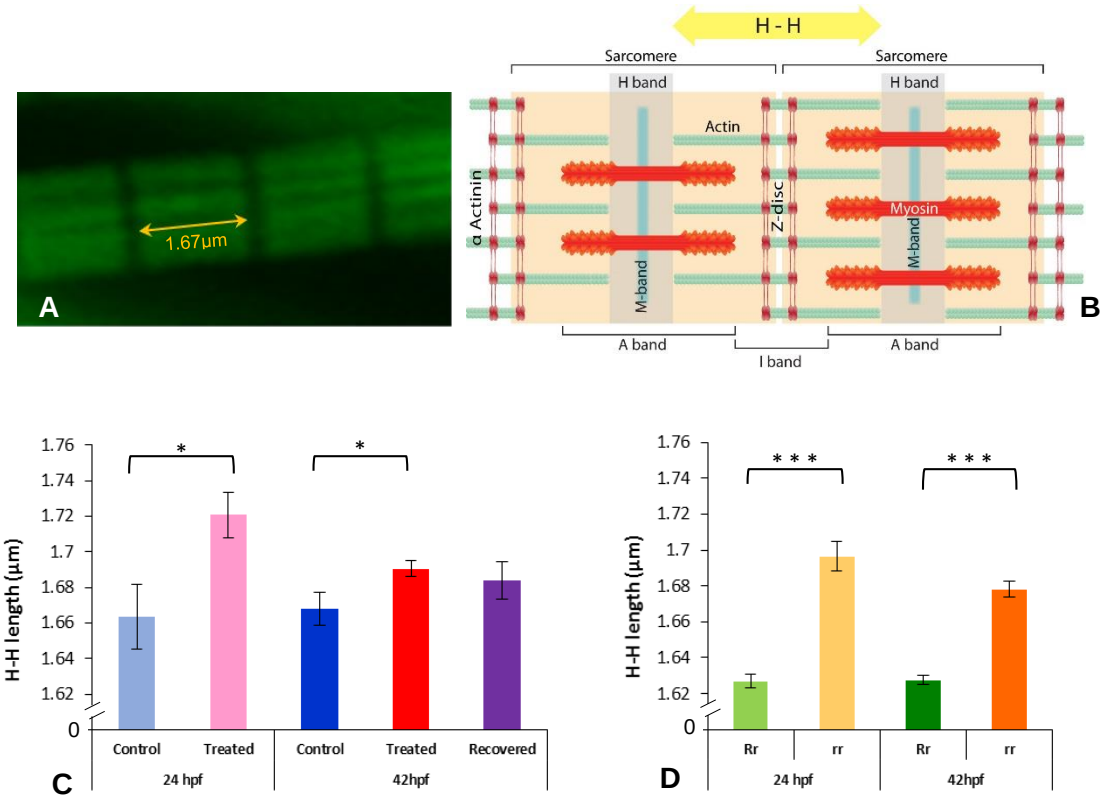

Figure 3.7: Paralysis leads to actin lengthening in both *relaxed* mutant and Tricaine treated embryos, subsequent movement restoration in recovered embryos leads to actin length complete rescue. [A&B] H-H measurement. Confocal images of actin filaments stained with phalloidin (1/40) were taken, measurement were made in between H bands, across Z discs and sarcomeres. **[C]** 17-24hpf paralysis caused a significant lengthening of actin filaments H-H at 24hpf (*p<0.05) (n=20 in 5 controls, n=15 in 3 treated embryos, t test). At 42hpf, recovered embryos (17-24hpf paralysis) showed a full recovery (n=50 in 10 control embryos, n=40 in 8 recovered embryos, unpaired t-test), in contrast with treated embryos (17-42hpf paralysis) which did not recover (n=50 in 10 control embryos, n=135 in 27 treated,*p<0.05). **[D]** Immotile *relaxed* mutants, rr, showed a very significant lengthening of actin filaments H-H at 24hpf (***p<0.001) (n=115 in 23 immotile *relaxed* mutants rr, n=120 in 24 motile carriers Rr) and at 42hpf (***p<0.001) (n=105 in 21 immotile *relaxed* mutants rr, n=135 in 27 motile carriers Rr). Interestingly, in contrast with the Tricaine treated immotile embryos, the immotile *relaxed* mutant (rr) actin is still very significantly longer than the motile carrier (Rr) actin at 42hpf. It is noticeable that in the complete absence of movement up to 42hpf actin filaments showed a significant shortening between 24 and 42hpf in between both treated and control embryos and immotile *relaxed* mutants and motile carriers respectively (n=15 in 3 24hpf treated, n=135 in 27 42hpf treated embryos, *p<0.05 unpaired t-test ; and n=115 in 23 24hpf immotile mutants rr, n=105 in 21 immotile *relaxed* mutants rr, *p<0.05 unpaired t-test).

In summary, in the absence of contraction, actin filaments elongate and therefore their length appears to be regulated via contraction. However, results also show that the paralysis-induced elongation of actin at 24hpf appears to partially recover by 42hpf, indicative of a regulatory component that occurs independently of contraction.

3.2.4 Paralysis selectively affects the localisation of the actin-capping protein Tropomodulin 1 but not Tropomodulin 4

Actin filament elongation was observed in immotile embryos and is likely to be controlled via capping proteins, specifically Tropomodulins (Tmod). Therefore the expression and localisation of Tmod1 and 4 in both *relaxed* mutant and pharmacologically treated embryos was assessed in immotile embryos. In control embryos, Tmod1 was located in the nucleus of skeletal muscle fibres prior to movement at 17hpf (Figure 3.8 A) but by 24hpf the distribution of the protein had changed, it had left the nucleus and migrated into the cytosol (Figure 3.8 B). By 42hpf the staining appeared punctate, linear and regularly arranged within the cytoplasm of the myofibrils themselves (Figure 3.8 C). In contrast to control embryos, Tricaine treated immotile embryos displayed nuclear localisation of Tmod1 at both 24hpf (Figure 3.8 D) and 42hpf (Figure 3.8 E) exclusively. Whereas in recovered motile embryos (Figure 3.8 F) at 42hpf, Tmod1 was found to be displayed in a similar cytosolic linear staining pattern to control embryos. In summary, prior to movement (initiated at 17hpf) and in immotile embryos (at 24 and 42hpf) Tmod1 staining is observed within the nucleus, whilst in motile embryos it is located in the cytoplasm of the myocytes. These observations were investigated further within the skeletal muscle of the immotile *relaxed* mutant line *cacnb1*^{ts25}. Carrier motile embryos already display cytosolic Tmod1 staining at 20hpf (Figure 3.8 G) which was conserved up to 42hpf (Figure 3.8 H) and was similar to the patterns observed in control and recovered motile embryos. Immotile *relaxed* mutant embryos display a nuclear localisation of Tmod1 at both 20hpf (Figure 3.8 I) and 42hpf (Figure 3.8 J), similar to that observed in Tricaine treated immotile embryos. In summary these results suggest that the relocation of Tmod1 from the nucleus to the cytoplasm of the myocytes is driven by embryonic movement in zebrafish.

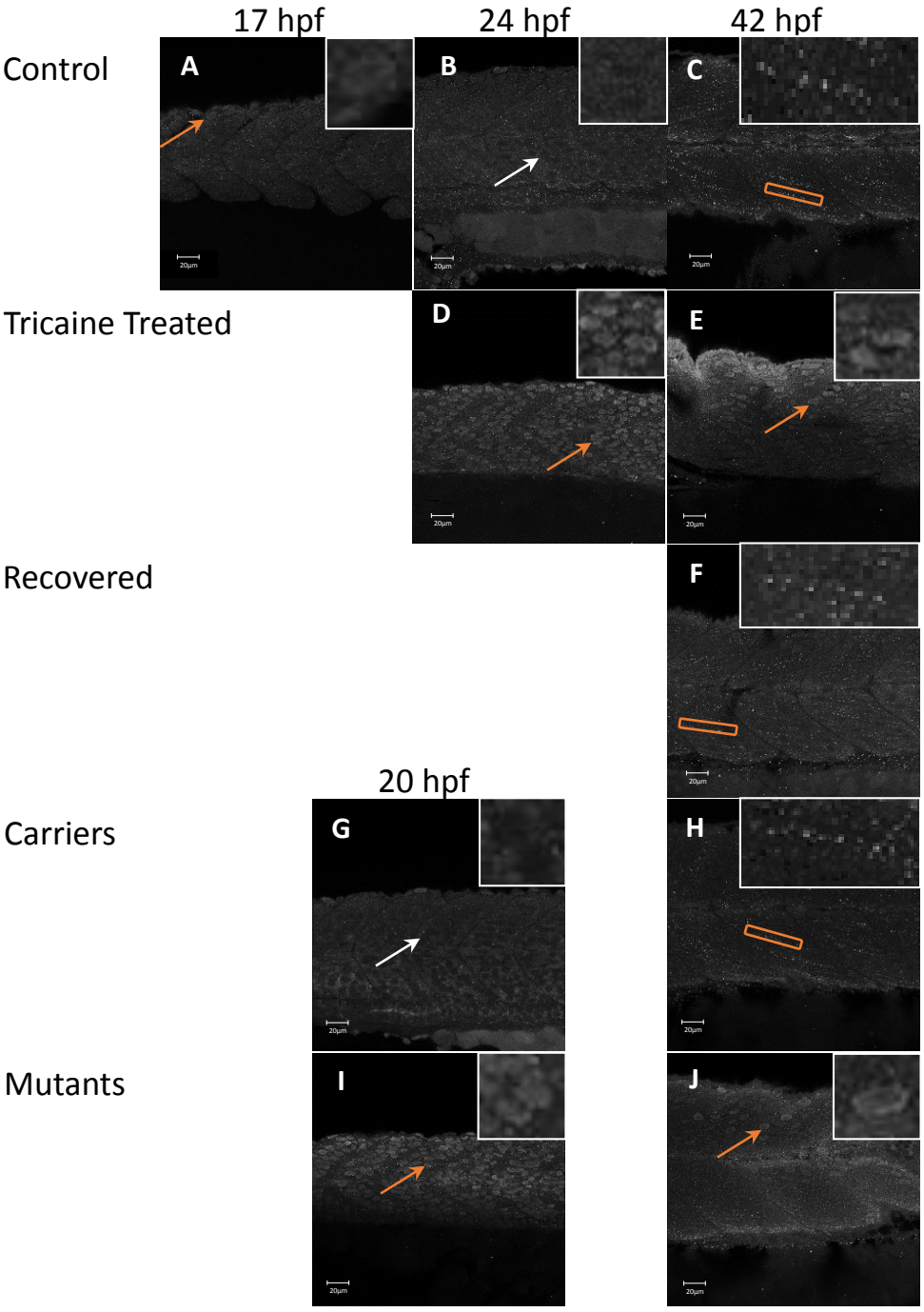

Figure 3.8: Tropomodulin 1 localisation within the fast skeletal muscle cell from 17hpf up to 42hpf in immotile and control embryos. In control embryos **[A,B,C]** Tmod1 is initially located in the nucleus of the skeletal muscle cell at 17hpf (orange arrow) **[A]** and then migrate into the skeletal muscle cell cytosol at 24hpf (empty nuclei, white arrow) **[B]** where it stays and get organised linearly by 42hpf (orange box) **[C]**. Tricaine treated immotile embryos **[D,E]** display a nuclear localisation of Tmod1 at both 24hpf **[D]** and 42hpf **[E]** (orange arrows). Recovered motile embryos **[F]** display at 42hpf a similar cytosolic linear pattern of Tmod1 as control embryos (orange box). Carrier motile embryos **[G,H]** display a cytosolic pattern of Tmod1 from 20hpf **[G]** (empty nuclei, white arrow) which is linearised by 42hpf **[H]** (orange box) as control and recovered embryos. Immotile relaxed mutants embryos **[I,J]** display a similar nuclear localisation of Tmod1 at both 20hpf **[I]** and 42hpf **[J]** as Tricaine treated embryos (orange arrows).

We then addressed the distribution of Tmod4 in both immotile models (Tricaine treated and *relaxed* mutant). In control embryos, Tmod4, is located initially in the nucleus of the muscle cell at 17hpf (Figure 3.9 A) but by 24hpf (Figure 3.9 B) the protein had left the

nucleus and appeared in a striated staining pattern within the cytosol of the myocytes, where it remained at 42hpf (Figure 3.9 C). In Tricaine treated immotile embryos, Tmod4 displays a cytosolic localisation from 24hpf onwards (Figure 3.9 D&E) and recovered motile embryos (Figure 3.9 F) also display cytosolic staining of Tmod4 at 42hpf. Both heterozygote motile and homozygote immotile *relaxed* embryos also display Tmod4 within the myocytes cytosol from 20hpf onwards (Figure 3.9 G-J). In summary, these results suggests that the relocation of Tmod4 from the nucleus to the cytoplasm of the myocytes is independent of embryonic movement.

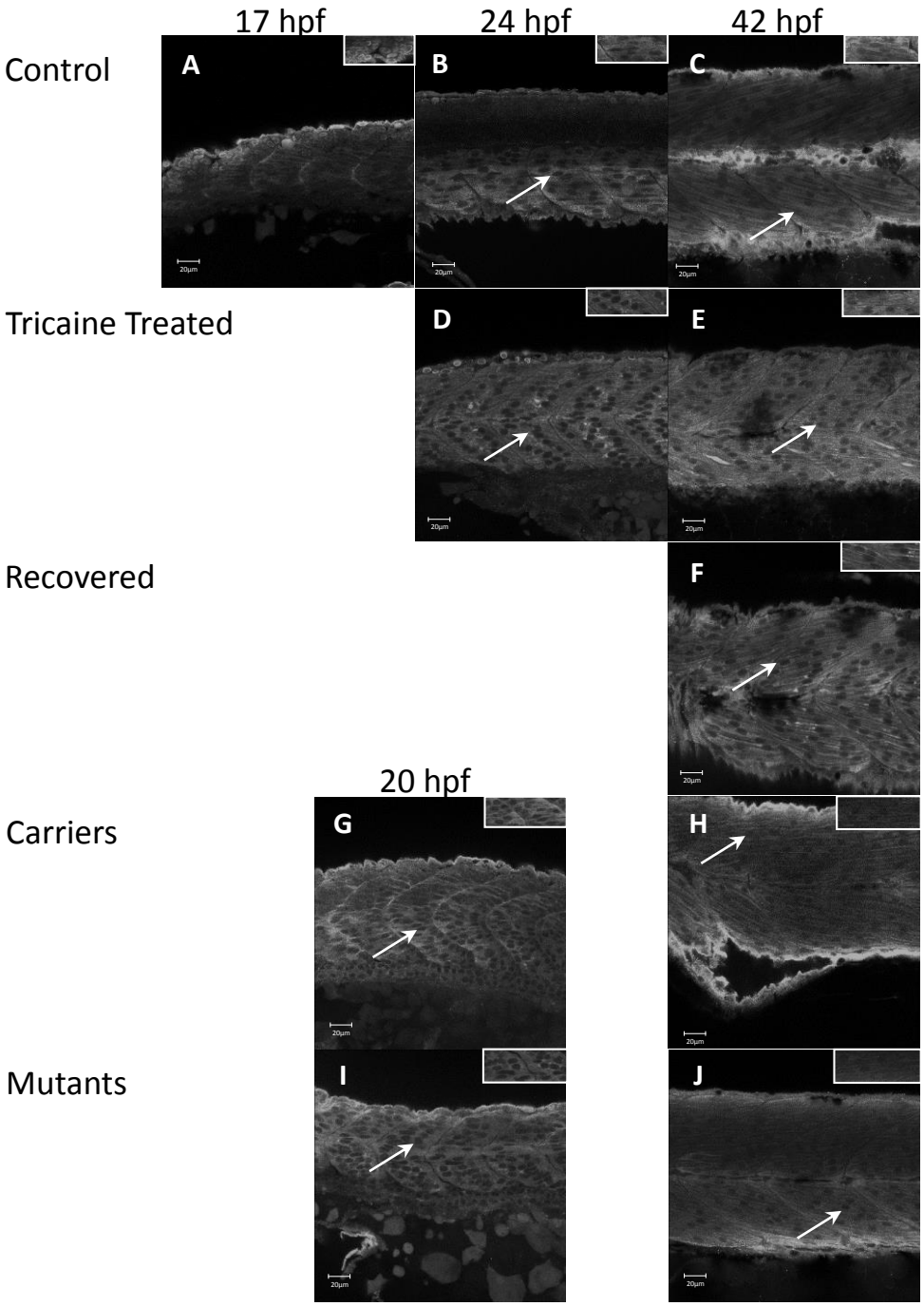

Figure 3.9: Tropomodulin 4 localisation within the fast skeletal muscle cell from 17hpf up to 42hpf in immotile and control embryos. In control embryos **[A,B,C]** Tmod4 is initially located in the nucleus of the skeletal muscle cell at 17hpf (orange arrow) **[A]** and then migrate into the

skeletal muscle cell cytosol at 24hpf **[B]** where it remains up to 42hpf (empty nuclei, white arrows) **[C]**. Tricaine treated immotile embryos **[D,E]** display a cytosolic localisation of Tmod4 at both 24hpf **[D]** and 42hpf **[E]** (empty nuclei, white arrows). Recovered motile embryos at 42hpf **[F]** display a similar cytosolic localisation of Tmod4 as control and Tricaine treated embryos (empty nuclei, white arrows). Carrier motile embryos **[G,H]** display a cytosolic localisation of Tmod4 from 20hpf **[G]** which is maintained up to 42hpf **[H]** (empty nuclei, white arrows). Immotile *relaxed* mutants embryos **[I,J]** display a similar cytosolic localisation of Tmod4 as carrier embryos at both 20hpf **[I]** and 42hpf **[J]** (empty nuclei, white arrows).

In summary, the results showed that during normal development Tmod1 and 4 are located in the nuclei of skeletal muscle cells, prior to the initiation of movement at 17hpf. After the onset of movement, at 24hpf and later at 42hpf Tmod1 and 4 are no longer concentrated at the nucleus but show a strong cytosolic expression in the developing skeletal muscle. Paralysis selectively affects the localisation of the actin-capping protein Tmod1, which is retained in the myocyte nuclei, rather than in the cytosol; this suggests that the initial contractile events drive the translocation of this actin-capping protein from the nucleus into the cytosol of the developing myofibrils. In contrast, the expression of Tmod4 was unaffected by paralysis and its cellular localisation is not dependent of movement.

3.3 Discussion

An experimental paradigm to explore how the restoration of contraction after paralysis affects myofibril organisation in developing zebrafish was established. Inhibition of contraction between 17 and 24hpf caused a significant increase in length and decrease in width of myofibrils. The restoration of contractile movement led to a full recovery of myofibril length but not width, whereas in the absence of movement myofibril width but not length fully recovered. Lattice spacing at the myofilament level was unaffected by both paralysis (*relaxed* mutants) and paralysis followed by recovery (Tricaine). In the absence of contraction, actin filaments were observed to elongate; however, the paralysis-induced elongation of actin at 24hpf was shown to recover by 42hpf. Examination of the capping proteins Tmod1 and 4 revealed localisation in the nuclei of skeletal muscle cells, prior to the initiation of movement at 17hpf. After the onset of movement at 24hpf, and later at 42hpf, Tmod1 and 4 are no longer concentrated at the nucleus but show a strong cytosolic expression. Paralysis selectively affects the localisation of the actin-capping protein Tmod1, which is retained in the myocyte nuclei, rather than in the cytosol. In contrast, the expression of Tmod4 was unaffected by paralysis and it underwent relocation from the nucleus to the cytosol. Overall, the results show that during zebrafish embryogenesis the later steps of myofibrillogenesis are regulated by a dual mechanism, of which only one is driven by movement.

(1) Movement-dependent regulation of myofibril assembly

In mature mammalian muscles, immobilised muscle has been shown to adapt by adjustment of sarcomere number and length, resulting in optimum overlap of myosin and actin filaments (Williams and Goldspink, 1978). These studies highlight the importance of these parameters for force generation in the muscles, which ultimately allows normal growth to occur (Williams and Goldspink, 1971). This process appears to be true for developing muscle as in zebrafish, immobility generates an increase myofibril length alongside shortening of sarcomeres and sarcomere addition (Brennan et al., 2005; Lahne et al., 2009). Evidence in avian (Kagawa et al., 2006), amphibian (Ramachandran et al., 2003) and cell culture (Soeno et al., 1999; De Deyne, 2000) studies, show that muscle contractility is required for sarcomere assembly. Indeed contraction has been proposed to be key during the later stages of myofibril assembly (Sparrow and Schöck, 2009). In this study inhibition of contraction between 17 and 24hpf causes a significant increase in myofibril length, as shown previously (Brennan et al., 2005), furthermore the restoration of movement leads to a full recovery. This later work is the first direct evidence that the restoration of movement regulates myofibril length *in vivo*.

Actin is a key protein of the sarcomere thin filaments, which allow the spring like action necessary for force transmission along the myofibrils. In this study, results revealed that in the absence of contraction actin filaments elongate and therefore their length appears to be regulated via contraction. This data fits with our observations at the myofibril level and suggests that movement-induced regulation of actin polymerisation and thin filament length may be an underlying factor of myofibril organisation, namely elongation during development. Previous work has shown that myofilaments and sarcomere length are disrupted by paralysis (Etard et al., 2005) and our observations of actin lengthening during paralysis are consistent with this idea.

Actin length regulation was examined by assessing the effect of paralysis on Tmod1 and 4 localisation. Tmod1 and 4 are actin-capping proteins that promote polymerisation and depolymerisation (Littlefield and Fowler, 2008). Tmod1 has been shown to regulate actin filament length in mice (Gokhin et al., 2014). It's over expression leads to a decrease in actin incorporation and shortening, whilst it's under expression has the reverse effect (Gokhin and Fowler, 2011). It is argued that its normal role in muscle fibres is to control length by inhibiting polymerisation and lengthening of filaments. We observed an initial expression of Tmod1 in the nuclei of the muscle cells and subsequent movement-dependent translocation to the cytosol. Contraction-driven movement in different cellular compartments has been demonstrated for other sarcomeric proteins (Lange et al., 2006; Clark et al., 2002). Furthermore, in immotile embryos Tmod1 is absent from the cytosol

and this correlates with a significant lengthening of actin filaments. Taken together these observations suggest that the absence of movement and the lack of Tmod1 in the cytosol results in elongation of actin filaments. In conclusion, Tmod1 appears to act to limit contraction-driven actin regulation during sarcomere maturation. Furthermore, Tmod1 is directly involved in skeletal muscle contractility regulation by enhancing actomyosin crossbridge formation (Ochala et al., 2014), thus creating a positive feedback loop: contractility leading to Tmod1 localisation and Tmod1 regulating contractility.

Tmod4, shows an early nuclei localisation followed by translocation into the cytosol, which occurs simultaneously with Tmod1. The expression of Tmod4 was unaffected by paralysis and its cellular localisation is not dependent of movement. However, although Tmod4 is not regulated by contraction, its translocation still occurs concurrently with Tmod1, which suggests that another signal induces its transfer at this specific developmental stage. Therefore the shortening of actin observed between 24 and 42hpf in immotile embryos is very likely to be the result of the regulating action of Tmod4, as in these embryosTmod1 is missing at the actin pointed ends. In contrast, actin shortening in the motile recovered embryos can be attributed to both Tmod1 and Tmod4, which are capping actin pointed ends. This could explain why the recovered embryos are the only one to restore actin length to its normal size, suggesting that both Tmod1 and 4 are required to complete this process.

This study showed that during normal zebrafish skeletal muscle development, Tmod1 and 4 are located in the nuclei of skeletal muscle cells prior to the onset of movement at 17hpf. The nuclear transport of Tmod was described previously in mammals and suspected to be a conserved phenomenon across species (Kong and Kedes, 2004; Kong and Kedes, 2006). Our data in zebrafish suggests indeed that the transport of Tmod to the nucleus may be conserved at least in vertebrates. This initial nuclear localisation could indicate additional roles for Tmod in the myocyte; for example, they might be interacting with actin filaments in this location. Nuclear Tmod has also been proposed to have a role in the regulation of proliferation and differentiation processes in skeletal muscle cells (Kong and Kedes, 2004). Similar interactions have been described in cardiac muscle where tropomodulins are associated at the plasma membrane before they locate to the sarcomeres (Ehler et al., 2004; Chu et al., 2003). Tropomodulins, by controlling actin length, ultimately control the regular array of sarcomeres within the skeletal muscle myofibrils, leading to proper myofibril organisation.

(2) Movement-independent regulation of myofibril assembly

The results showed that inhibition of contraction between 17 and 24hpf causes a significant decrease in width of the myofibrils; however, over time the data revealed that recovery occurs independently of movement. This finding indicates that, from 24hpf onwards, there is also a movement-independent mechanism that regulates myofibril width during zebrafish embryonic skeletal muscle development. This hypothesis of a myofibril regulation mechanism independent of movement is supported by previous study in our laboratory that showed that the disruption of myofibril organisation in chemically paralysed embryos was milder when the drug was applied at later developmental stages (Lahne et al., 2009) (Chapter 1 Figure 1.10). These milder phenotypes could be due to the fact that when the drug was applied later during development, the 17-24hpf contractile development event had occurred preventing myofibril disorganisation. If the 17-24hpf contractile development event is the only event regulating myofibril organisation, the later phenotypes should show a similar level of disruption. However, this is not the case as the later the drug is applied the milder the phenotype, suggestive of movement independent myofibril organisation regulatory mechanisms that appear from 24hpf onwards and counterbalancing the immobility-induced myofibril disruption. It is most likely that myofibril organisation is regulated by a combination of both contraction and contractile independent mechanisms.

At the myofilament level, the lattice spacing was found to be regulated independently of movement. Results also show that the paralysis-induced elongation of actin at 24hpf appears to partially recover by 42hpf, indicative of a regulatory component that occurs independently of contraction. These findings support the observations of the myofibril width recovery, which is also independent of movement. Furthermore, the X-ray data indicates that by 6dpf, myofilaments lattice spacing is not disrupted by paralysis. It is assembled and allows attaching of cross bridges even in immotile *relaxed* mutants which do reach rigor state in the presence of cyanide. A possible mechanism could involve the filament protein Desmin which wraps around the Z-disc thus stabilising this structure, as proposed in Costa et al., 2004 review. Although the expression of Desmin in zebrafish embryos has not been shown, its emerging presence from 24hpf onwards may be one of the factors that prevents paralysis-induced disruption via the stabilisation of the sarcomeric structure. Further work could include Desmin labelling throughout embryogenesis to identify the onset of its expression in skeletal muscle. This demonstrates that the actin and myosin myofilament lattice spacing is regulated independently of movement, as is myofibril bundling.

3.4 Conclusion

These observations suggest that myofibril organisation is regulated by a dual mechanism involving movement-dependent and movement-independent processes. The initial contractile event itself drives the localisation of Tmod1 to its sarcomeric position, capping the actin pointed ends, ultimately regulating actin length. This process is an underlying factor of myofibril length regulation and contributes to myofibril organisation, which is necessary for establishing proper skeletal muscle structure and function during development *in vivo* in zebrafish. However, our study also revealed that contraction is not the only driver of myofibril organisation, additional mechanisms independent of movement are involved in other aspects of myofibril organisation, namely myofibril bundling. Movement independent processes are also observed at the myofilament level with the movement independent assembly of the myofilament lattice, and the translocation of Tmod4 into its actin capping position allowing some actin length regulation to occur even in immotile embryos.

3.5 Future work

The ‘two segment model for thin filament architecture’ (Gokhin and Fowler, 2013) is based on the action of tropomodulins, another capping protein, CapZ, and the ruler protein nebulin. This zebrafish tropomodulin study would be enhanced by the analysis of both CapZ and nebulin. Antibodies raised against fish nebulin were tested in 24 and 48hpf zebrafish, but no staining was observed, suggesting a lack of specificity. Antibodies raised against CapZ are also available but have not been tested in zebrafish to date. This part of the project would benefit from improved access to zebrafish specific antibodies raised against sarcomeric proteins.

Tmod4 translocation from the nucleus to the cytosol occurs at the same time as Tmod1 and it is shown to be independent of movement. The mechanism that drives Tmod4 relocation to the cytosol is unknown but the data from this study suggests that it is an important developmental step in the organisation of actin myofilaments. The contribution of Tmod4 could be investigated by inhibiting expression of the protein (either by knock-down or knock-out studies). These models would allow the investigation of Tmod1 alone and enable the assessment of the relative importance of the mechanisms that drive both Tmod1 and Tmod4 translocation on myofilament organisation. It would also further test our finding that Tmod1 and 4 are required for the actin length to be established correctly in vivo. A further complication is the functional equivalence of Tmod4 and Lmod3 during sarcomere assembly (Nworu et al., 2015), therefore investigating the nuclear transport of Lmod3 as well as Tmod4 would provide a better insight into the mechanism that drives

Tmod4 relocation. Ultimately, this work would improve our understanding of the importance of mechanotransduction versus an alternative developmental event on actin regulation and myofibril organisation. In mature muscle (as in other tissues) function rather than form, is a critical evolutionary determinant (Russell et al., 2000). These studies would also establish to what extent form follows function during skeletal muscle development.

We have established that movement is a driver of myofilament and myofibril elongation ultimately allowing the correct patterning of the skeletal muscle and muscle function. Determining how the muscle cells senses the mechanical stretch signals and establishing which mechanotransduction pathways are involved is crucial. The involvement of Fak and Src proteins of the focal adhesion complexes of costameres and myotendinous junction, structures known as tension sensors, will be investigated in the next chapter.

CHAPTER 4

THE ROLE OF FOCAL ADHESION COMPLEXES (FAC) IN MECHANOTRANSDUCTION-DRIVEN MYOFIBRIL ORGANISATION

4. The role of Focal Adhesion Complexes (FAC) in mechanotransduction-driven myofibril organisation

4.1 Introduction

Mechanotransduction, the translation of external mechanical signals into cellular chemical signals, is already known to play a key role in maintaining the structure of mature striated muscle (Boonyarom and Inui, 2006). In zebrafish, previous work has shown that the inhibition of the excitation-contraction pathway disrupts both sarcomere and myofibril length (Brennan et al., 2005). This suggests that intrinsic contractile activity contributes to the maintenance of the skeletal muscle fibres structure. This study has established that a contraction-driven myofibril organisation pathway exists during zebrafish development (Chapter 3). However, the contraction-driven signals that regulate the cytoskeletal architecture within the developing muscle fibre (i.e. myofibril formation) are not well defined. The contractile event itself has been proposed as the primary regulator of myofibril length regulation during embryogenesis *in vivo,* i.e. movement rather than Ca^{2+} signalling is necessary for myofibril organisation (Lahne et al., 2009) (Chapter 3). The components of the mechanotransduction pathway that contribute to skeletal muscle development remain undefined and will be investigated in this chapter.

In mature skeletal muscle, mechanical force and regulatory signals are sensed and transmitted from the extracellular matrix into the cell interior (cytoplasm) via specialist transmembrane linkages, myotendinous junctions and costameres, which connect the sarcolemma with the cytoskeleton (as reviewed in Clark et al., 2002). These linkages are made up from membrane/cytoskeletal junctions, large macromolecular complexes, one of which is the integrin-based focal adhesion complex (FAC) (Figure 4.1). The FAC integrin transmembrane receptors physically connects the actin cytoskeleton of the cells to the ECM at focal adhesions, and thus, mediates migration and adhesion in many cells (as reviewed in Turner, 2000 and Schwartz, 2001). The role of mechanotransduction in skeletal muscle development will be explored by examining the expression and role of identified proteins of FAC.

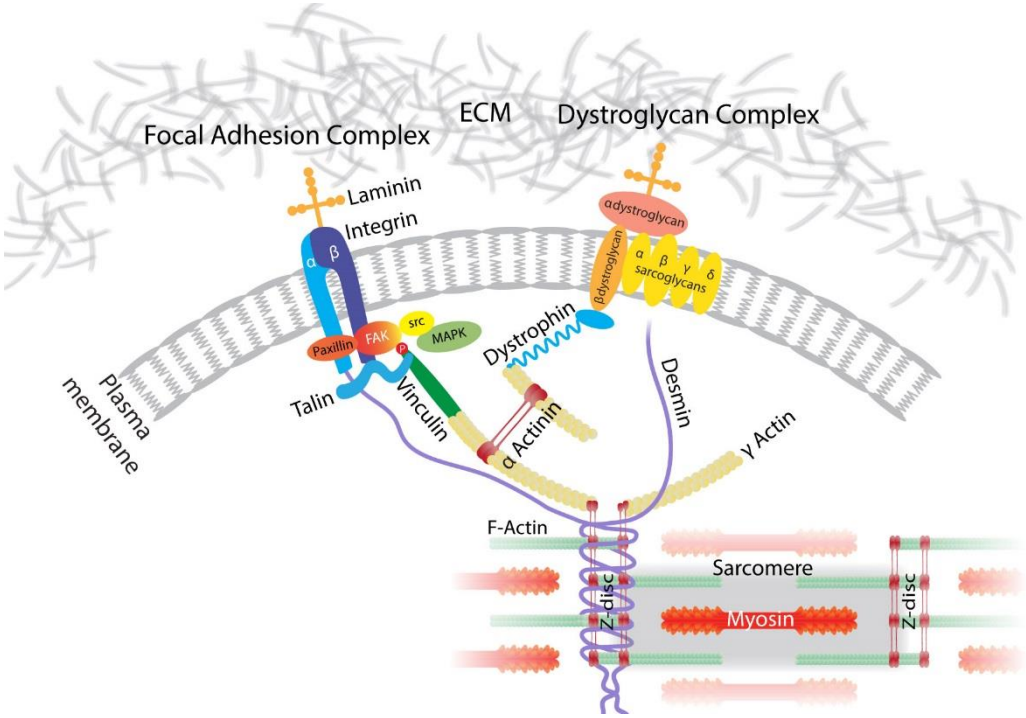

Figure 4.1: Schematic representation of a costamere. Two laminin receptors, a dystroglycan complex and focal adhesion complex (integrin receptor complex) are among the sarcolemmal structures (Pardo et al., 1983) that link the contractile apparatus of muscle fibres with the surrounding basal lamina. Components of both receptors, i.e. both dystrophin and the integrin-associated cytoskeletal proteins (talin, vinculin, α-actin), co-localise in subsarcolemmal complexes (Pardo et al., 1983) which connect through γ-actin and the intermediate-filament proteins desmin to the Z-disk of skeletal muscle fibres (Patel and Lieber, 1997); (Rybakova et al., 2000).

It was proposed that the mechanosensitive FACs are the structures through which contraction regulates myofibril organisation, specifically length, within skeletal muscle. FAC are known to have key roles in responding to external and internal forces by changing their size and signalling activity (Wolfenson et al., 2011). Over 50 different proteins reportedly localise to FAC, they are arranged by function, and include cytoskeletal proteins (e.g. vinculin, paxillin), tyrosine kinases (e.g. Fak, Src*)* and other enzyme groups (Zamir and Geiger, 2001*)*. In this study, we focused on the role of non-receptor tyrosine kinases already known to be implicated in mechanotransduction, namely focal adhesion kinase (Fak) and the protein kinase Src.

4.1.1 Focal adhesion kinase (Fak)

Fak is a 120kDa protein, non-receptor tyrosine kinase that binds paxillin. As well as its scaffolding properties, Fak plays a role in the phosphorylation of many proteins within the FAC. Integrin-mediated Fak autophosphorylation of its Tyr^{397} site generates a binding site for Src, which in turn phosphorylates a number of other tyrosine residues on Fak (Figure 4.2). Consequently, the phosphorylation state of Tyr^{397} is considered indicative of Fak's activity. There is also evidence that Fak, located on the sarcolemma, is involved

in sensing and transducing the mechanical forces in skeletal muscle. Durieux et al. have shown in mammalian cells (mouse) that Fak becomes activated and Tyr^{397} is phosphorylated, after cells have been submitted to mechanical loads (Durieux et al., 2009). Further study by Flück et al. highlighted Fak's preferential localisation at myotendinous junctions and costameres, important sites of mechanotransduction (Fluck et al., 1999). Furthermore, Fak knockout mice embryos die with mesodermal defects at a very early developmental stage (E8.5, 14-16 pairs of somites) illustrating the importance of Fak in early development (Furuta et al., 1995).

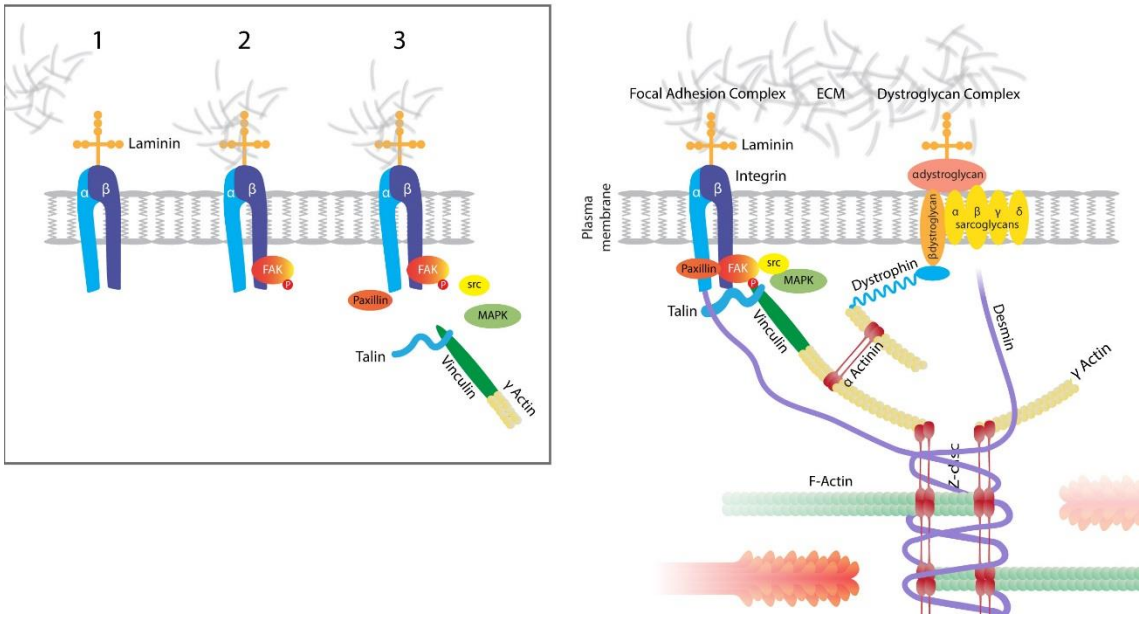

Figure 4.2: Schematic representation of the focal adhesion complex (FAC). Integrin-based FACs bridge cortical γ-actin to the extracellular matrix (ECM). Integrin in the sarcolemma of the muscle fibre acts as an anchor for the actin fibres in the sarcomere. Actin is bound to vinculin, which is then attached to the integrin β-subunit through focal adhesion kinase (Fak).The inset indicates schematically the proposed involvement of Fak in the formation of FACs. Occupancy of integrins with ECM ligand (1) causes phosphorylation (red circle) of integrin-associated Fak (2) which, in turn, promotes recruitment of both cytoskeletal (paxillin, vinculin, talin and γ-actin) and signalling molecules (e.g. MAPK and Src kinase) to integrins (3) (Miyamoto et al., 1995; Durieux et al., 2009)**.** Adapted from Fluck et al., 2002.

Fak is involved in integrin mediated phosphorylation signalling cascades and many of its domains are highly conserved in between species (Figure 4.3). However, as a result of the teleost genome duplication, zebrafish has two *fak* genes and divergent Fak proteins (Jaillon et al., 2004), *fak1a* is segmentally expressed in somites throughout the embryogenesis and *fak1b* is expressed ubiquitously as the dominant isoform during early development (Crawford et al., 2003).

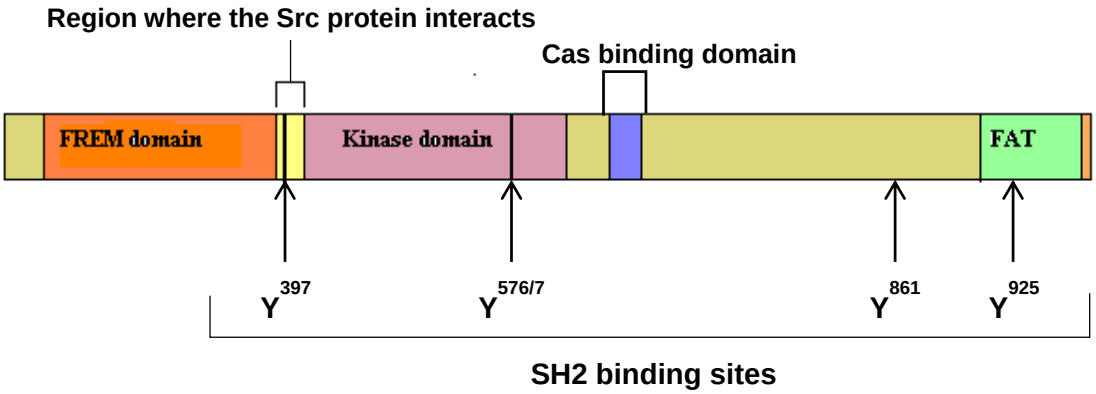

Figure 4.3: Diagram showing the main conserved regions of the focal adhesion kinase. The amino acid sequence of zebrafish *fak1b* is 69% identical compared with zebrafish *fak1a* or with human *FAK1*. The kinase domain is very highly conserved being 94% identical to zebrafish *fak1a* and 93% identical to human *FAK1*. The focal adhesion-targeting domain (FAT) of zebrafish *fak1b* is also highly conserved, 93% with zebrafish *fak1a* and 92% with human *FAK1*. The proline-rich Cas binding domain (amino acids 714–724) is identical between all three *FAK* sequences. The FERM2 phosphotyrosine binding domain, NYFY at amino acids 144–147, is identical for *fak1a* and *fak1b* and similar to *Hum FAK* (NFFY) (Garcia-Alvarez et al., 2003). Of importance, is that the SH2 binding sites surrounding Tyr^{397} and Try^{925} are identical for zebrafish *fak1a, fak1b*, and human *FAK1* and that the SH2 binding sites for $Tyr^{576/7}$ and Tyr^{861} are identical except for a few conservative changes. Although the SH2 binding sites are similar for the zebrafish and human FAK proteins, there are significant differences between them and the SH2 binding sites of human FAK. Those areas that differ most significantly between zebrafish *fak1a, fak1b*, and human *FAK* are the N-terminal ends, two areas of the FERM3 domain, and the areas between the proline-rich Cas binding domain and the FAT domain. These areas are not usually conserved between species. Zebrafish *fak1b* maps to linkage group 19 (LG19), which is a duplicate of LG 16 containing *fak1a* (see AAK31154 and AY196213). Both LG19 and LG16 share syntenies with the distal tip of human chromosome 8, the site of the human *FAK* locus. (Diagram modified from Crawford et al., 2003). (Furuta et al., 1995).

Furthermore, in mammals, Fak is essential to mesodermal development (Furuta et al., 1995), and has been localised at sites of strong cell-ECM adhesion in embryos. In *Xenopus* and mouse embryos Fak was shown to be prominent at somite borders and in the brain (Hens and DeSimone, 1995; Polte et al., 1994). In early zebrafish development, at the time of gastrulation (5hpf) Fak Tyr^{397}residue, localised within SH2 binding site of Fak, is increasingly phosphorylated, indicative of Fak activation allowing a strong adhesion between the cell and the extracellular matrix. At 24hpf phosphorylated Fak is found at the somite boundaries where it mediates their stabilisation, and in a ring like pattern connecting the notochord to its peripheral sheath (Figure 4.4). Also, it is noticeable that during somitogenesis, the abundance of *fak1a* increases (Henry et al., 2001; Crawford et al., 2003).

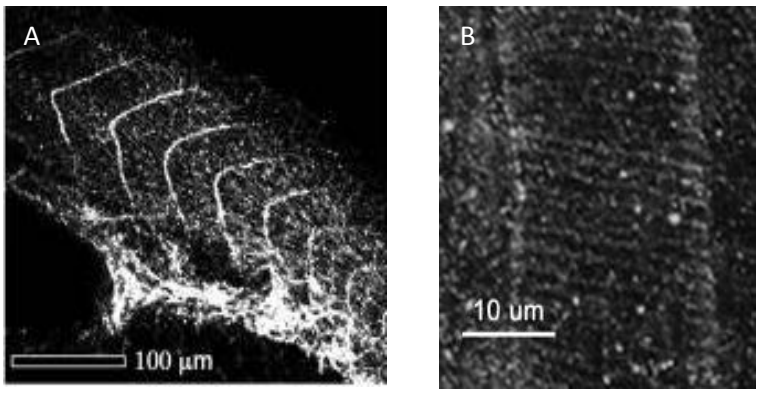

Figure 4.4: Phosphorylated Fak are concentrated at somite boundaries and in the notochord, at sites of cell-matrix adhesion. [A] Lateral views of 24hpf embryos stained with anti-pY^{861}Fak shows somite boundaries (dorsal up). **[B]** Projection of confocal sections of the notochord of a 24hpf embryo stained with anti-pY^{861}Fak shows circumferential striations (anterior up, dorsal to the right). Adapted from Crawford et al.,2003.

As stated previously, work in this chapter is aimed at exploring the role of mechanotransduction in skeletal muscle development by identifying the components of the FAC components implicated in the regulation of myofibril organisation *in vivo,* using the zebrafish as a model. Fak meets several of these criteria as it (i) is an important component of the focal adhesion complex, (ii) is involved in signalling between the extracellular matrix and the cytoskeleton and (iii) is expressed in early zebrafish development.

4.1.2 Src protein

Src, a tyrosine kinase, was also examined, because of its key role in Fak phosphorylation. Src kinases are a family of non-receptor kinases, responsible for the phosphorylation of tyrosine residues on many molecules. The Src kinase family consists of nine members: Src, Yes, Fyn, Fgr, Lck, Hck, Blk, Lyn and Frk (Koegl et al., 1994). Src kinases have been shown to be involved in B-cell antigen receptors, cell adhesion, cell motility and morphology, bone reabsorption and focal adhesion complexes (FAC) (Kurosaki et al., 1994; Roskoski, 2004). The Src family proteins have a conserved domain organisation which is very important for the Src function (Figure 4.5). The SH3 and SH2 domains are the binding sequences of the protein. The SH2 domain binds to pYEEI protein sequences in the target protein. The SH3 domain binds to a left handed helical motif in target proteins, this is due to a rich proline sequence usually found in the helical motif. The SH3 binding affinity is less sequence specific, this is due to the secondary structure, the left handed helix, of the protein. Src is found to phosphorylate several components in the focal adhesion complexes of muscle fibres, which suggests an important role for this protein in skeletal muscle.

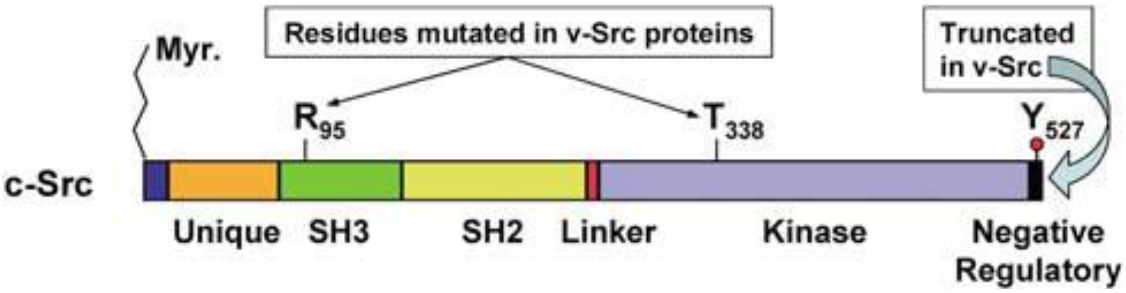

Figure 4.5: Domain Structure of Src family kinases. Members of the Src family exhibit a conserved domain organisation, which includes a myristoylated N-terminal segment, followed by SH3, SH2, linker and tyrosine kinase domains, and a short C-terminal tail. Src activity is regulated by intramolecular interactions controlled by tyrosine phosphorylation, SH2 and SH3 domains mediate protein–protein interactions with sequences containing phosphotyrosine and proline-rich motifs. Adapted from Parsons and Parsons, 2004.

Unlike Fak, the localisation and role of Src has not been explored to any great extent in skeletal muscle, nor in zebrafish development and it is not currently known whether it is involved in mechanotransduction. The relevance of Src protein in zebrafish skeletal muscle development was therefore explored.

Hypothesis: Fak and Src proteins are known to be involved in mechanosensing processes in mammals. However, their role in zebrafish muscle development is unclear. This chapter has explored the proposal that Fak and Src proteins are involved in the mechanotransduction pathway driving myofibril organisation in zebrafish. Fak is already known to be expressed in zebrafish embryos (Crawford et al., 2003), in this study its expression levels were assessed in both motile and immotile embryos in order to evaluate its involvement in mechanosensing. In contrast, Src expression remains undocumented in zebrafish, therefore its expression pattern and its mechanosensing role was established in immotile versus motile embryos.

4.2 Results

The role of Fak in contraction-driven muscle development was initially addressed by examining its developmental expression levels in motile versus immotile zebrafish embryos. This study will characterise changes of *fak* expression levels in the *relaxed* mutant line compared to wildtype controls. These observations will allow us to test specific hypotheses about the function of Fak, in the mechanosensitive pathway driving myofibril organisation and movement (Stickney et al., 2000).

4.2.1 *fak* expression levels in *relaxed* mutants vs. controls, preliminary study

The first aim was to determine whether there was a difference in *fak* expression levels in between motile controls and immotile *relaxed* mutant embryos. A preliminary study

investigated the expression of *fak1a*, *fak1b* and *βactin* using RTPCR, in both homozygotes *relaxed* mutants and heterozygotes controls at 24hpf, as well as in wild type total RNA (Figure 4.6).

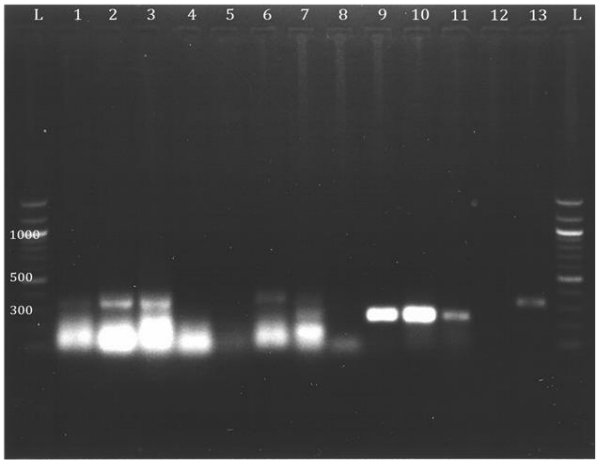

Figure 4.6: RTPCR of *fak1a*, *fak1b* and *βactin* in homozygote *relaxed* mutant, heterozygotes control and wildtype 24hpf whole embryo. L: Ladder 100bp, **1**: *fak1a* – relaxed mutant, **2**: *fak1a* – heterozygote control, **3**: *fak1a* – wildtype total RNA, **4**: *fak1a* – DEPC H2O, **5**: *fak1b* – *relaxed* mutant, **6**: *fak1b* – heterozygote 'normal', 7: *fak1b* – wildtype total RNA, **8**: *fak1b* – DEPC H2O, **9**: *βactin* – *relaxed* mutant, **10**: *βactin* – heterozygote control, **11**: *βactin* – wildtype total RNA, 12: *βactin* – DEPC H2O, **13**: kit positive control. (*fak1a*: 353bp, *fak1b:*346bp, *βactin:* 238bp)

We found that *fak1a* is expressed at a very low level in homozygotes *relaxed* mutants, but is found strongly expressed in both heterozygotes controls and in wildtype total RNA, the negative control is clear. *fak1b* is not expressed in homozygotes *relaxed* mutants, and very low levels of expression are observed in both heterozygotes controls and in wildtype total RNA, the negative control is clear. Finally, our housekeeping gene, *β-actin*, is strongly expressed in both homozygotes *relaxed* mutant and heterozygotes controls, a little less in wildtype total RNA, the negative control is clear. The positive control provided by the kit is positive.

In summary, differences in *fak1a* and *fak1b* expression were observed in between immotile *relaxed* mutants and their controls.

4.2.2 At 24hpf, the levels of *fak* expression are comparable in immotile *relaxed* mutants and motile wildtype embryos

The RTPCR pilot study pointed to differences between *fak* expression in the immotile *relaxed* mutant compared to controls. These findings were explored further, variations in the *fak1a* and *fak1b* gene expression within immotile *relaxed* mutant embryos versus wildtype and motile *relaxed* carriers were assessed using qRTPCR at 24hpf. This is one of the most powerful and sensitive gene analysis techniques available. It measures PCR amplification as it occurs, rather than to collect the results once the reaction is complete as in traditional PCR, this allows determination of the starting concentration of nucleic

acid. In addition to *fak1a* and *fak1b* we also analysed the expression of *foxm1* a human proto-oncogene known to play a key role in human embryonic development (Teh et al., 2002). The *foxm1* gene was included as a qRTPCR control as the conditions of the qRTPCR for this gene have already been defined. Furthermore, *foxm1* is a transcription factor expressed mainly in epidermal cells and unlikely to be found at high levels in skeletal muscle. Therefore, we assumed that *foxm1* gene expression will not be affected by paralysis and will remain at a constant level within the three genotypes, acting as a positive control of the technique. In addition, zebrafish *GAPDH* and *βActin* genes were used as reference housekeeping genes for quantification of *fak1a, fak1b* and *foxm1* mRNA levels. The data showed that at 24hpf, there is no significant difference in *fak1a, fak1b* and *foxm1* expression levels in between the three genotypes (immotile *relaxed* mutants, motile *relaxed* carriers and wildtypes embryos) (Figure 4.7).

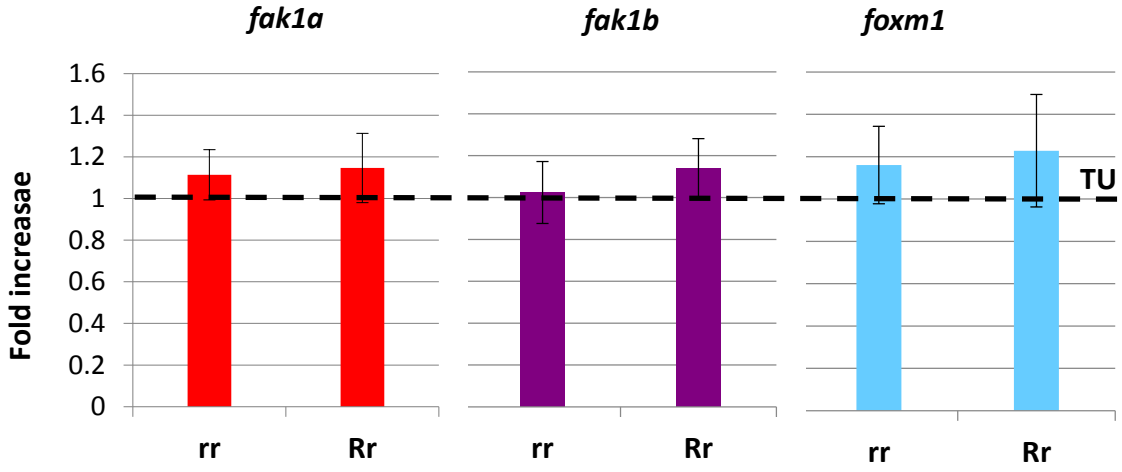

Figure 4.7: *fak1a, fak1b* and *foxm1* expression levels in the immotile *relaxed* mutant cacnb1^{ts25-}/cacnb1^{ts25-} (rr) and the motile *relaxed* carrier *cacnb1^{ts25+}/cacnb1^{ts25-}* (Rr) do not differ from wildtype (TU) at 24hpf. Expression of *fak1a, fak1b* and *foxm1*, in immotile *relaxed* mutant cacnb1^{ts25-}/cacnb1^{ts25-} (rr) and motile *relaxed* carrier *cacnb1^{ts25+}/cacnb1^{ts25-}* (Rr) embryos is shown as fold increase compared to gene expression in wildtype embryos (TU) at 24hpf. A dotted line indicates where the fold increase is one and no differential expression exists between the immotile *relaxed* mutant (rr), the motile *relaxed* carrier (Rr) and the wildtype (TU) at 24hpf. RNA extracted from whole embryos.(Mean ±SEM, *fak1a* rr n=7, Rr n=7, TU n=9, p=0.6917 ; *fak1b* rr n=11, Rr n=7, TU n=11, p=0.7733 and *foxm1* rr n=7, Rr n=10, TU n=10, p=0.7560, ANOVA).

4.2.3 *fak* expression patterns are comparable throughout development in immotile *relaxed* mutants and motile wildtype zebrafish

Initially, Fak was proposed to be involved in mechanotransduction during the 17-24hpf contractile development event in zebrafish, and its expression levels thought to be movement dependent. However, as demonstrated in the previous section, no differential expression of *fak1a* and *fak1b* in the absence of movement was observed at 24hpf. Evidence from mammalian studies suggests that Fak is involved with mechanotransduction signalling in skeletal muscle and these initial results suggest that the role of Fak in zebrafish is different to that in mammals. This is based on observations

from one early time point and did not take into account the fact that *fak* expression levels may be affected later during development. Therefore, the expression of the *fak* genes was determined at later developmental stages, specifically 24hpf, 48hpf, 72hpf and 96hpf.

Firstly, the expression of endogenous *foxm1*, an important factor in mitotic division, was assessed. As development progressed and cell division rate decreased, *foxm1* expression showed an extremely significant decrease for the three genotypes as expected (Figure 4.8 A, B, C). Although all three genotypes exhibit the same pattern of *foxm1* expression throughout development it is interesting to notice that at 96hpf the immotile *relaxed* mutant display a significant decrease compared to both its motile *relaxed* carrier siblings and the wildtypes. It is also important to note that for both motile genotypes, carriers and wildtypes, the level of expression of *foxm1* are similar at 96hpf (Figure 4.8 D). This difference possibly reflects a slowing down of mitotic division rate in the immotile *relaxed* mutant (Appendix D).

Using in situ hybridization, Crawford et al. has shown that in zebrafish embryos *fak1b* is initially expressed ubiquitously whereas *fak1a* is expressed much more specifically later in developing skeletal muscle (Crawford et al., 2003). Therefore, in this study the mRNA levels of *fak1a* and *fak1b* were predicted to reflect the spatial expression described in these in situ studies. Specifically, the low level of *fak1a* expression observed in the early phases of development will increase and that the high level of *fak1b* expression will decrease. Results showed that between 24 and 96hpf, the level of *fak1a* expression significantly increased in wildtypes (Figure 4.8 F) but not in *relaxed* mutants and carriers embryos. At 96hpf the level of expression was found to be similar in immotile *relaxed* mutant compared to motile carrier but was significantly down regulated compared to wildtype embryos (Figure 4.8 D, E). Finally, the overall level of *fak1a* expression in the motile carrier appeared lower than both its sibling's immotile *relaxed* mutants and the wildtypes (Figure 4.8 E), but this was only found to be significantly different when compared to the wildtype at 96hpf. These results are in contrast with the pilot study and the drawbacks of using RTPCR against qRTPCR are discussed in Appendix B. Furthermore, it should be noted that in both the immotile *relaxed* mutants and the motile carriers, wide variations in the expression levels of *fak1a* were observed and this made statistical comparisons difficult (Figure 4.8 D, G). Considerations about the use of heterozygotes against wildtypes embryos as controls in molecular studies are examined in Appendix B. The levels of *fak1b* expression were compared over the four developmental time points and were found to be the same and to decrease in a significant manner in the wildtype, motile carrier, and immotile *relaxed* mutants (Figure 4.8 H, I, J).

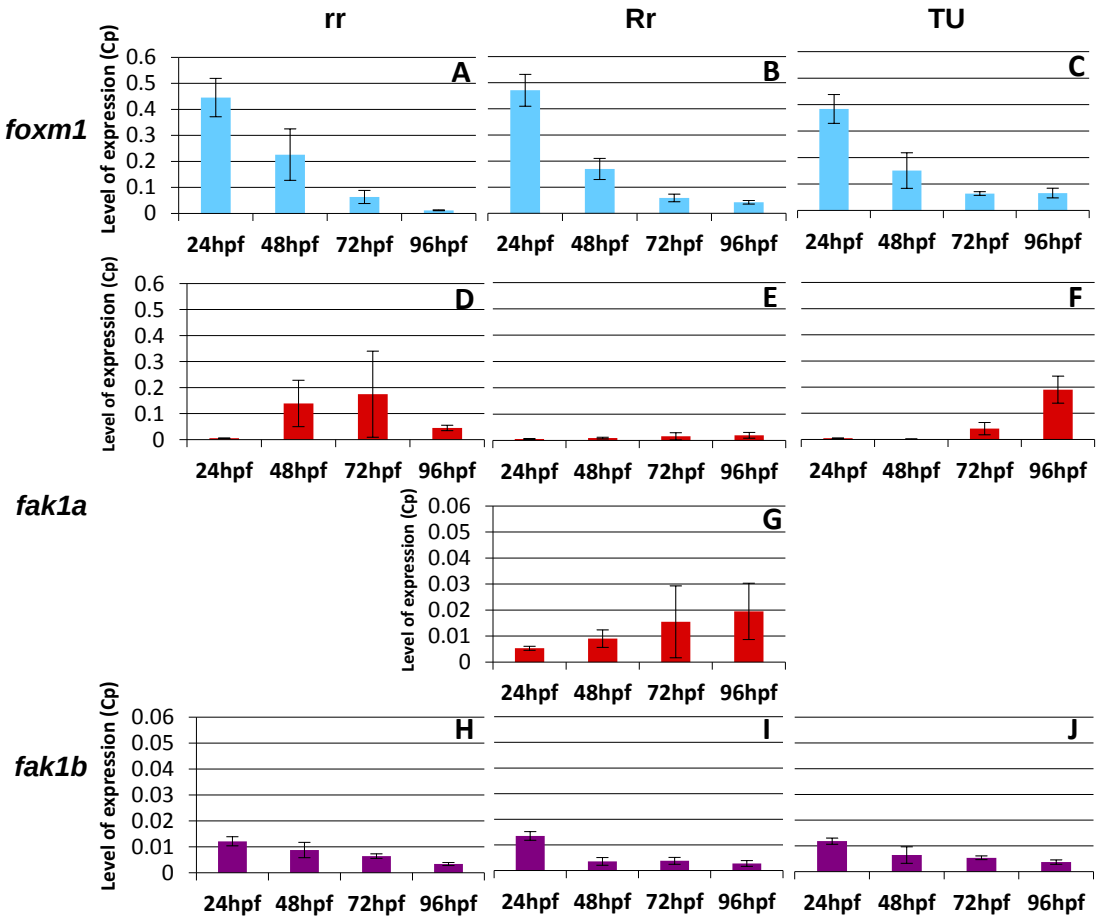

Figure 4.8: *foxm1, fak1a* and *fak1b* expression overtime for the *relaxed* mutant rr, the carrier Rr and the wildtype TU. Level of expression (Cp) of *foxm1* (blue), *fak1a* (red), *fak1b* (purple) in the immotile *relaxed* mutant rr **[A,D,H]**, the motile carrier Rr **[B,E,G,I]** and the wildtype TU **[C,F,J]** at 24hpf, 48hpf, 72hpf and 96hpf. The level of expression of *foxm1* significantly decreases overtime for all three genotypes (rr $p=0.0026$, Rr $p<0.0001$, TU $p<0.0001$, ANOVA). At 96hpf, the level of expression of *foxm1* is comparable for Rr and TU ($p=0.3460$, t test) however it is significantly lower in rr compared to Rr ($p=0.0052$, t test) and TU ($p=0.0683$, t test). The level of expression of *fak1a* significantly increases overtime for TU ($p=0.0002$, ANOVA) but not for rr ($p=0.4381$, ANOVA) and Rr ($p=0.4163$, ANOVA) respectively. However, at 96hpf the levels of *fak1a* expression are significantly different in rr ($p=0.0142$, t test) and Rr compared to TU ($p=0.0237$ t test). Note that graph **G** is similar to graph **E**, showing *fak1a* Rr expression but on an expanded y-axis. Levels of *fak1b* expression decreased for TU ($p=0.025$), for Rr ($p<0.0001$) and for rr ($p=0.0954$). There were no significant differences of the level of expression of *fak1b* for all three genotypes at each time point ($0.1511<p<0.8954$, t-test).

4.2.4 Switch of prevalence of *fak1a* and *fak1b* expression levels throughout early zebrafish development

Crawford et al. showed, using mRNA in situ hybridisation, that *fak1b* is ubiquitously expressed in the embryos from 5hpf (start of gastrulation), whereas *fak1a* is exclusively expressed in the developing skeletal muscle from 14hpf (10 somites) (Crawford et al., 2003). The spatial expression of these genes suggests that at 24hpf the levels of *fak1b*, which is ubiquitously expressed, would be higher than *fak1a*, which is confined to one tissue type. We found here that the level of *fak1b* expression is significantly higher

(approximately three fold) than *fak1a* expression in all three genotypes at 24hpf (Figure 4.9 A). Based on the in situ data as described by Crawford et al., we predicted that this expression ratio would reverse as development progressed (Crawford et al., 2003).

Therefore we examined the quantitative expression ratio at 96hpf, compared to that at 24hpf. Our data showed that at 96hpf, overall the relative expression level of *fak1b* compared to *fak1a* is very significantly lower. Furthermore, the levels of *fak1a* expression were significantly increased in wildtype embryos compared to both immotile *relaxed* mutants and motile carriers. The results also showed that the level of *foxm1* expression was significantly higher at the early stages of development, for all three genotypes, the immotile *relaxed* mutants, the motile carriers and the wildtypes (Figure 4.9 B). This is in accordance with evidence showing that *foxm1* expression levels will be highest when the mitotic activity is at its maximum level during early development (Teh et al., 2002). Furthermore, although the level of *foxm1* expression decreases throughout development for all three genotypes, at 96hpf it is significantly lower for the immotile mutant against both motile genotypes the carriers and the wildtypes.

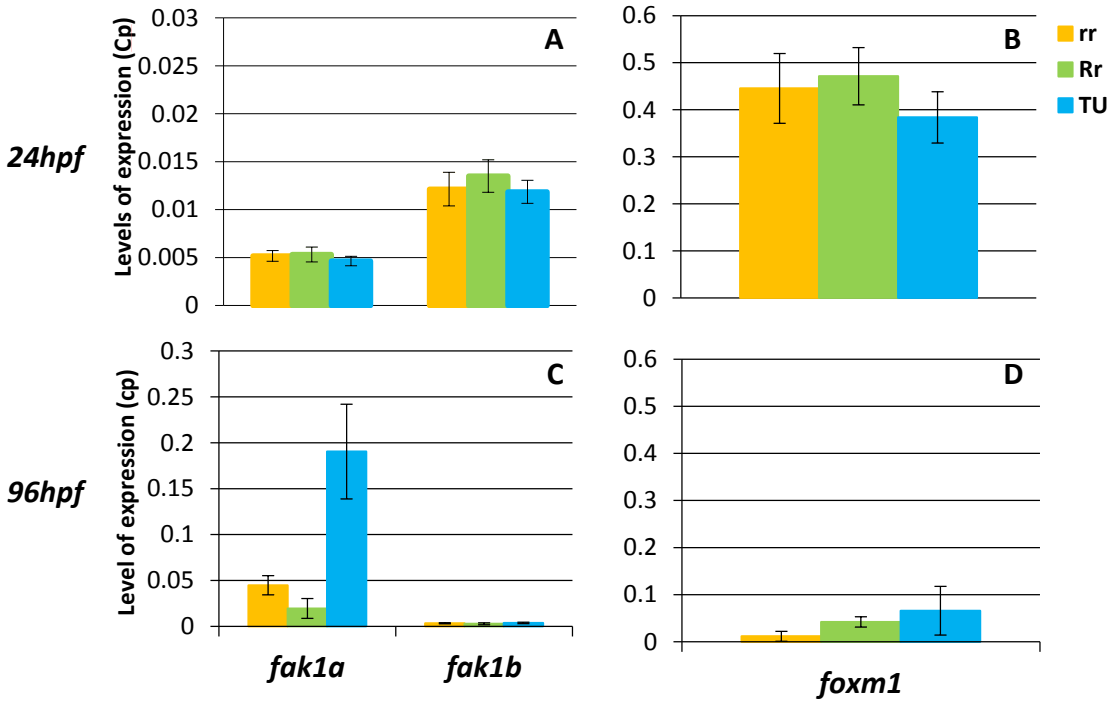

Figure 4.9: *fak1a, fak1b* and *foxm1* differential expression levels at 24hpf and 96hpf. [A] At 24hpf, *fak1a* expression level is significantly lower than *fak1b,* p=0.0007 and **[B]** *foxm1* is highly expressed for all three genotypes (TU blue, Rr green and rr yellow). **[C]** At 96hpf, *fak1a* expression level is significantly higher than *fak1b* p=0.0035, the levels of *fak1a* compared to *fak1b* expression were significantly increased in the immotile *relaxed* mutant (rr, p=0.0134, t test) in the wildtype (TU, p=0.0069 t test) and in the motile carrier (Rr, p=0.0659, t test). At 96hpf *fak1a* expression level in the immotile *relaxed* mutant and the motile carrier is significantly lower compared to the wildtype (TU) (rr p=0.0142, Rr p=0.0237). **[D]** At 96hpf *foxm1* expression level is very significantly decreased compared to that at 24hpf, and its expression level for the immotile *relaxed* mutant (rr) is significantly lower than for both the motile carrier (Rr, p=0.0052) and the wildtype (TU, p=0.0683).

In summary, the results show a steady decrease of *fak1b* expression through the first four days of development which is unaffected by paralysis. A steady increase of *fak1a* expression was also observed during this time period. The *fak1a* expression levels were found to be highly variable in the *relaxed* mutant line (both in mutants and carriers) and therefore it is difficult to state categorically whether *fak1a* expression is affected by paralysis.

4.2.5 Src is expressed in the sarcolemma and at the somite boundaries in developing embryos

Preliminary data has shown that zebrafish embryos treated with PP2, a Src kinase inhibitor, displayed disrupted embryonic tail formation, myofibril organisation (wavy misaligned myofibrils), and movement (Ashworth & Punn, personal communication). This suggested that Src is involved in muscle development; however Src expression and localisation in zebrafish embryo has yet to be described. Based on the structure of focal adhesion complexes from other systems, where Fak interacts with a variety of proteins including Src, it would be reasonable to propose that these proteins will also be present in zebrafish muscle. Whole mount immunohistochemical staining, using a phosphorylated Src antibody, was used to assess whether the protein was expressed in the developing somites during skeletal muscle formation from 24hpf. Results revealed phosphorylated Src expression at the plasma membrane of cells located within the mesoderm of the extreme rostral region of the embryo (Figure 4.10 A). In addition, within anterior somites phospho-Src is expressed at the sarcolemma of differentiated muscle fibres, with particularly strong expression at the somite boundaries (Figure 4.10 B&C). The specific localisation of the Src protein suggests that, along with focal adhesion kinase, it is part of FAC in both costameres and myotendinous junctions within zebrafish developing muscle.

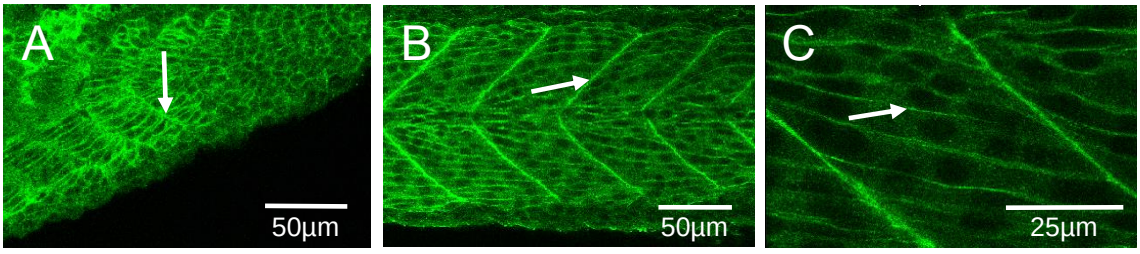

Figure 4.10: Src expression in the presomitic mesoderm and developing skeletal muscle within zebrafish embryos. Zebrafish embryos were fixed at 24hpf and stained with a phospho-Src antibody and Alexa Fluor® 488 Goat Anti-Rabbit IgG. Images were taken using laser scanning confocal microscopy and viewed with an X63 objective (HCX PL APO CS 63.0x1.30 GLYC 21°C UV) and **(A&B)** X1 and **(C)** X3 zoom. **[A]** Arrow denotes boundary of last forming somite. **[B]** Arrow denotes accumulation of the phospho-Src at the myotendinous junction. **[C]** Arrow denotes accumulation of phospho-Src along the sarcolemma. Anterior towards the right and dorsal towards the top of the images. (Scale bar is 50µm in A&B, 25µm in C)

4.2.6 Inhibition of Src disrupts tail development and embryonic movement in developing embryos

Previous work in our laboratory had indicated that treatment with PP2, a tyrosine kinase inhibitor, disrupted embryonic tail formation and possibly movement in zebrafish embryos (Ashworth & Punn, personal communication). We set out to investigate this phenotype disruption in more detail. The mechanism of action of PP2 is not fully understood, but it is thought that it binds to an ATP binding pocket on the Src domain preventing full activation of the protein. PP2 was selected over other kinase inhibitors due to its potency to inhibit Lck and Fyn kinases (Src family kinases), its low potency for EGFR (epithelial growth factor receptor), and as it does not activate PKA (protein kinase A), JAK2 and ZAP-70 (Karni et al., 2003).

The toxicity of PP2 on embryonic survival was tested initially to determine an optimal sub-lethal dose to use in experiments, as described in supplementary data (Appendix C). At 24hpf, after a 7 hours exposure to PP2 the tail of PP2 treated embryos appeared to be shorter and wider than controls. By 42hpf, after a 20 hours exposure to PP2, the PP2 treated embryos have developed a distinctive curve in their tails, compared to control embryos whose tails have straightened as expected (Kimmel et al., 1995). By 48hpf, the embryos have been exposed to PP2 for 26 hours, the phenotypes of the PP2 treated embryos are comparable to the 42hpf, but they also displayed pericardial oedema. Furthermore, PP2 treatment did produce a dose dependent disruption in embryonic development, the 'tail flip' phenotype is more prominent at higher PP2 concentrations (Figure 4.11).

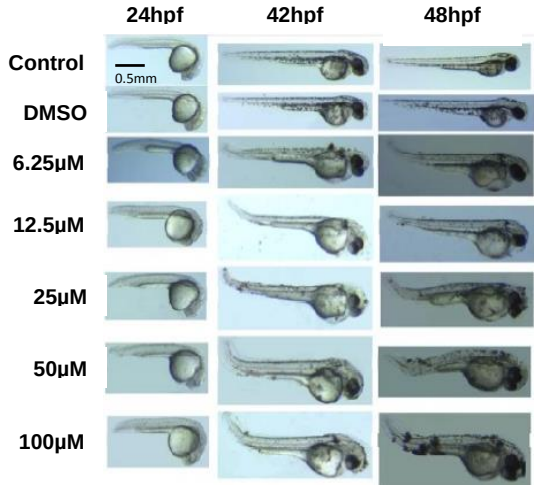

Figure 4.11: Treatment with PP2 disrupts tail formation in zebrafish embryos. Zebrafish embryos were treated with PP2 from 17hpf and images were taken at 24hf, 42hpf and 48hpf. At 24hpf after 7 hours of exposure to PP2, the embryos showed little variance in phenotype compared to controls. The embryos at 42hpf started to show a variance in detail, as the rear third of the tail has begun to "flip", and there seems to be signs of dose effect. At 48hpf the embryos had been exposed to 31 hours of PP2, and the phenotype is distinctive. Embryos exposed to the same concentration across the three time points show progression of tail flip and worsening of cardiac oedema.

The effect of the PP2-induced tail flipping was investigated further by examining the motility of the PP2 treated embryos when exposed to a light touch, namely the touch-evoked escape response. At 24hpf, control and treated embryos responded to touch by displaying a weak tail flip without travel. At 42hpf the embryos were more active and the motion varied, the control and DMSO embryos were able to escape with very strong rapid movements in response to touch. In contrast, treatment revealed a dose effect, with embryos incubated in lower concentrations showing either a normal escape response or a tail flip and higher concentrations showing a weak tail flip or no escape response. At 48hpf the control and DMSO embryos had a very rapid escape response and the PP2 treated embryos showed a dose effect, with those incubated in lower concentrations showing a tail flip and those in higher concentrations lacking escape response altogether. In summary, the pharmacological inhibition of Src show a dose dependent disruption of embryonic tail development and movement, with a progressive decrease in spontaneous and touch-evoked escape.

4.2.7 Inhibition of Src disrupts boundaries and somite patterning

Tail straightening in the developing embryo depends on several processes, of which somitogenesis is a key factor. Therefore observation that tail formation was affected by PP2 treatment suggests that the process of somitogenesis may be disrupted. Somite boundary formation was investigated by assessing the expression of β-sarcoglycan, which is expressed in the myotendinous junctions. Control and DMSO embryos showed sharp, well defined and continuous expression of β-sarcoglycan at the somite boundaries, in contrast in PP2 treated embryos the boundary structure was diffuse, undefined and fragmented. This effect was dose dependent, with a loss of the boundary apex for the higher concentrations of PP2 (Figure 4.12). This interesting observation suggests that Src plays a role in somite boundary formation, as its inhibition leads to the dispersion of β-sarcoglycans.

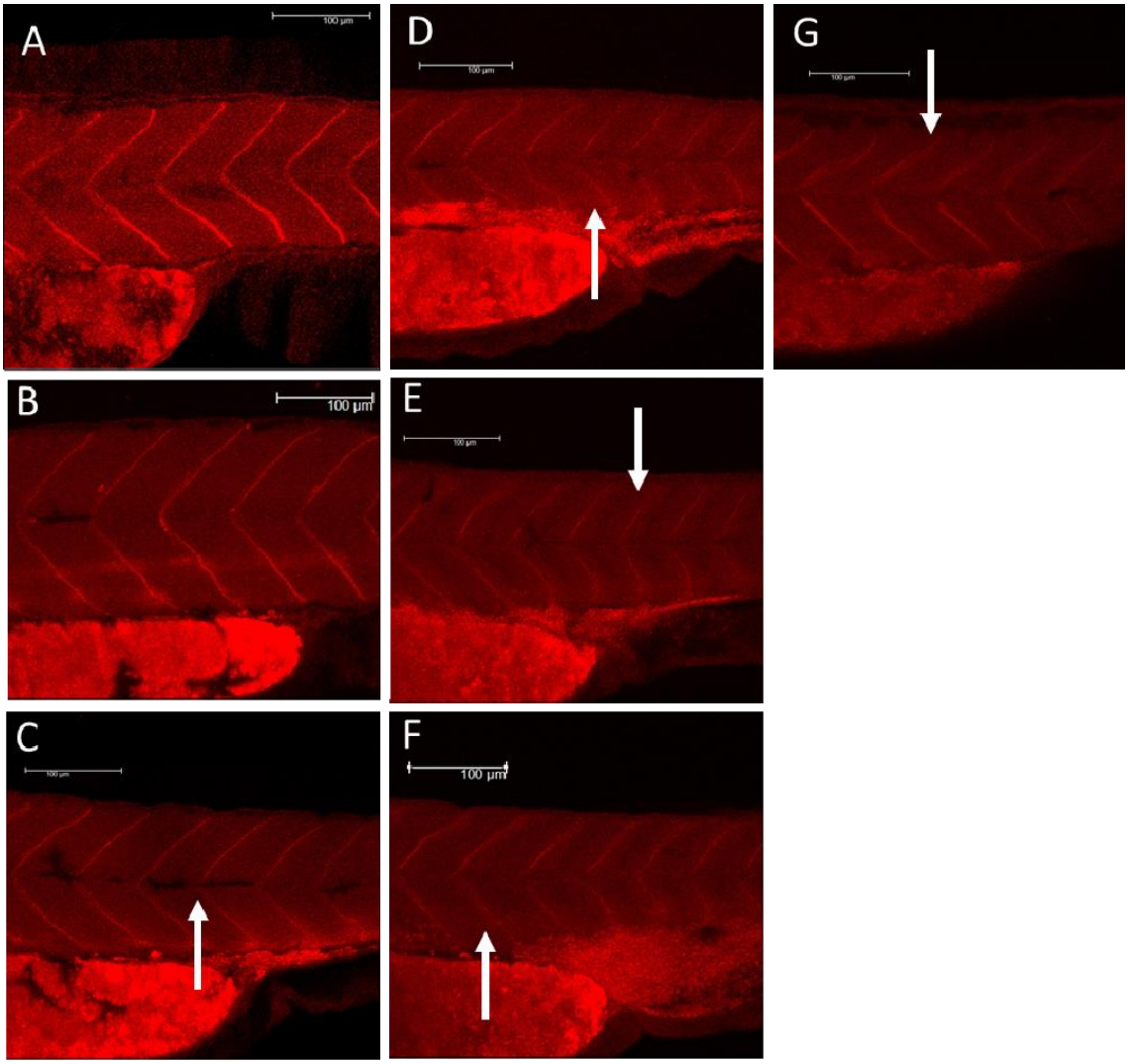

Figure 4.12: Prevalence of boundaries at increasing PP2 concentrations. Embryos kept at 25°C were put into their respective PP2 concentrations at 17hpf and further incubated at 28.5°C for 24 hours. The embryos were then fixed in paraformaldehyde and stained with a β-sarcoglycan with a Cy-5 linked secondary antibody**. [A]** Control embryo kept in Embryo Medium have clear somite boundaries, a solid line with no visible breaks. **[B]** DMSO control embryo shows similar boundary characteristics as the control embryo. **[C]** Embryo incubated in 6.25µM PP2, display a reduction of boundary prevalence at its apex (white arrow). **[D]** Embryo incubated in 12.5µM PP2 shows a reduction of its ventral boundary structure (white arrow). **[E]** Embryo incubated in 25µM PP2 shows a reduction in boundary prevalence at its apex and his ventral boundary as well as his dorsal boundary (white arrow). **[F]** Embryo incubated in 50µM PP2 displays the same boundary defects as the 25µM embryos and his ventral boundaries have lost the tight structure seen in the controls (white arrow). **[G]** Embryos incubated at 100µM displays all the boundary defects observed in the 25µM embryo and the dorsal boundaries have lost their tight structure (white arrow).Scale bars 100µm.

The role of Src on somite patterning was explored further, to assess whether somite length was disrupted by PP2 treatment. In zebrafish, the first somite furrow can be observed from 10hpf and somites appear sequentially with the anterior ones developing first. Somite addition at a standard temperature of 28.5°C occurs at a set rate and provides a useful staging tool, so that by 17hpf zebrafish embryos have a total of 16 fully formed somites (see Chapter 1). In our experiments, PP2 was introduced at the 17hpf

stage and somite length was measured in somites 15 to 19 (Figure 4.13). Somite 15 and 16 will have formed just prior to drug treatment, whereas somites 17 to 19 will have formed post PP2 treatment. PP2 treatment produced a significant shortening in somite length of approximately 10µm at every somite number (* $p<0.01$). This effect was dose dependent, higher concentration of PP2 leading to shorter somites. Notably, the gradients of the graphs were similar to controls (-2.5708 σ = ±0.275), which indicates that the rate of somite elongation and their size remains proportional in the PP2 treated embryos. Furthermore, the overall somite number was also conserved. This suggests that whilst PP2 slows down the rate of somite elongation, it does not disrupt the timing of somite addition.

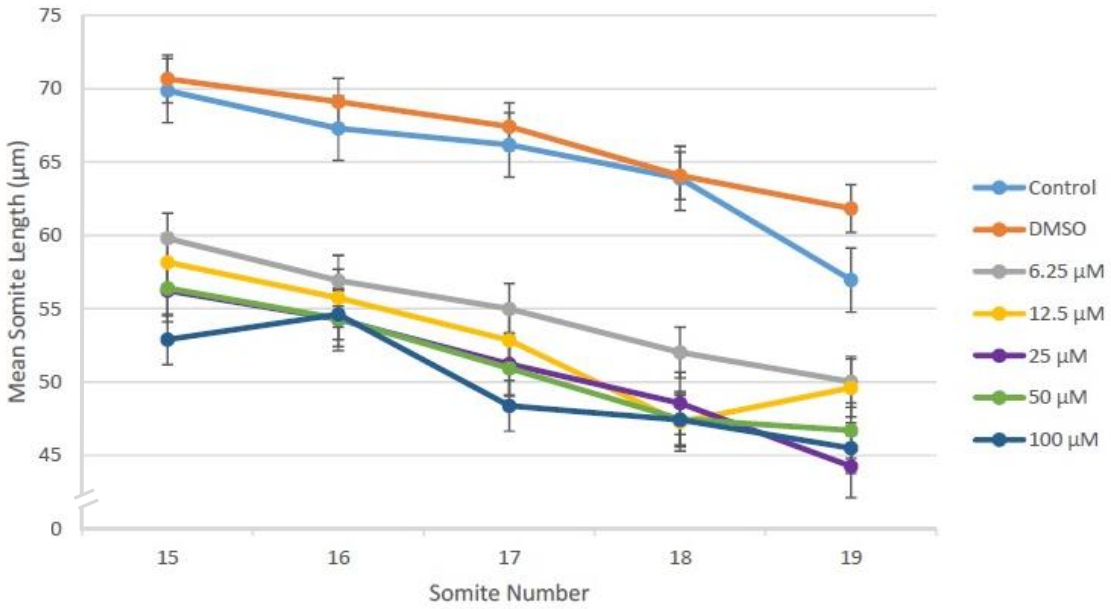

Figure 4.13: Effect of PP2 on somite development. Embryos were put into their respective PP2 concentrations at 17hpf and further incubated at 28.5˚C for 24 hours. The embryos were then fixed in paraformaldehyde and stained with a β-sarcoglycan with a Cy-5 linked secondary antibody. Somite length was measured from boundary to boundary. The control and DMSO embryos showed no significant difference, and the embryos kept in PP2 showed a negative dose effect for somite length, the higher the concentration the shorter the somite ($F(6,897) = 134.072$ $p<0.01$, 4 embryos/treatment n=3). The overall somite number showed no interaction with PP2 treatments, therefore somite addition is independent of the PP2 treatments ($F(28,897) = 0.738$ $p=0.836$, 4 embryos/treatment, n=3).

In summary, PP2 treatment affects both the initial stages of somite formation, namely boundary generation, and somite elongation, indicative of a later role for Src in somite maturation. Further this gross alteration of somite shape might be ultimately responsible for the ‘tail flip’ phenotype.

4.2.8 Inhibition of Src disrupts myofibril organisation

Our study showed that Src is expressed in the skeletal muscle of zebrafish possibly in FACs of both costameres and myotendinous junctions, and that its inhibition leads to both structural and functional defects of the skeletal muscle. These findings are indications of its possible involvement in mechanotransduction. Therefore, we investigated whether it was contributing to the contraction-driven myofibril organisation pathway in the developing zebrafish skeletal muscle. Results showed that at 48hpf, after a 26 hours exposure to PP2, the myofibril organisation is disrupted and the myofibrils appeared wavy and disorganised compared to control embryos. Furthermore, a positive dose effect can be observed when comparing the embryos exposed to increasing PP2 concentration, the myofibril disorganisation is more prominent at higher PP2 concentration (Figure 4.14). In summary, Src inhibition leads to myofibril disorganisation.

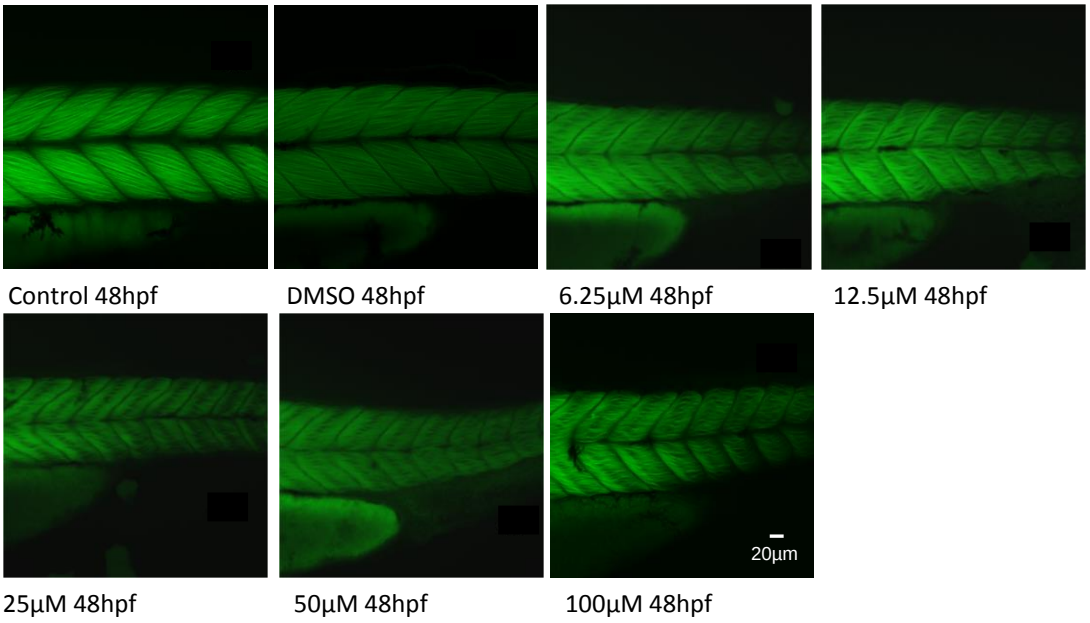

Figure 4.14: Treatment with PP2 causes disruption to myofibril organisation. At 17hpf embryos were incubated at 28.5°C in their respective PP2 concentrations. The embryos were then fixed and stained with phalloidin at 42hpf. (Scale bar is 20µm)

4.2.9 Inhibition of Src disrupts swimming behaviour

This study has shown that PP2 treatment disrupts myofibril organisation, somite patterning and ultimately tail formation leading to the 'tail flip' phenotype. These structural defects impact on the embryo's motility and a reduction of embryonic movement, namely touch-evoked escape response, was observed up to 48hpf (see 4.2.6).

The impact of PP2 treatment on movement was further assessed by a detailed analysis of swimming behaviours in PP2 treated compared to control larvae at 72hpf, using the

Ethovision™ tracking software. Three different measurements (i) the total distance travelled (ii) rotations about one axis, and (iii) mean angular frequency were collected. PP2 treated larvae displayed a significant dose dependent decrease in the total distance travelled compared to controls and DMSO treated larvae (Figure 4.15). In addition, PP2 treated larvae also displayed a reduction of their rotations and of their mean angular velocity. A tank effect was also tested for and established that there was no significant environmental/tank effects that potentially could have arisen from the fish housing or the Ethovision™ tracking system. This confirmed that the differences observed in swimming behaviour were due to PP2 treatment and no other external conditions. In summary, PP2 treated larvae showed a dose dependent decrease of their swimming behaviour when compared to controls at 72hpf.

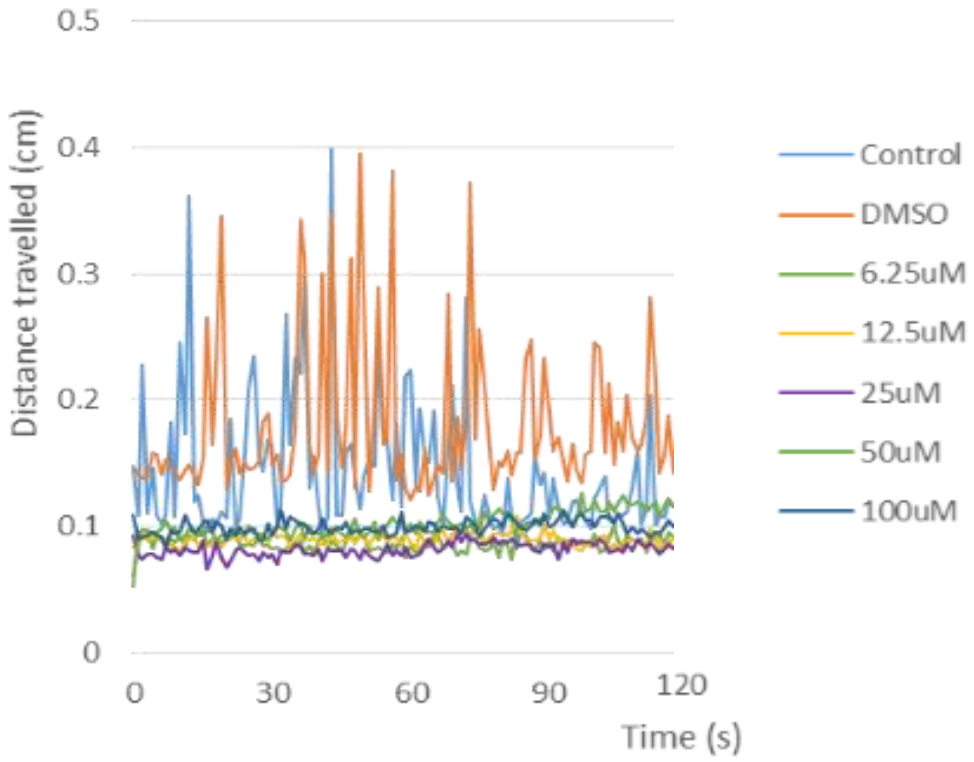

Figure 4.15: Effect of PP2 treatment on zebrafish swimming behaviour. Embryos were put into their respective PP2 concentrations at 17hpf and incubated at 28.5˚C for 55 hours. Their swimming behaviour was then monitored during 2 minutes using a camera equipped with the Ethovision™ tracking software. PP2 treated embryos total distance travelled was reduced compared to controls embryos (one-way ANOVA $F(6,27114)=79.473$ $p<0.01$), in an inversely proportional manner to the PP2 concentrations applied (compared by a LSD post hoc test). Rotations and mean angular velocity were also reduced compared to control embryos ($F(6, 27114)=123.247$ $p<0.01$ and ($F(6,27114)=575.617$ $p<0.01$ respectively).

4.3 Discussion

Expression of *fak1b* mRNA decreases, whereas expression of *fak1a* mRNA increases throughout the first four days of embryonic zebrafish development. *fak1b* expression was found to be unaffected by paralysis. Pharmacological inhibition of Src revealed a dose dependent disruption in embryonic tail development, swimming behaviour, somite formation and myofibril organisation. Overall, the results indicate that Fak is unlikely to be involved in the mechanotransduction pathway that regulates skeletal muscle development, specifically myofibril organisation. In contrast Src has been shown to have a role in somitogenesis and myofibril organisation during embryonic skeletal muscle development.

(1) The role of Fak in myofibril organisation

In mammals, Fak is known to be a key component of FAC and is essential to the mechanotransduction pathways linking extracellular matrix to the cytoskeleton (Durieux et al., 2007; Durieux et al., 2009; Klossner et al., 2009). In zebrafish embryos Fak is located at the somite borders and in notochord cells (Henry et al., 2001; Crawford et al., 2003) and is proposed to play a role in mechanotransduction. The role of Fak in contraction-driven myofibril organisation in zebrafish was initially assessed in immotile *relaxed* mutant embryos versus motile wildtype controls. If Fak was involved in the mechanotransduction driven pathway regulating myofibril elongation, its level of expression would be diminished in immotile embryos; however, the levels of *fak* expression were similar at 24hpf and remained constant throughout development up to 96hpf. At 96hpf a significant decrease in expression levels of *fak1a* was detected in carriers and *relaxed* mutants compared to wildtypes. However, this result was attributed to embryonic death, as the mitotic indicator *foxm1*, used as a control, was also reduced (Appendix D). In summary, this data suggests that, in zebrafish, *fak* expression is not dependent on contraction.

Furthermore, preliminary data from our laboratory has also revealed that treatment of wildtype embryos with a Fak inhibitor that prevents autophosphorylation at Tyr^{397} (Fak inhibitor 14) (Crawford et al. 2003) at the onset of movement (17-24hpf), did not disrupt myofibril alignment or body movement at 24hpf (Figure 4.16) (Ashworth and Karunarathna, personal communication).

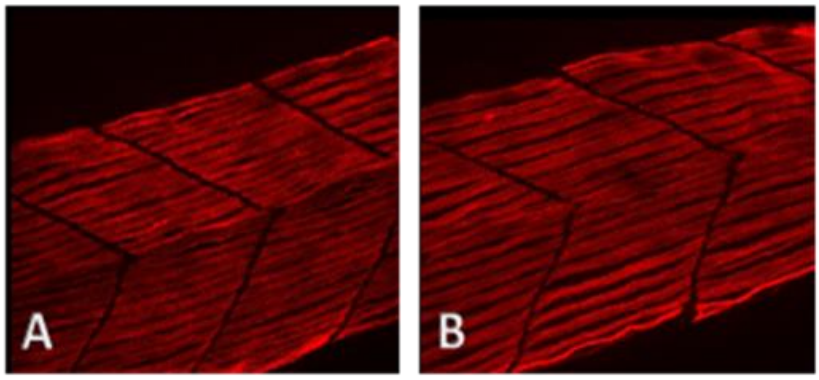

Figure 4.16: Treatment of wildtype embryos with Fak inhibitor, Inhibitor 14, did not affect muscle development at 24hpf. Skeletal muscle morphology of Inhibitor 14 treated wildtype embryos. **[A]** Non treated wildtypes, controls. **[B]** 100μM Inhibitor 14 treated wildtypes. Embryos were fixed and stained with myosin antibody (F59) and fluorescent secondary antibody. (Ashworth and Karunarathna, personal communication).

The normal, undisrupted phenotype in the Fak inhibitor treated embryos suggests that Fak is not involved in skeletal muscle development at this stage. However, there are several caveats that still need to be addressed. We know that zebrafish *fak1a* and *fak1b* are highly conserved (93% identical to human *FAK1*) and it is therefore likely that Inhibitor 14, initially designed and used for mammalian studies, will bind and inhibit zebrafish Fak; however, this was not tested directly. Furthermore, uptake of the drug into the embryo was not examined.

Taken together, experimental issues aside, both of these studies suggest that, in zebrafish, *fak1a* and *fak1b* are unlikely to be sensors of the mechanotransduction pathway driving myofibril organisation. These results do not fit with the evidence from mammalian studies that have shown that Fak is involved in mechanosensitive signalling and suggests that there may be mechanistic differences in the way in which zebrafish skeletal muscle operates. One interpretation of this data could be explained by the fact that the teleost genome duplication has led to genetic divergence and a change in protein function (Jaillon et al., 2004). Zebrafish, indeed teleosts in general, have two divergent isoforms of the Fak protein, Fak1a and Fak1b, which are similar in terms of their sequence but display entirely different expression and localisation patterns within the embryo. *fak1a* is segmentally expressed in somites throughout embryogenesis, whereas *fak1b* is expressed ubiquitously as the dominant isoform during early development (Crawford et al., 2003). The divergent expression of these two *fak* isoforms suggest that they may have different roles. Further, in mammals Fak initiates activation of signalling within the focal adhesion complex; however, in zebrafish Fak may reside downstream and play a secondary role. If this is the case, and Fak only has a minor role in zebrafish, Fak inhibition would not result in a major disruption of muscle phenotype. It would be worth exploring these dissimilarities in more detail as they could lead to the discovery of novel signalling and/or sensing mechanisms of the contraction-driven myofibril

organisation pathway. Zebrafish work can indeed potentially inform studies in mammals and lead to a better understanding of muscle function and organisation, uncovering unknown evolutionary breakpoints that occurred in the human genome in the past 450 Myr (Jaillon et al., 2004) and ultimately enhance medical research in humans (Sato et al., 2009).

(2) The role of Src in myofibril organisation

Evidence from this study suggests that the mechanotransduction signalling pathway in mammalian FAC may be different to that in zebrafish. Potentially, although similar protein signalling molecules are present their function may differ. Most relevant to this study was the investigation of their overall contribution to contraction-driven myofibril organisation in zebrafish. Src kinase was chosen as a key candidate because of its activation role within the phosphorylation cascade in FACs in mammals. This protein is known to be part of the focal adhesion complexes (FAC) and to co-operate with Fak and Paxillin to regulate cell adhesion and motility (Kratimenos et al., 2014; Moroco et al., 2014). We initially established that Src was present in zebrafish at the sarcolemma and at the somite boundaries where it colocalised with Fak and Paxillin (Kratimenos et al., 2014; Brown et al., 2005) (Figure 4.17).

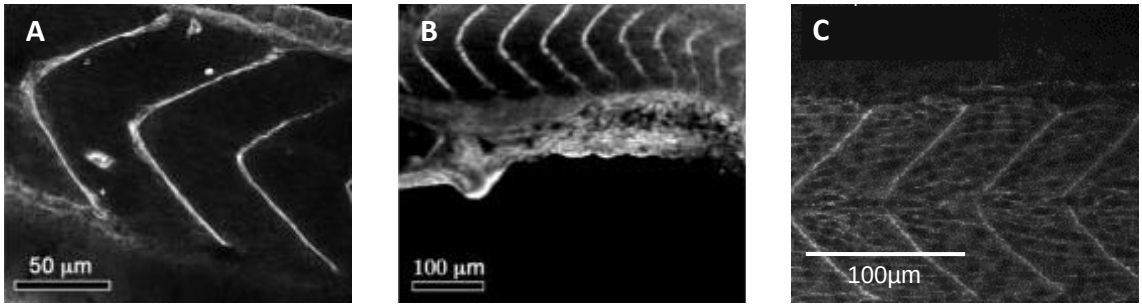

Figure 4.17: Colocalisation of Fak, Paxillin and Src at the somite boundaries. In 24hpf zebrafish embryo Fak **[A]** and Paxillin **[B]** are localised at the somite boundaries (Crawford et al., 2003), and in this study Src colocalises at the somite boundaries and is also found at the sarcolemma **[C]** (see **4.2.5.**).

Src localisation at the FAC of costameres and myotendinous junction led to the hypothesis that, in zebrafish, it might be Src rather than Fak that would be involved in skeletal muscle development, namely in the mechanotransduction pathway regulating myofibril organisation.

The role of Src was investigated using a pharmacological inhibitor and the disruption of skeletal muscle structure and function was analysed. Our results revealed that Src may have multiple roles in skeletal muscle development, as discussed below.

Somitogenesis disruption was observed in PP2 treated embryos, which displayed shorter somites. This suggests that Src has a role in somite maturation and is involved in the somite elongation process. This process occurs during the later stages of the clock and wave front mechanism for somite formation (Baker et al., 2006). This rhythmic phenomenon is a gene regulatory network that operates in the presomitic mesoderm of developing vertebrate embryos and generates transcriptional oscillations that direct the rhythmic and sequential formation of body segments in concert with embryonic elongation (Schroter et al., 2012). In the case of PP2 treated embryos, disruption to somite elongation gave rise to shorter somites. This could be explained by two different alterations of the mechanism. Either, the somite clock mechanism is accelerated and shorter somites formed faster, due to a reduced amount of elongation. Although, considering that the control and treated embryos had an equal number of somites, that would also mean that the somite clock mechanism is altered in another way, allowing for a time delay in between elongation and the formation of the next somite, to avoid supernumerary somites. Or, another simpler and more likely interpretation would be that somite elongation is solely slowed down, which involves only one defect of the somite clock mechanism.

Another aspect of skeletal muscle disruption following Src inhibition was the reduction of the somite boundary prevalence, observed on β-sarcoglycan immunostaining. This suggests that Src kinase has a role during somite boundary formation. A reduction and dispersion of the somite boundary protein, β-sarcoglycan, was observed in PP2 treated embryos. β-sarcoglycans are part of the dystrophin/glycoprotein complex and have no direct interaction with Src kinase which is part of the integrin complex, FAC. However, both these complexes are part of specialist transmembrane linkages, myotendinous junctions and costameres. These linkages transmit mechanical forces and regulatory signals from the extracellular matrix into the cell interior (cytoplasm) via co-localised subsarcolemmal complexes (Pardo et al., 1983) which connect through γ-actin and the intermediate-filament protein Desmin to the Z-disk of skeletal muscle fibres (Patel and Lieber, 1997) (Figure 4.18). Therefore there is an indirect link between β-sarcoglycan and Src kinase. Src inhibition generated somite boundary disruption, this might be the result of FAC not forming a connection between the Fak and Vinculin. This disruption of FAC might have caused a distortion of Desmin and α-actinin resulting in an irregular dispersion in β-sarcoglycan. Therefore, the diffuse somite boundary observed in PP2 treated embryos (Figure 4.12G) suggests that Src inhibition induced a decrease in the affinity in between FAC and dystrophin/glycoprotein complex.

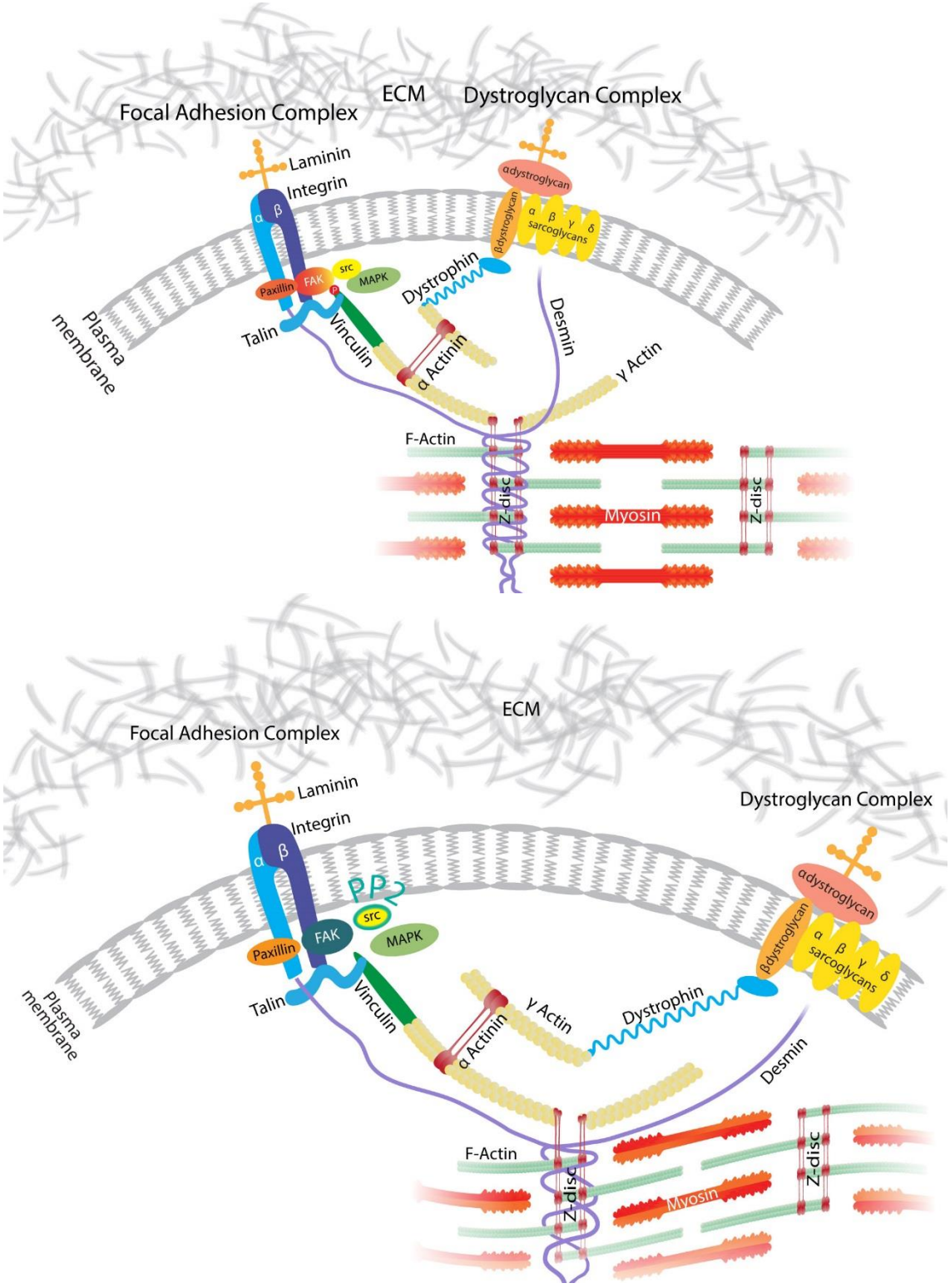

Figure 4.18: Schematic model of the PP2 induced disruption of the cytoskeletal filament linkages at the sarcolemma of striated muscle: integrin-based focal adhesion complex (FAC) and dystroglycan complex (DGC). Integrin-based FAC and the DGC act as transmembrane receptors for ECM components and link the ECM with the actin cytoskeleton. Integrins associate with Talin, α-actin and Vinculin to form a strong mechanical link to actin filaments. The DGC consists of the transmembrane complex β-dystroglycan, Dystrophin, the sarcoglycans, and other components not depicted here. Importantly, these linkage complexes bind to the submembraneous Actin (γ-actin) and are probably interlinked through this association as well as other unknown interactions. It is this association that might be disrupted in PP2 treated embryos, inducing a decrease of FAC and DGC affinity. Adapted from Clark et al., 2002.

Furthermore, actin staining revealed that Src inhibition disrupted myofibril organisation, which appeared increasingly wavy with both the drug concentration and the incubation time. Taken together with its localisation, this suggests that Src has a role in the contraction-driven myofibril organisation pathway. However, this disruption of the myofibrils could also be linked to the somitogenesis disruption observed in PP2 treated embryos. Therefore, we cannot conclude whether myofibril misalignment is directly linked to Src activity.

Src inhibition led to a disruption of myofibril organisation, somite boundaries and somitogenesis, and is accountable for the gross anatomical disorder first noted, the 'tail flip' phenotype. Defective tail straightening is often associated with disruption of somite development (Stickney et al., 2000). Taken together with the fact that Src inhibition also disrupts skeletal muscle function, with a reduction in swimming behaviour, this suggests that Src plays a key role in skeletal muscle development.

4.4 Conclusion

Our results show that paralysis does not affect the expression level of *fak* during early zebrafish development and it is therefore unlikely to be a gene candidate involved in the mechanotransduction pathway that regulates myofibril organisation in zebrafish. This result is in contrast with mammalian studies, which have implicated Fak in skeletal muscle development. Src, on the other hand, was shown to be present in the costameres and found in the myotendinous junctions at the somite boundaries in zebrafish. Furthermore, Src was found to be involved in several aspects of muscle structure and function during development. In contrast to mammalian studies, in zebrafish Src appears to have a major role in skeletal muscle development whereas Fak does not, this is a novel finding and could be explained by a remodelling of FAC in teleosts, with a shift in the relative importance of the signalling proteins.

4.5 Future work

Following on from this study, future work could address the experimental caveats identified. Pharmacological inhibition of Fak needs to be confirmed, by ensuring that Inhibitor14 does binds to Fak in zebrafish and stops its autophosphorylation activation mechanism. This could be addressed by immunostaining using both Fak and phosphorylated-Fak antibodies, a down regulation of the latter would be expected. In addition, this work could be combined with experiments using newly developed more specific Src-family kinase inhibitors, such as Saracatnib, Bosuntib, Dasantanib or KX2-391 (Lieu and Kopetz, 2010). These Src inhibitors are more specific to one type of Src rather than PP2, which is effective for multiple Src-family kinases. Another possibility to

study the action of Src during development is the use of morpholinos. This would enable the suppression of a specific Src-family kinase mRNA from being transcribed. DNA encoding Src-family kinases have been identified in the zebrafish genome, '*she*' gene (accession number: BX470239) codes for a Src-family kinase that has shown high levels of expression in striated muscle in mice, and is the only Src-family kinase to date expressed in muscle (Table 4.1). Zebrafish is a prime candidate for morpholino studies on striated muscle, both skeletal and cardiac, as they are able to survive up to 5dpf without a functioning heart as gases can diffuse through the skin. The advantage of using morpholinos as compared to pharmacological inhibitors is that it enables specific inhibition of the protein kinase of interest. Furthermore, emerging technologies, such as CRISPR/Cas9 allow to introduce genome modifications at the targeted genomic locus of interest. This new and powerful genome editing technique, would be perfectly suited to Src knockdown (Hisano et al., 2014).

Src family kinase	Accession	Function
CSK	BC125943	Epidermal growth factor signalling
fynA	BC075763	
fynB	BC098534	T-Cell receptor signalling
SHC1	-	Antagonise cell proliferation
SHC2	BX470234	-
SHC3	-	Found in nucleus accumbens (dopaminergic?)
shda	BX24831	Calcium release from sarcoplasmic reticulum
shdb	BX470234	
SHF	-	-
she	BX470239	Expressed in heart, lung, brain and skeletal
skap1	BC129162	T cell adapter protein
skap2	BC057253	Expressed in Thymus and T cells, interacts with
sla1	BC103485	Lymphocyte migration
sla2	BC155558	Bone marrow macrophages
sla3	-	Ubiquitously expressed in cardiac and
SRC	BC116544	Pulmonary microvascular endothelial cells
SRCIN1	-	-

Table 4.1: 17 Src kinase genes in the zebrafish genome. The function of these proteins is not fully known in zebrafish, the function indicated here refers to the function of ortholog genes found in other model organisms.

Finally, the identification of additional signalling proteins of the mechanotransduction pathway and their associated role would facilitate the understanding of contraction-driven skeletal muscle development. Prior to this project a microarray approach had been used to compare immotile *relaxed* mutant and motile carriers with the aim of identifying novel genes affected during paralysis. Further details of this work can be found in Appendix E.

CHAPTER 5

MYOFIBRIL DISRUPTION AND FORCE TRANSDUCTION

5. Myofibril disruption and force transduction

5.1 Introduction

The zebrafish has proved useful as a vertebrate model to explore the loss of E-C coupling on subsequent skeletal muscle development *in vivo*. Previous studies have shown that paralysis disrupts myofibril and sarcomere organisation (Behra et al., 2002) (Brennan et al., 2005; van der Meulen et al., 2005; Lahne et al., 2009). One advantage of the *in vivo* approach is that it enables the study of physiological events allowing complex interactions between tissues, here nerve and muscle, to be examined. My work has now shown that contraction driven increase of myofibril length can be rescued by recovery of movement. This can be taken as evidence that skeletal muscle function, that is contraction, can regulate structural organisation. Further to this, studies in other models have shown that the structural organisation of myofibrils will affect its functional properties, ultimately controlling force generation and movement (Williams and Goldspink, 1978). Thus, it can be argued that there is a positive feedback loop whereby function regulates structure and vice versa. It is likely therefore that the paralysis driven disruption to myofibrils observed in zebrafish developing muscle will affect its mechanical properties. However, the impact of altered structure on muscle function in zebrafish has not been explored in detail.

One parameter of muscle function, extensively studied in mammalian systems is their passive and active force generation. Normally in mammalian systems, muscle fibres are isolated in order to mount them on force transducers with the aim of manipulating their environment. Despite the size of zebrafish larval muscle fibres, it has proved possible to isolate them and to measure force (Iorga et al., 2011). However, of greater advantage has been the development of a technique in Professor Arner's laboratory that allows the mounting of whole larval fish, enabling muscle properties to be explored in intact animals (Dou et al., 2008; Li et al., 2013). Using this approach skeletal muscle can be assessed in an environment in which they are capable of differentiating into the full range of definitive muscle-types. Zebrafish larvae were mounted in a physiological bath, using aluminium clips trapping their head and tail (Figure 5.1). Within the bath they are mounted on one side on a force transducer and on the other side on a micrometer screw allowing length adjustments. Stimulations were performed using platinum electrodes.

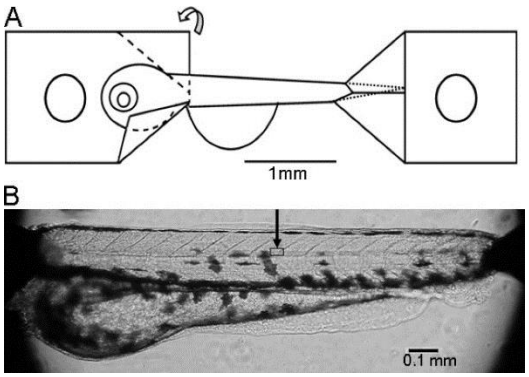

Figure 5.1: Zebrafish larvae preparation. [A] Schematic illustration of preparation attachment using aluminium foil clips at both ends of the larvae. The aluminium foil is folded along the dashed lines as shown on the left clip. A small hole is made in each clip for mounting. **[B]** Photograph of the preparation mounted on the microscope stage (Dou et al., 2008).

In this chapter we examined, in collaboration with Professor Arner (Karolinska Institutet, Stockholm, Sweden), the functional consequences of paralysis using the technique he pioneered to study the mechanical properties of developing muscle in zebrafish larvae (Dou et al., 2008; Li et al., 2013). Immotile *relaxed* mutants, and pharmacological treatments were used to assess the effect of paralysis and recovery on the developing skeletal muscle mechanical properties. However, due to technical limitations, larvae could only be mechanically assessed from 4-5dpf. Therefore, comparison of muscle function between immotile, recovered and control fish was established by exploring length-force relationships at 5 and 7dpf. Passive force measurements were taken in all fish by stretching the muscle and active force was measured in recovered compared to control embryos. In addition, sarcomere length was determined using light microscopy to assess whether, as shown in the motility mutants *nic1* (Brennan et al., 2005), zebrafish immotile *relaxed* mutants and pharmacologically treated fish displayed shorter sarcomeres.

Finally, to complete the assessment of the positive feedback in between muscle structure and function, the effect of paralysis on zebrafish subsequent swimming behaviour was also assessed, using the Ethovision™ tracking software. Previous studies have shown that immobilisation of embryos did not appear to disrupt subsequent swimming behaviours of developing zebrafish larvae (Saint-Amant and Drapeau, 1998). However, this study has revealed that whilst paralysis-induced myofibril disorganisation is reversible, this process takes several days to fully recover (Chapter 3). The delay in myofibril structural recovery, as observed in this study, may well have a knock-on effect on the swimming behaviour in developing larval fish.

The aim of this chapter is to analyse the disruption of sarcomere length and force production in the zebrafish skeletal muscle and ultimately swimming behaviour, in response to paralysis.

Hypothesis: Work from chapters 3 and 4 have shown that paralysis leads to structural disruption, causing myofibril disorganisation. As the structure of muscle fibres is critical to the maintenance of function, it was proposed that paralysis-induced disruption will impact on force production and ultimately swimming behaviour. In this chapter the hypothesis was tested using force measurement and a swimming tracking system.

5.2 Results

5.2.1 Active and passive tension measurements in 5dpf carrier control larvae

Passive and active tensions were measured at different degrees of stretch relative to slack length (Ls) in 5dpf (Figure 2). The length of the samples (L) was increased in steps from slack length (Ls) and at each relative stretch (L/Ls) active and passive tension were recorded as a voltage and converted into force measurements (mN). To generate active tension, muscle were stimulated at supramaximal voltage (10% above the maximal) with single pulses (0.5ms) to give rise to a single twitch contraction via direct stimulation of the whole fibre (Figure 5.2 A). The active tension was measured at the peak of the single twitch contraction. Passive tension was measured just before the electrical stimulus and stretch increment (Figure 5.2 B).

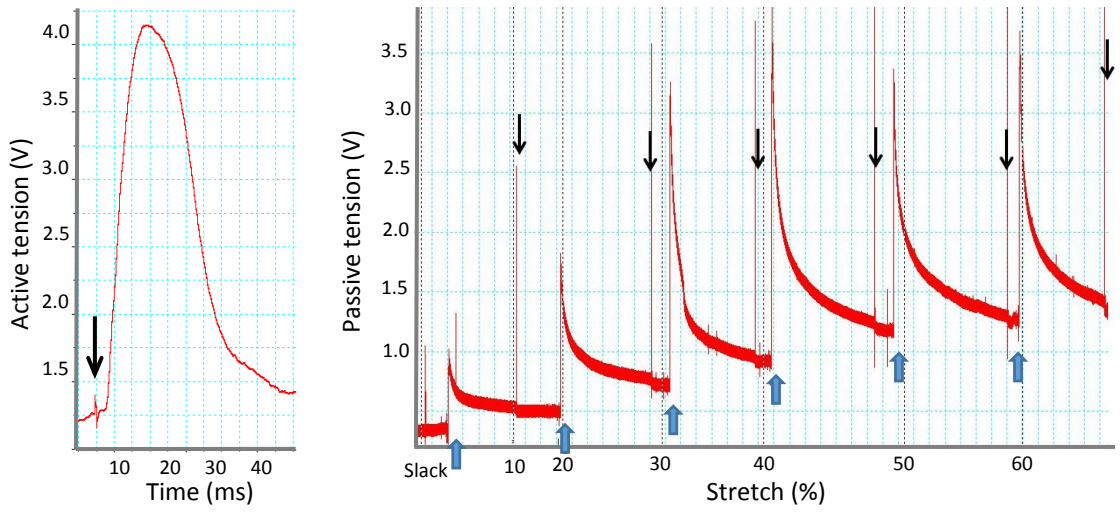

Figure 5.2: Active and passive tension recorded in a 5dpf carrier control larvae. To examine the mechanical function of immobilised and recovered larvae, larval muscle preparations were mounted for force recording. **[A] Active tension**: single twitch contraction at 40% stretch, contraction occurs after a short delay after the stimulus (black arrow) and reaches a peak in about 10-20ms. **[B] Passive tension** was measured just before the electrical stimulus (top black arrows) and stretch increment (bottom blue arrows).

5.2.2 Paralysis and passive tension

It was proposed that myofibril disorganisation affects the mechanical properties of skeletal muscle. Thus, changes in the passive elastic properties in paralysed versus control embryos were examined by measuring passive length force relationships at different degrees of stretch using both the immotile *relaxed* mutant line and pharmacologically treated larvae, during paralysis and after recovery.

5.2.2.1 Effect of paralysis on passive tension in *relaxed* mutant muscle

At 5dpf, immotile *relaxed* mutants, were found to have a similar passive tension to their motile carrier siblings, up to 30% stretch. When stretched above 50% of the slack length, motile carriers muscle teared off (often at the attachment of the aluminium clips), whereas immotile *relaxed* mutants muscle allowed up to 100% of the slack length. However, this final increase in stretch did not result in an associated increase in the passive tension of the immotile *relaxed* mutant muscles, which plateaued (Figure 5.3 A). The increase in stretch above 50% in immotile *relaxed* mutants muscle could be due to a number of factors (i) an increase in muscle size, (ii) myofibril disorganisation (lengthening) and (iii) sarcomere elasticity. *Relaxed* immotile mutants have similar cross-sectional area to carrier motile controls indicative that muscle size has not changed (Figure 5.3 B). Myofibrils, are long and wavy at both slack length and 30% stretch (Figure 5.3 C). The average stretch (L/Ls) at the point where force is maximal is similar in both carriers and *relaxed* mutants, indicative of similar sarcomere elasticity (Figure 5.3 D). In summary, the results show that it is the paralysis-induced myofibril lengthening, rather than gross muscle size or sarcomere elasticity, that potentially contributes to the ability of the *relaxed* mutant muscle to undergo further stretch above 50% without an associated increase in passive tension.

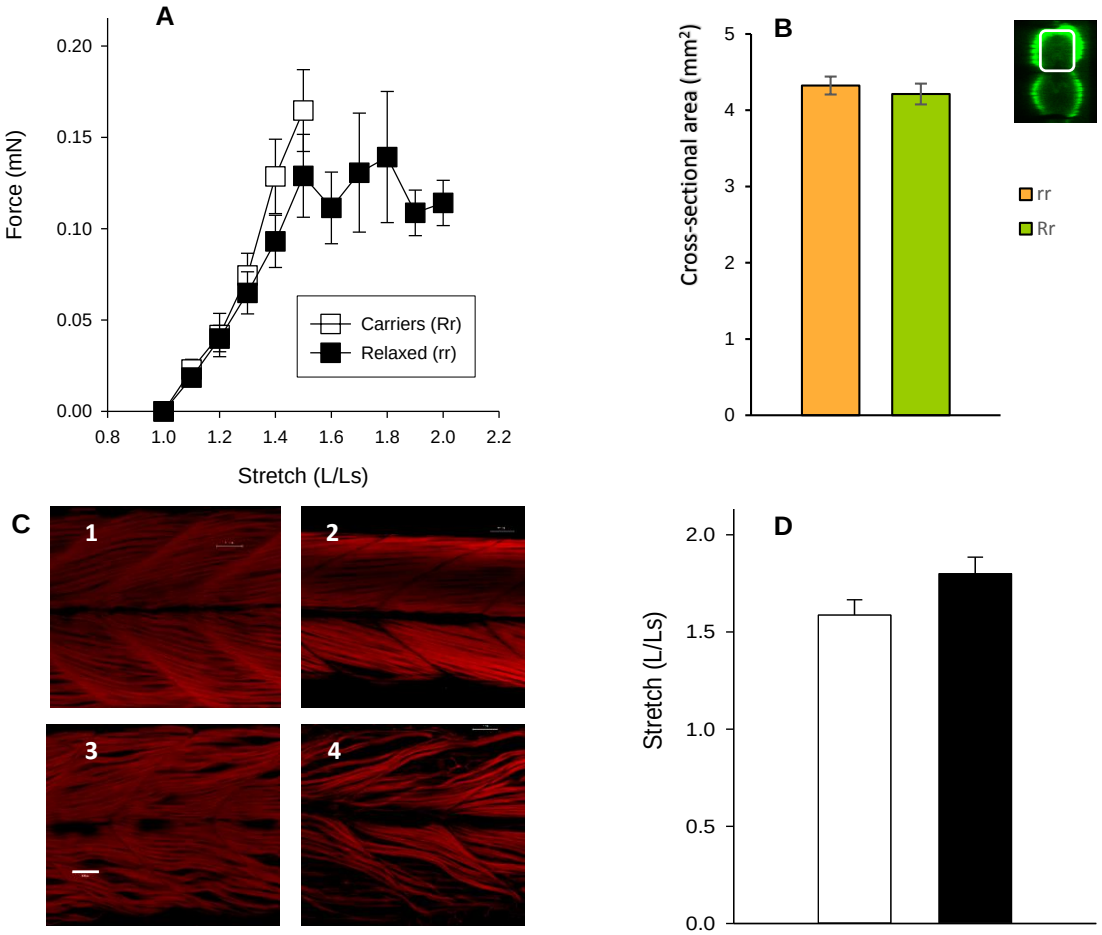

Figure 5.3: Measurement of passive tension and associated factors in the *relaxed* mutant muscle at 5dpf. [A] Passive tension (Force mN) was plotted against stretch at different lengths, relative to slack length (L/Ls)**,** carriers (Rr, white), *relaxed* mutants (rr, black). Controls tended to break at stretches above 1.5. Whereas *relaxed* mutants were able to stretch without breaking, up to twice the slack length, without an associated increase in passive tension (above about 1.5-1.6). **[B]** Cross-sectional area was measured on transversal sections through the dorsal region of the somite. *Relaxed* mutants (yellow), carriers (green). (n=9, p=0.54655, ns) **[C]** Actin within the somites stained with rhodamine phalloidin to demonstrate the myofibril phenotype in **1:** carrier at slack, **2:** carrier at 30% stretch, **3:** *relaxed* mutant at slack, **4:** *relaxed* mutant at 30% stretch. **[D]** Average stretch (L/Ls) at the point where force is maximal in both carriers (white) and *relaxed* mutants (black) (n=7 *relaxed* mutants & 8 carriers, p=0.0948, NS) (Scale bar is 100µm).

5.2.2.2 Effect of paralysis and subsequent recovery on passive tension in drug treated larvae

In order to be able to assess the same batch of fish during paralysis and once movement is restored, the pharmacological protocol was adapted and the embryos were paralysed up to 5dpf. Movements in zebrafish embryos prior to 24hpf are driven by slow muscle, therefore the Na^+ channel blocking anaesthetic Tricaine, rather than BTS, was found to be most effective at inhibiting the initial embryonic movements (up to 29hpf). Conversely, BTS, specific reversible inhibitor of the fast muscle myosin II ATPase, was shown to be

a more effective reversible paralysing agent and to have a better survival rate compared to Tricaine from 29hpf up to 5dpf, (Appendix F).

At 5dpf, immotile Tricaine-BTS treated fish were found to have a similar passive tension compared to the motile DMSO control fish, up to 60% stretch. As with the *relaxed* mutants and their carriers, when stretching further, motile DMSO control fish muscle teared off (often at the attachment of the aluminium clips), whereas immotile Tricaine-BTS treated fish muscle allowed up to 100% of the slack length. However, in contrast with the *relaxed* mutant data, the Tricaine-BTS treated larvae showed a continuous associated increase of their passive tension above 60% stretch (Figure 5.4 A). As for the immotile *relaxed* mutants, possible factors involved in stretch increase were explored, i.e. increase in muscle size, myofibril disorganisation (lengthening) and sarcomere elasticity. Tricaine-BTS treated immotile larvae have similar cross-sectional area to DMSO motile control larvae, indicative that muscle size has not changed (Figure 5.4 B). However, although myofibril waviness was observed at slack length, it was less apparent in Tricaine-BTS treated fish than in *relaxed* mutants, and disappeared at 30% stretch (Figure 5.4 C). Furthermore, the average stretch (L/Ls) at the point where force is maximal is similar in both Tricaine-BTS treated and DMSO control larvae, indicative of similar sarcomere elasticity (Figure 5.4 D). In summary, the results show that, as with the *relaxed* mutant data, it is the paralysis-induced myofibril lengthening, rather than gross muscle size or sarcomere elasticity, that potentially contributes to the ability of the Tricaine-BTS treated larvae muscle to undergo further stretch above 50%. However, in contrast to the *relaxed* mutant data, stretch in the Tricaine-BTS treated larvae muscle is accompanied by an associated increase in passive tension.

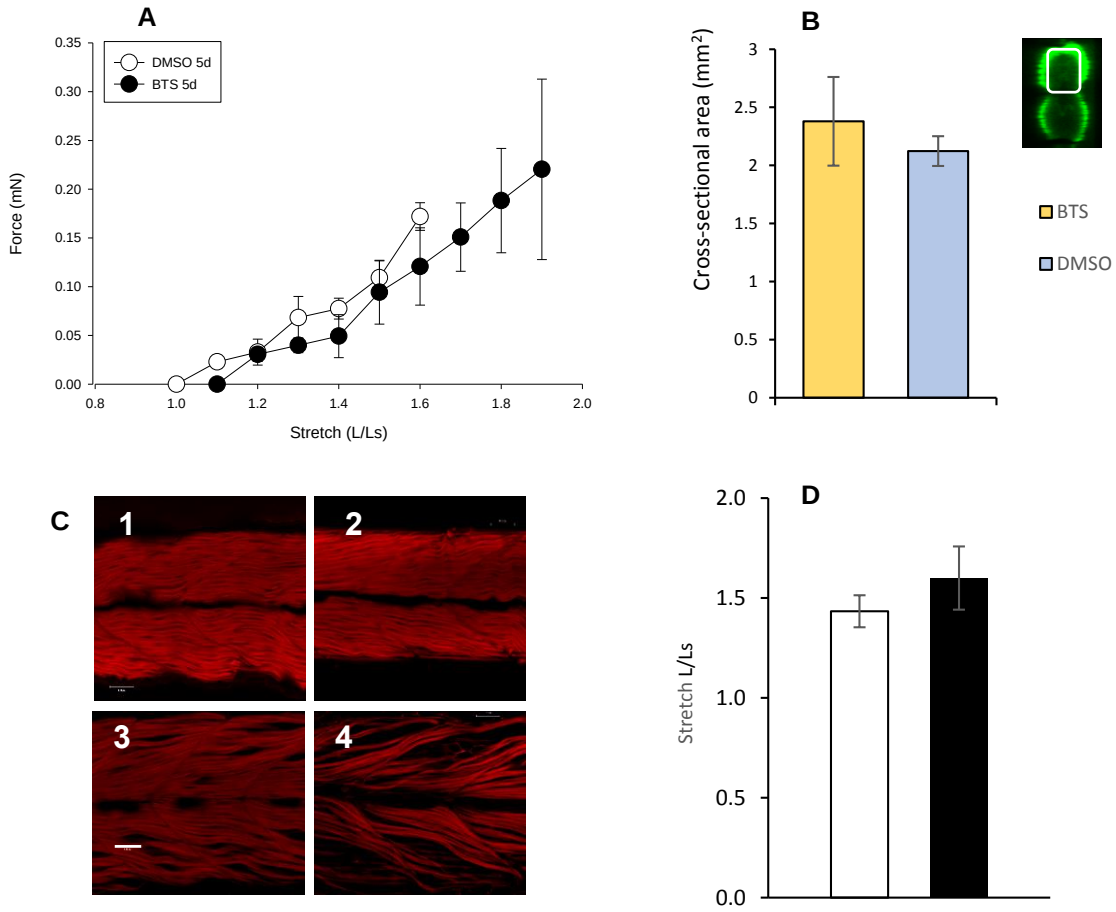

Figure 5.4: Measurement of passive tension and associated factors in the Tricaine-BTS treated and DMSO control larvae at 5dpf. [A] Passive tension (Force mN) was plotted against stretch at different lengths, relative to slack length (L/Ls)**,** DMSO controls (DMSO 5d, white), Tricaine-BTS treated (BTS 5d, black). DMSO controls tended to break at stretches above 1.6. Whereas the Tricaine-BTS treated larvae were able to stretch without breaking, up to twice the slack length. **[B]** Cross-sectional area was measured on transversal sections through dorsal region of the somite. Tricaine-BTS (yellow), DMSO control (blue) (n=9, p=0.558354, ns). **[C]** Actin within the somites stained with rhodamine phalloidin to demonstrate the myofibril phenotype in **1:** slack Tricaine-BTS slack, **2:** 30% stretch BTS, **3:** *relaxed* mutant at slack, **4:** *relaxed* mutant at 30% stretch. **[D]** Average stretch (L/Ls) at the point where force is maximal in both DMSO controls (white) and Tricaine-BTS treated larvae (black) (n=5 BTS & 6 DMSO, p=0.347274, ns) (Scale bar is 100µm).

The next step in the experimental approach was to test whether the effect of paralysis remained when movement was restored. The effects of two paralysis protocols were compared, the combined Tricaine-BTS paralysis up to 5dpf followed by 2 days recovery and the initial 17-24hpf Tricaine alone paralysis followed by 6 days recovery. Myofibril structure and cross-sectional surface area were compared at 5dpf, prior to Tricaine-BTS recovery. Myofibril structure was compared at slack length, Tricaine-BTS immotile treated larvae were the only group to display a mild wavy myofibril phenotype. Motile Tricaine recovered larvae presented a similar myofibril structure to both the motile DMSO and Embryo Medium (EM) controls (Figure 5.5 A). Cross-sectional areas were similar in all groups, however it is noticeable that Tricaine-BTS treated larvae displayed wider

variations, which might be accountable for their thinner appearance, as observed in Figure 5.5 A1 (Figure 5.5 B).

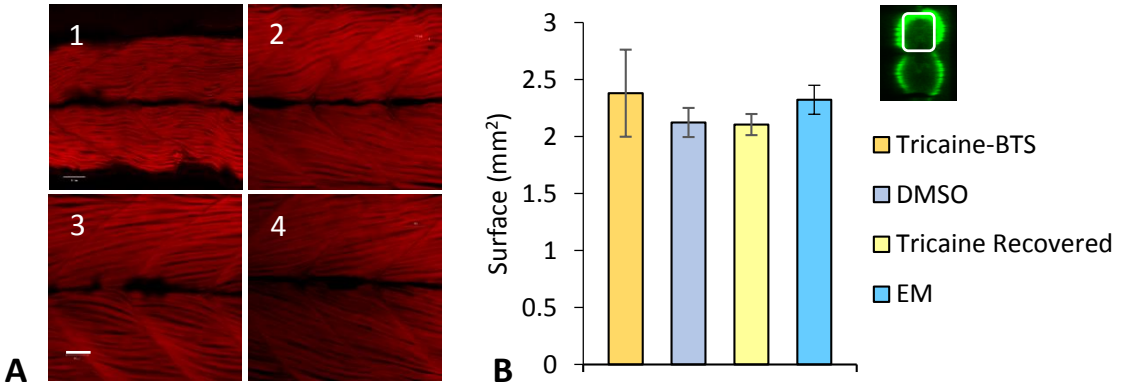

Figure 5.5: Effect of paralysis and recovery on myofibril structure and muscle volume in drug treated larvae at 5dpf. [A] Actin within the somites stained with rhodamine phalloidin to demonstrate the myofibril phenotype in **(1)** Tricaine-BTS treated larvae, **(2)** DMSO control larvae, **(3)** Tricaine recovered larvae, **(4)** EM control larvae. Scale bar 100µm. **[B]** Cross-sectional area was measured on transversal sections through dorsal region of the somite. Tricaine-BTS 5d (orange), DMSO controls (grey), Tricaine recovered (yellow), EM controls (blue) (n=4, p=0.74572, ns) (Scale bar is 100µm).

Passive tension was assessed, at 7dpf, once movement recovery had occurred in both Tricaine-BTS recovered and Tricaine recovered larvae. Motile Tricaine-BTS recovered larvae passive tension was assessed, after 5 days paralysis and 2 days recovery. Their muscle could be stretched up to 110% of the slack length, against 90% for the DMSO controls (Figure 5.6 A). In both Tricaine-BTS recovered and DMSO controls passive tension increased continuously. Passive tension was assessed in motile Tricaine recovered larvae, after 17-24hpf paralysis and 6 days recovery. Their muscle could be stretched up to 100% of the slack length, against 50% for the EM controls (Figure 5.6 B). Their passive tension increased continuously up to 50% stretch before plateauing. Furthermore, these larvae muscles displayed a significantly higher passive tension from 30% of stretch onwards compared to EM controls (Figure 5.6 C). The average stretch (L/Ls) at the point where force is maximal is similar in Tricaine-BTS and DMSO larvae, and in Tricaine and EM control larvae indicative of similar sarcomere elasticity (Figure 5.6 D).

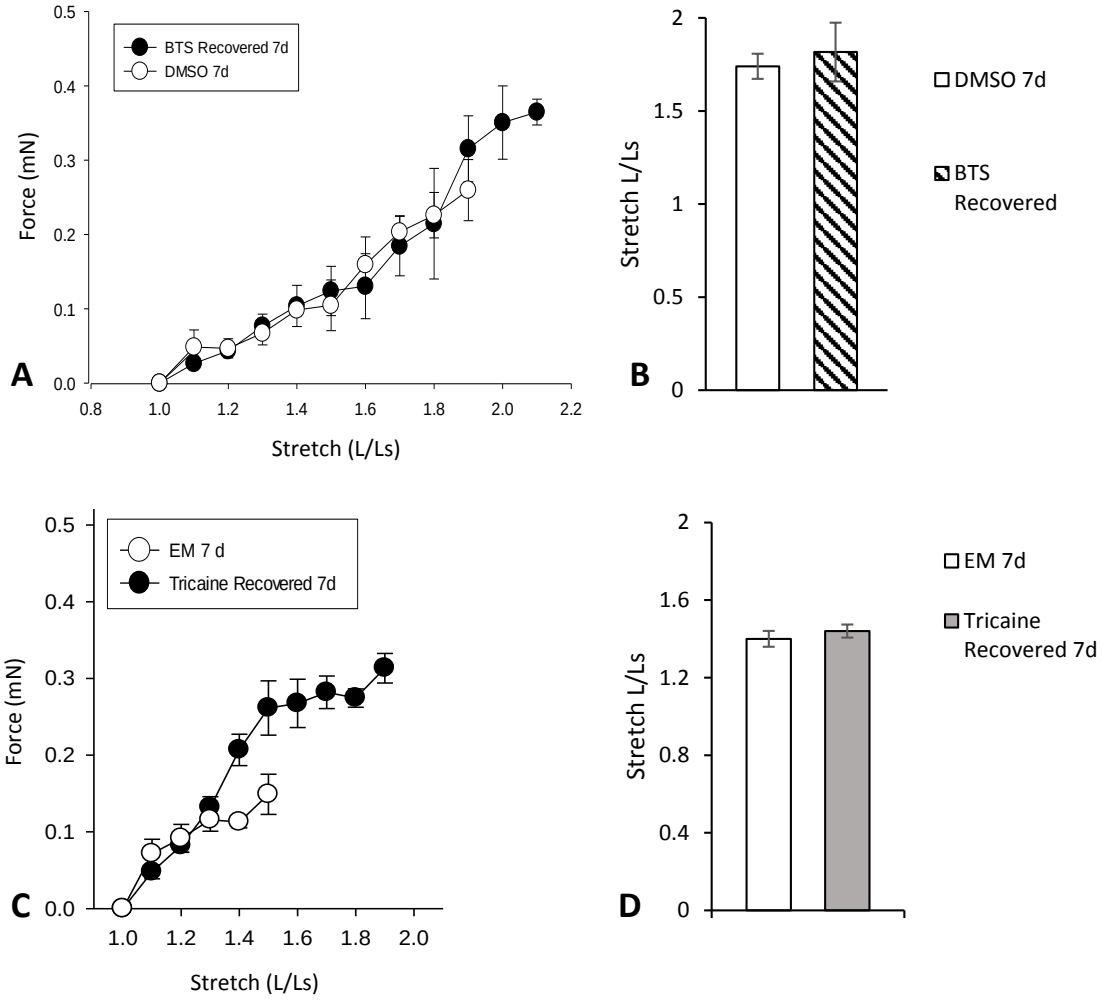

Figure 5.6: Measurement of passive tension and associated sarcomere elasticity in the Tricaine-BTS recovered, Tricaine recovered, DMSO and EM control larvae at 7dpf. [A] Passive tension (Force mN) was plotted against stretch at different lengths, relative to slack length (L/Ls)**,** Controls (DMSO 7d, white), Tricaine-BTS recovered larvae (BTS Recovered 7d, black). **[B]** Average stretch (L/Ls) at the point where force is maximal, DMSO controls (DMSO 7d, white), Tricaine-BTS treated (BTS Recovered 7d, hatched) (n=6 BTS Recovered & 5 DMSO, p=0.669042, ns). **[C]** Passive tension (Force mN) was plotted against stretch at different lengths, relative to slack length (L/Ls)**,** Tricaine recovered larvae (Tricaine Recovered 7d, black symbols), embryo medium control larvae (EM, white symbols). Higher passive tension was observed from 30% stretch in Tricaine recovered larvae **[D]** Average stretch (L/Ls) at the point where force is maximal, EM controls (EM 7d, white), Tricaine recovered (Tricaine Recovered 7d, grey) (n=4 EM & 10 TR, p=0.476036, ns).

In summary, the results show that the drug treated and recovered larvae muscle have an increase ability to undergo further stretch. Another paralysis-induced effect was also unveiled in the Tricaine recovered muscle, as 17-24hpf paralysis leads to a significantly higher passive tension from 30% of stretch. This data shows that the increase in stretch observed during drug induced paralysis at 5dpf remains evident after movement recovery at 7dpf. Furthermore, myofibril structure was found to be restored after movement. Taken together, this data indicated that the increase stretch observed after recovery is unlikely to be due to myofibril disruption.

5.2.3 Paralysis and sarcomere length

Paralysed larvae, showed an overall increase of their passive tension, as their muscles allowed up to 50% additional stretch for the *relaxed* mutants (Figure 5.3 A) and 40% for the Tricaine-BTS treated larvae (Figure 5.4 A). In both cases, data suggest that it is the elongation of the myofibrils during paralysis that is accountable for the increased ability to undergo further stretch. It was previously established that the lack of E-C coupling in the skeletal muscle of immotile zebrafish also led to a shortening of the sarcomere and to an increase in sarcomere number within the elongated myofibrils (Brennan et al., 2005). Therefore, using light microscopy, the sarcomere length was determined at different degrees of stretch for the immotile *relaxed* mutants, their motile siblings and the motile Tricaine-BTS treated larvae at 5dpf. The results show that the sarcomere length increased linearly against stretch in each groups (as shown in figure 5.7). Furthermore, individual sarcomere stretch is proportional to that of whole muscle in all groups (with correlation coefficient for carriers of r=0.9808, for *relaxed* mutants of r=0.9631 and for Tricaine-BTS treated larvae of r=0.9024). However, sarcomere length was significantly shorter at all degrees of stretch in both the immotile *relaxed* mutants and Tricaine-BTS treated larvae at 5dpf compared to the motile carriers controls (Figure 5.7). Furthermore, the sarcomere elasticity of both immotile *relaxed* mutant and Tricaine-BTS treated larvae, allowed an additional 20% stretch compared to the motile carrier controls.

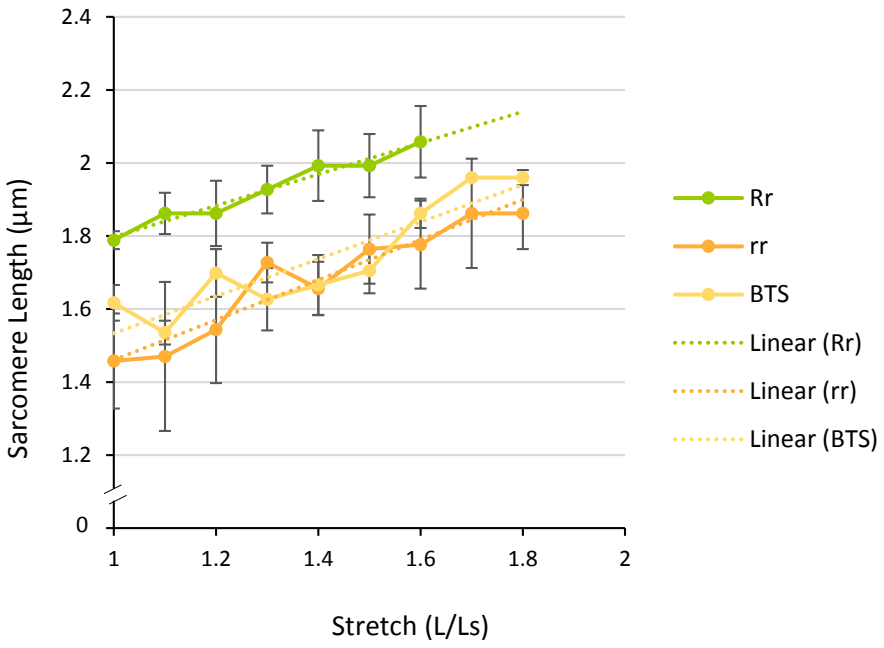

Figure 5.7: Sarcomere length at each degree of stretch for *relaxed* mutants, carriers, and Tricaine-BTS treated larvae. Sarcomere stretch is proportional to muscle stretch (carriers r=0.9808, *relaxed* mutants r=0.9631 and Tricaine-BTS treated larvae r=0.9024). At stretches above 60% the controls (carriers, Rr) tended to break. The Tricaine-BTS and *relaxed* mutant larvae were possible to stretch significantly further without breaking, up to 80%. However, the sarcomere length did not increase further above 70%. Sarcomere length is shorter in immotile *relaxed* and Tricaine-BTS treated larvae. Carriers (Rr, green), *relaxed* mutants (rr, orange), and Tricaine-BTS treated larvae (BTS, yellow).

In summary, paralysis induces sarcomere shortening in the immotile muscles of *relaxed* mutants and Tricaine-BTS treated larvae. This data has shown that myofibril lengthening is associated with shorter sarcomeres and potentially enables their muscle fibres to stretch up to an extra 20% stretch.

5.2.4 Paralysis and active tension

In addition to passive tension, active tension was measured. Active tension is elicited in response to an electrical impulse, which allows assessment of the ability of the muscle to generate force in response to stimulation. Active tension was measured in immotile *relaxed* mutants and drug treated larvae, during paralysis and after recovery at each degree of stretch.

As expected, no contraction was elicited in the *relaxed* mutant in response to the single twitch electrical stimuli (0.5ms) and the tetanic stimulation (200ms 200Hz). In skinned *relaxed* mutant embryos contraction can be elicited by exposure to Caffeine (Zhou et al., 2006). However, in this study, intact *relaxed* mutant embryos were assessed and 80mM KCl or 20mM Caffeine did not elicit contraction. In contrast, carriers did develop a typical contractile response to electrical stimulation with an increase of active force relative to stretch, peaking at 40% (Figure 5.8 A). At 5dpf, during paralysis, Tricaine-BTS treated larvae showed an absence of active force (less than 4% of the DMSO control value). At 7dpf, in Tricaine-BTS recovered larvae, the active tension was partially rescued to approximately 60% of that in the DMSO control larvae (Figure 5.8 B). Furthermore, Tricaine recovered larvae active tension was fully rescued to EM control values, with an optimal length at 40% stretch (Figure 5.8 C).

Further, using active tension recordings and sarcomere length measurements, a sarcomeric optimal length of 1.99 ±0.097µm value established for motile carriers and of 1.66 ±0.082 µm at 40% stretch was established in Tricaine-BTS recovered larvae.

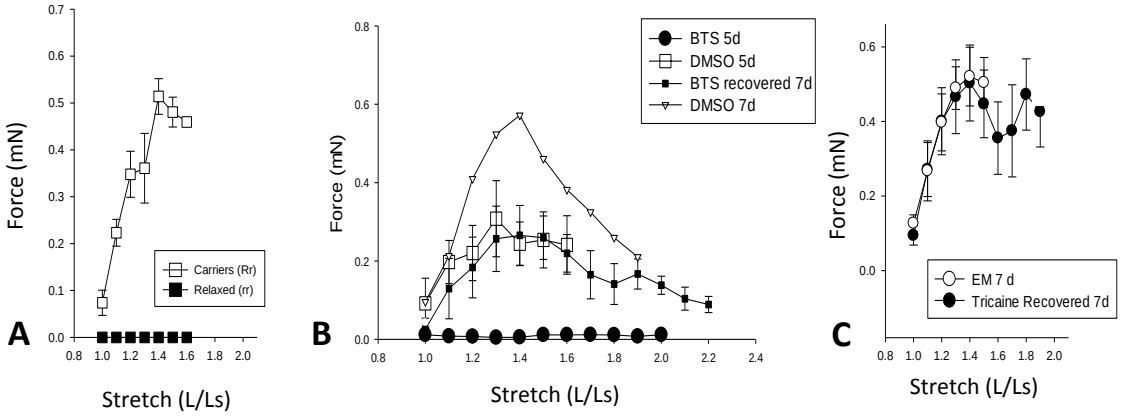

Figure 5.8: Active tension measurements recordings. [A] *Relaxed* mutants and carriers. No contraction could be elicited in the *relaxed* mutant group with a single twitch stimulus. **[B] Tricaine-BTS treated larvae during paralysis and after recovery.** At 5dpf a significant reduction in active tension, to less than 4% of the control values, was observed, at all degrees of stretch, in Tricaine-BTS treated larvae (BTS 5d). At 7dpf, when BTS was removed for 2 days recovery, the larvae muscles recovered about 60% of their active tension, at all degrees of stretch (BTS recovered 7d). **[C] Tricaine recovered.** At 7dpf, Tricaine recovered larvae displayed an active tension similar to EM controls.

In summary, at 5dpf active tension could not be induced in the immotile *relaxed* mutants, and the immotile Tricaine-BTS treated larvae. At 7dpf the active tension in the muscle of recovered motile larvae, treated with Tricaine-BTS for 5 days, was partially restored. Whilst the active tension in the muscle of recovered motile larvae, treated with Tricaine only from 17-24hpf, was fully restored to control values.

5.2.5 Recovery of swimming behaviour after drug induced paralysis

The recovery of movement after pharmacological immobilisation was shown to be accompanied by a recovery of the muscle structure and function. Ultimately, the role of skeletal muscle is to generate locomotion, therefore the swimming behaviour of Tricaine and Tricaine-BTS recovered larvae was assessed.

Tricaine treated embryos were allowed to recover, after 17-24hpf paralysis, and their swimming behaviour, namely distance covered and rotation frequency, was tested against controls at 3, 5, 7 days and 1 month. No difference in swimming behaviour was observed between controls and Tricaine recovered fish from 3dpf onwards (Figure 5.9A). Tricaine-BTS larvae were allowed to recover, after 5 days of paralysis, and their swimming behaviour, namely distance covered and rotation frequency, was tested against DMSO controls at 3 months. No difference in swimming behaviour was observed between DMSO controls and Tricaine-BTS recovered fish at 3 month (Figure 5.9 B).

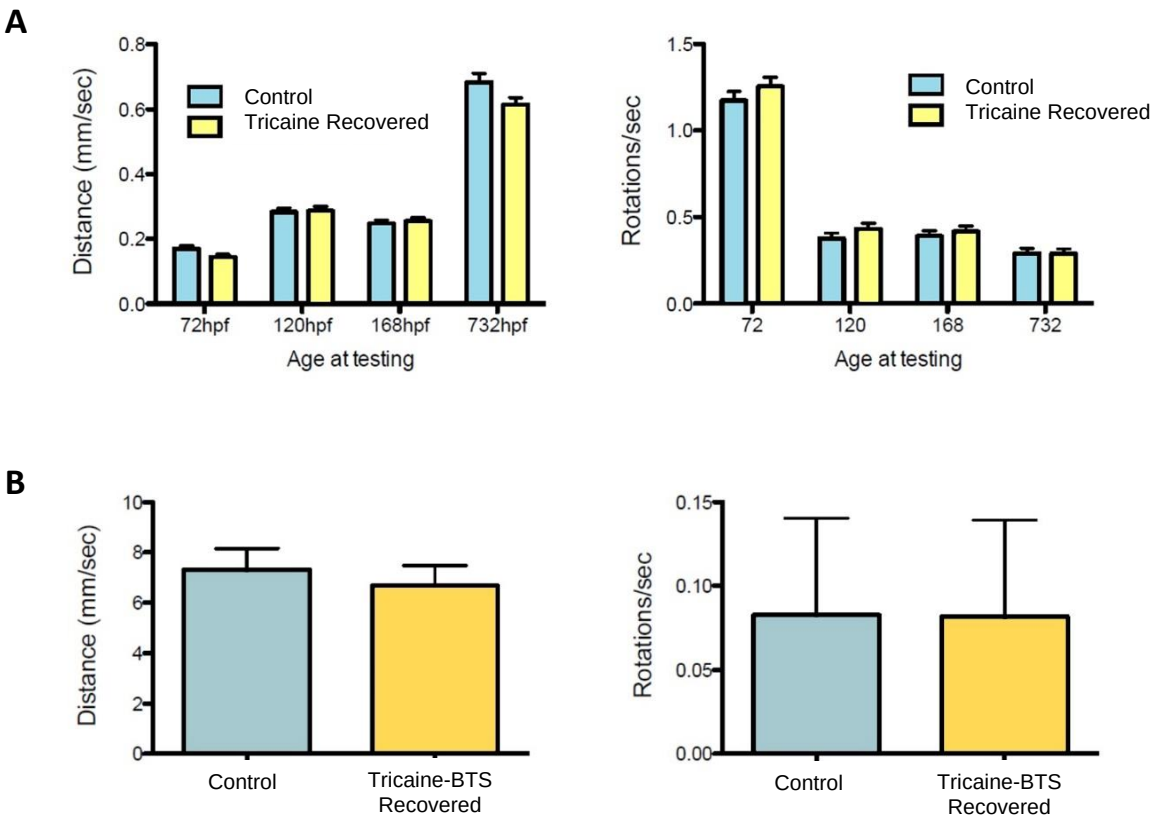

Figure 5.9: Swimming behaviour analysis. [A] Tricaine recovered fish swimming behaviour, distance and rotations, was assessed at 3, 5, 7 days and 1 month. No difference was observed. **[B] Tricaine-BTS recovered** fish swimming behaviour, distance and rotations, was assessed at 3 months. No difference was observed.

In summary, results show that larvae, after an initial period of paralysis and associated myofibril disorganisation, recover their muscle mobility, and subsequently normal swimming behaviour.

5.3 Discussion

Skeletal muscle has both passive and active mechanical properties. Passive properties relate to the ability of muscle both to stretch and to generate passive tension, whereas the active properties relates to active tension.

At 5dpf, paralysis in immotile *relaxed* mutants leads to an increase in stretch but not passive tension which plateaus, whereas in Tricaine-BTS treated larvae stretch is accompanied by a continuous increase in passive tension. At 7dpf, Tricaine-BTS recovered larvae show an increase in stretch accompanied by a continuous increase in passive tension, whereas in Tricaine recovered larvae passive tension is increased from 30% stretch and plateaus during stretch increase (60% stretch onwards). Furthermore, sarcomere shortening was also observed as a result of paralysis. In addition, paralysis inhibits active tension, which recovers progressively once contractile recovery is restored, ultimately resulting in normal swimming behaviour.

(1) Movement-dependent regulation of passive tension

In this chapter, paralysis was shown to disrupt the passive properties of the muscle, mainly its increased ability to stretch. Sarcomere length was also found to be affected by paralysis, with a significant reduction of sarcomeric optimal length in motile Tricaine-BTS recovered larvae (1.66 ±0.082 µm) compared to the 2.1µm value previously established by Li et al. in wildtype larvae (Li et al., 2013). Furthermore, this result is supported by previous studies that have shown sarcomere shortening in immotile mutant (*nic1*) disorganised myofibrils (Brennan et al., 2005). The movement dependent increase in stretch and sarcomere shortening correlates with the fact that myofibril organisation is a movement-dependent mechanism. This hypothesis is strengthened by the fact that paralysis did not impair muscle size nor sarcomere elasticity. Therefore, we propose that paralysis-induced myofibril lengthening is the factor allowing further stretch of the muscle fibres, with stretch 'taking up' the slack of these long myofibrils, rather than gross muscle size or sarcomere elasticity itself. Thus, skeletal muscle passive tension is a movement-regulated mechanism. Overall, movement regulates myofibril organisation which in turn regulates the passive property of the skeletal muscle, this demonstrates the positive feedback between structure and function in muscle.

It was proposed that the earliest embryonic movements are crucial for subsequent organisation of muscle structure (Chapter 3). The observation that Tricaine recovered larvae, paralysed between 17-24hpf, display an increase in passive tension despite movement recovery indicates that this event is also key for establishing functional properties of the muscle. This increase in passive tension translates into an increase stiffness of the muscle. Titin is an early, crucial, multifunctional sarcomeric component, notably it is a molecular spring that generates the main source of myofibrillar stiffness, i.e. passive tension (Clark et al., 2002; Gautel, 2011). One interpretation of the increased passive tension observed in Tricaine recovered larvae is that early paralysis disrupts the titin recruitment process during myofibrillogenesis. Titin is also a strain sensor involved in muscle cell signalling, its enzymatic function is thought to be modulated by mechanically induced conformational changes (Sparrow and Schöck, 2009; Gautel, 2011). We propose based on the data from the Tricaine recovered larvae, that during myofibril assembly titin relies on its mechanosensing properties, to adjust its structural organisation within the sarcomere and regulate its mechanical passive property. Therefore, one possible explanation is that when paralysis occurs during myofibrillogenesis, the positive mechanical feedback (contractile activity) is suppressed and titin generates an extra level of passive tension, resulting in the increased stiffness observed in Tricaine recovered larvae. However, data from the paralysed *relaxed* mutants and Tricaine-BTS treated larvae, in which skeletal muscle passive tension was

found to be similar to control larvae, did not support the theory that early paralysis causes an increase in stiffness. Therefore, this part of the project is difficult to interpret without further work and the link between paralysis and increased stiffness remains uncertain.

(2) Movement-independent regulation of active tension

In this chapter, the active property of skeletal muscle was also examined in drug treated recovered larvae. A striking observation was that Tricaine recovered larvae, paralysed from 17-24hpf, displayed an active tension that was comparable to control values. Skeletal muscle active tension hinges on the ability of myofilaments to form cross-bridges, and this in turn relies on the correct myofilament spacing. The organisation of the myofilament lattice was shown to be a movement-independent process in Chapter 3. Therefore, the potential of paralysed muscle to generate active tension is also likely to be independent of movement. This hypothesis is supported by the ability of immotile *relaxed* mutants to reach rigor when exposed to cyanide (Chapter 3). Thus, the ability of the skeletal muscle to generate active force is not determined by the initial spontaneous contractile event in zebrafish embryos.

Observations also showed that Tricaine-BTS recovered larvae, paralysed for 5 days (due to mechanical assessment technique limitations), displayed a significant reduction in force production. This result is in contrast with the Tricaine data described above, as it suggests that active tension may be affected by paralysis. However, experiments with BTS could be interpreted differently to those performed with Tricaine, due to technical issues. BTS wash out after short exposure leads to rapid recovery (Dou et al., 2008), whereas here after long term treatment active tension is only partially restored. We propose that this lowering of active tension is due to structural changes, i.e. reorganisation and reestablishment of the contractile apparatus. BTS treatment was shown to disrupt myofilament spacing, reducing the lateral distance in between actin and myosin filaments (Chapter 3). This disruption might be the result of a BTS-induced alteration of a Ca^{2+} driven feedback mechanism. BTS is the only paralysis treatment used that blocks the E-C coupling downstream of Ca^{2+} release, both Tricaine treated and *relaxed* mutants cannot generate Ca^{2+} release. Therefore, myofilament lattice shrinkage might be the result of BTS treated muscle Ca^{2+} transients failing to generate contraction. Furthermore, active force development was previously shown to be inhibited by compression of the myofilament lattice in osmotically compressed skinned frog muscle fibres (Maughan and Godt, 1981). However, experiments performed in zebrafish showed that osmotic swelling of BTS treated larvae did not improve active tension (Li, personal communication). Interestingly, at 5dpf, upon BTS wash out, larvae started to swim even

if their lattice had not recovered by then. Furthermore, structural and functional paralysis-induced muscle disruption did not impact on long term swimming behaviour patterns.

5.4 Conclusion

Our results show that the passive properties of skeletal muscle are disrupted by paralysis, which always induced an increase in stretch. This has been linked to paralysis induced structural defects, namely myofibril elongation. Conversely, our results show that the active properties of skeletal muscle are not disrupted by paralysis and correlates with the correct spacing of myofilaments. As it has been established that myofibril elongation is a movement dependent process and that myofilament spacing is not, we propose that passive tension is regulated by movement but not active tension. Therefore, there is a link between skeletal muscle structure and function, that is the ability of myofibril length to determine stretch.

5.5 Future work

Induction of a rigor state in the *relaxed* mutants established that the myofilament spacing in the paralysed muscle is unaltered and allows the formation of cross bridges (Chapter 3). However, what remains to be determined is the level of active tension produced during rigor in the *relaxed* mutant and whether it is comparable to control larvae. Rigor can be induced using a number of chemical approaches including exposure to cyanide (as used in Chapter 3), the ionophore ionomycin or triton. This technique could be applied in the mechanical studies in order to determine active tension in a rigor state in the *relaxed* mutant larvae. The limitation of this experimental protocol, is that active tension and rigor would be elicited without subsequent relaxation, thus making it difficult to assess whether the *relaxed* mutants myofibrils are capable of generating a proper power stroke. One experiment design that could remediate this problem, would be to use a drug capable of reading through premature stop codons, ataluren (PTC124), as the *relaxed* mutant line carries a G-A non-sense point mutation in exon 13 of the gene *CACNB1*. This drug is already in the phase 2b of clinical trial in human Duchenne Muscular Dystrophy (DMD) clinical studies (Finkel, 2010; Peltz et al., 2013). Furthermore, it was also shown to efficiently rescue movement in the zebrafish DMD model, *sapje*, with an identical dose effect as the one observed in humans (Li et al., 2014). During my 6 weeks visit in Pr. Arner laboratory, I worked with Dr. Li and did a preliminary experiment to attempt motile rescue of *relaxed* mutant larvae, however the dose used for *sapje* larvae proved lethal for *relaxed*.

Another area that requires further work is the establishment of the mechanism that causes the myofilament shrinkage and active tension disruption observed exclusively in the Tricaine-BTS treated compared to Tricaine-treated and *relaxed* mutant larvae. As this Tricaine-BTS treatment is the only method that inhibits movement downstream of the calcium transients, it could be that the contraction is linked to a feedback mechanism that regulates calcium levels. In this scenario, the lack of contraction could potentially lead to a disruption of calcium signalling that would then lead to myofilament lattice shrinkage and subsequent active tension disruption. This paradigm could be tested by exposing *relaxed* mutant larvae to BTS, as their muscle is unable to generate Ca^{2+} transients their myofilament lattice should be protected from the BTS shrinking effect, which would verify our hypothesis. Furthermore, measurement of calcium levels in control and Tricaine-BTS treated larvae would determine whether there are significant changes that potentially drive myofilament lattice shrinkage.

CHAPTER 6

DISCUSSION

6. Discussion

The aim of this project was to determine the role of contraction in skeletal muscle development. To that effect the role of the initial contractile event observed in zebrafish embryos from 17 to 24hpf was examined. Both genetic and pharmacological approaches were used to study paralysis-induced disruption of skeletal muscle structure and function in the zebrafish model and ultimately determine the role of contraction during skeletal muscle development. It was established that, in zebrafish, the structural and the functional aspects of the developing skeletal muscles were regulated by dual mechanisms, involving both movement-dependent and movement-independent processes.

The work presented in this thesis has demonstrated that skeletal muscle structure and function are interdependent, myofibril length contributes to the ability of the skeletal muscle to stretch and this mechanism is regulated by movement. Previous work has shown that paralysis leads to an increase in myofibril length (Brennan et al., 2005); this study has now shown that recovery of contraction restores length. Taken together this proves that there is a contraction-driven myofibril organisation pathway (Figure 6.1 C-D). This is consistent with the findings of a recent study in Xenopus, that suggest a role for contractility in sarcomere maturation in vivo (Geach et al., 2015). The mechanism through which myofibril length is established is likely to occur at the sarcomere level. Paralysis induced actin lengthening along with shorter sarcomeres, will result in an increase amount of overlap between actin and myosin myofilaments. This disruption will affect active force production (contraction) and lead to the lengthening of myofibril. This elongation process might be due to the addition of extra sarcomeres, triggered by the lack of contraction, as suggested in previous studies (Williams and Goldspink, 1978; Lahne et al., 2009). Novel data from this study demonstrates that contraction can control sarcomere remodelling, namely the regulation of actin length, via movement driven localisation of the actin capping protein, Tropmodulin 1. Myofibril length was shown to be linked to the mechanical passive property, stretch, with lengthening leading to an increase of the muscle's ability to stretch. In summary, this work has shown that a movement dependent process links the structural organisation, namely myofibril length, with the functional mechanics of the skeletal muscle, specifically stretch.

In addition to the movement-dependent process described above, work presented in this thesis has also demonstrated that movement-independent processes are implicated in the regulation of developing skeletal muscle structure. Indeed, at the structural level, the initial paralysis-induced reduction of myofibril bundling, fully recovers despite a complete absence of movement over time. This finding was supported by sub-structural data

demonstrating that the myofilament lattice spacing is unaffected by paralysis in zebrafish. The lattice spacing is an underlying factor in the myofilaments ability to form cross-bridges, thus the capacity of the immotile *relaxed* mutant to reach rigor when exposed to cyanide, confirmed that the correct spacing of myofilaments is a movement-independent process. Developing skeletal muscle function, specifically their mechanical active property, active tension, rests on cross-bridge generated active force (Figure 6.1 A-B). Therefore, it was predicted that, recovery of movement after pharmacological paralysis of larvae, would lead to the restoration of active tension. This hypothesis was confirmed in Tricaine treated larvae, whose active tension was restored to a level comparable with control values after recovery of movement. Furthermore, in Tricaine-BTS treated larvae the paralysis protocol was shown to induce a compression of the myofilament lattice and as predicted led to an associated disruption of active tension. Recordings of the Tricaine-BTS active tension showed a reduced level of recovery. This finding is supported by the fact that the disruption of active tension in compressed myofilament lattice is known to be due to the hindrance of myosin head power stroke movement (Maughan and Godt, 1981; Adhikari and Fajer, 1996). Thus, the generation of the developing skeletal muscle function, active tension, was shown to be a movement-independent process, and myofilament lattice spacing determines the ability of the skeletal muscle to generate active tension.

The close interaction of skeletal muscle structure and function during development was established. It is particularly interesting to note that the mechanism leading to active force generation and eventually movement is robust and persists despite paralysis. Furthermore, as this mechanism generates the contractile activity, it regulates the movement-dependent mechanism linking myofibril length and passive tension generation. Finally, passive tension closes the feedback loop by determining the optimal force at which the muscle operates within their force-length relationship (Figure 6.1 E) (Azizi, 2014). This paradigm is supported by the idea that function, rather than form, is a robust evolutionary determinant, and that form follows function (Russell et al., 2000).

The role of contraction in skeletal muscle development was investigated further by exploring the signalling of the contraction-driven myofibril organisation pathway. Mechanosensing is typically considered to occur primarily through specialised transmembrane linkages, the costameres and myotendinous junctions, as reviewed by Burkholder (Burkholder, 2007). Focal adhesion complexes (FAC) are key components of these linkages and, in mammals, focal adhesion kinase (Fak) is known to be central to their mechanotransduction activity. In this study, it was established that the mechanisms of mechanosensitive signalling of the contraction-driven myofibril organisation pathway, were different in zebrafish and appeared to revolve around the

Src protein kinase rather than Fak (Figure 6.1). This shift of the role of the FAC signalling proteins shown in this thesis, is proposed to be due to a remodelling of FAC following on the teleost genome duplication and protein functional divergence (Jaillon et al., 2004). Furthermore, the description of Src localisation and sensing role in zebrafish skeletal muscle is novel. This finding could lead to a better understanding of the role of contraction in the developing skeletal muscle and ultimately enhance medical research in humans.

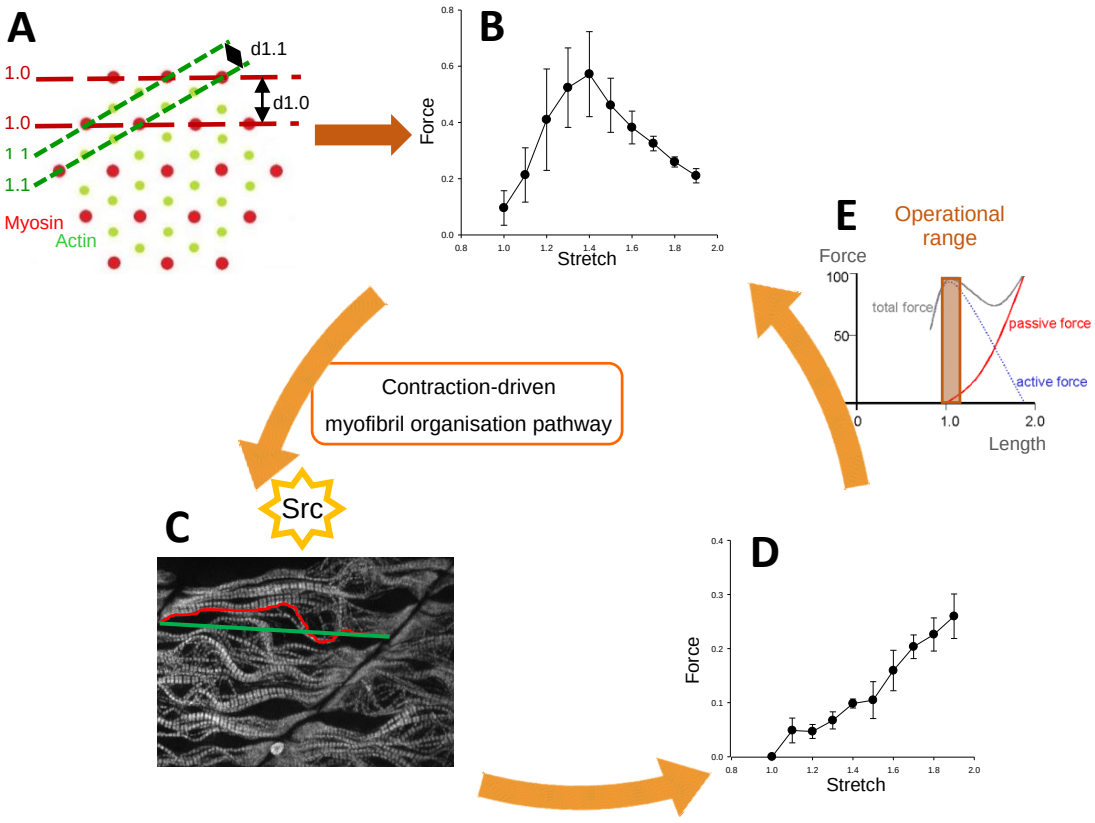

Figure 6.1: Skeletal muscle structure and function feedback loop. Skeletal myofilament lattice correct spacing **[A]** leads to the generation of active tension and movement **[B]**. This contractile activity is sensed by the Src protein within costameres and myotendinous junction and drives myofibril organisation. Correct myofibril length **[C]** leads to the generation of passive tension **[D]**, which in turn determines the operational range **[E]** of the active tension of skeletal muscle. This optimal functional window, varies with the type of muscle and their respective stiffness.

In summary, the role of contraction in the developing zebrafish skeletal muscle was established as a critical driver of myofibril organisation and resulting passive tension, which in turn regulates the 'fine-tuning' of muscle function and gives it its plasticity to ensure the complex needs of locomotion are met. Furthermore, the investigation of the signalling pathway involved in the developing skeletal muscle contractile activity led to the discovery of a novel role for Src in zebrafish skeletal muscle development. These two findings (i) that contraction is a driver of myofibril organisation and (ii) that Src is a

key protein of the skeletal muscle development could be further explored, for therapeutic purposes as described below.

The importance of contraction in skeletal muscle development, the direct impact on passive and subsequently active properties, could be important in understanding the role of foetal movements in humans. This could lead to a better understanding of the mechanism of foetal akinesia (absence, poverty or loss of movement) leading to amyoplasia, which is the most common form of arthrogryposis multiplex congenital (AMC). This sporadic condition, of heterogeneous etiology, is characterised by a generalised lack of skeletal muscle development which is replaced by dense fatty-fibrous tissue, leading to contractures and deformity of most joints in new-borns (Filges and Hall, 2013). This syndrome is the result of a lack of foetal movement in the womb. This lack of movement can be the result of maternal abnormalities restricting the foetal movements, for example a lack of amniotic fluid (oligohydramnios) or an abnormal shape of the uterus (bicornuate). In other cases, the foetal akinesia is due to foetal myogenic disruptions, such as muscular dystrophy. However, in many cases, the cause of this contractile disruption is still unknown, as reviewed by Hall et al. (Hall et al., 2014). In this study, we determined that movements in the developing zebrafish embryo led to the correct establishment of skeletal muscle passive tension, which then impacts on the determination of skeletal muscle operational ranges, necessary to the differentiation of diversified locomotive skeletal muscles. Perhaps this is also the case in human foetuses and zebrafish could be used as a model to study this akinesia-induced syndrome.

Another therapeutic aspect relating to the importance of contraction in skeletal muscle, would be to re-impose movement to paralysed muscles to prevent myofibril disorganisation and muscle stiffness. This idea is already implemented in the treatments of spasticity and hemiplegia following on from stroke, in humans. Several approaches have shown the efficiency of this mobility based treatment, namely with the application of localized 100Hz vibrations (Casale et al., 2014) or the constraint induced movement therapy after botulin toxin injection (Amano et al., 2015). Both these therapies reduce muscle spasticity and improve function, furthermore these non-pharmacological approaches could lead to a reduction of the cost of stroke treatments.

Recent techniques are also developing the idea of mobility based treatment by introducing the use of robotic training. This is either done in combination with conventional physiotherapy (Dundar et al., 2014), or following on from botulin toxin injection (in more severe cases) (Pennati et al., 2014) and effectively reduces muscle spasticity and improves function. Finally, these studies led to the development of lower limb exoskeletons to facilitate the recovery of walking after stroke (Murray et al., 2015) and of the Hybrid Assistiv Limb (HAL) robot suit for hemiplegic patients. This robot is able to realise spontaneous symmetric gait by storing the motion of the

unaffected limb during swing and providing motion support on the affected limb during the subsequent swing using the stored pattern to realize symmetric gait based on spontaneous limb swing (Kawamoto et al., 2014). However, the cost of these robotic training approaches are limiting.

Finally, the role of Src in skeletal muscle development could be explored further in the Duchenne muscular dystrophy (DMD) zebrafish model, *sapje* (Bassett et al., 2003; Bassett and Currie, 2004; Berger et al., 2010), as Src was shown to be involved in the mechanism of this muscle disease in the mdx mouse, model of DMD. Namely, it was shown that the ROS-Src-TRPC1/caveolin-3 pathway enhanced Ca^{2+} influx through stretch-activated channels and induced muscle-cell damage in the mdx mouse. PP2, the Src inhibitor also used on zebrafish in this study, reduced stretch-induced Ca^{2+} entry and increased force recovery (Gervasio et al., 2008). This experiment could be easily reproduced in the zebrafish *sapje* mutants, to determine whether stretch induced muscle damaged could be rescued using PP2. Exploring the mechanisms of DMD in multiple animal models, would allow a comparative approach and could lead to some novel findings. Furthermore, as seen in this study, zebrafish is a very advantageous vertebrate model, which allows rapid and robust high throughput studies.

CHAPTER 7

APPENDICES

7. APPENDICES

APPENDIX A - Spacing of the 1.1 reflection

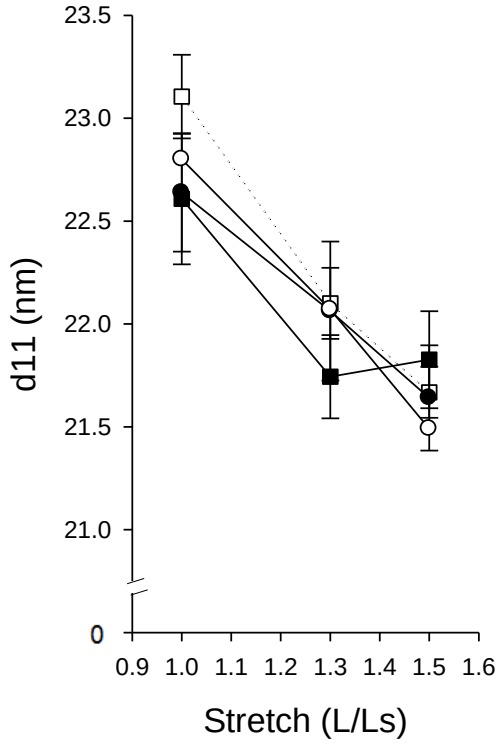

Figure A1: 1.1 reflection at different degrees of stretch

Small angle X-ray diffraction of larvae treated with Tricaine between 17 and 24hpf and recovered until 6dpf (black circles), their controls kept in embryo medium until 6dpf (white circles), immotile *relaxed* mutants (black squares), and their motile siblings (white squares) at 6dpf. The graph shows the spacing of the 1.1 reflection (d_{11}) determined at different degrees of stretch, expressed as length (L) relative to slack length (Ls). The spacing of the 1.1 reflection was similar in the four groups at all degrees of stretch.

APPENDIX B - Experimental considerations for the molecular biology work

PCR vs. qPCR

The RTPCR pilot study initially conducted showed a down-regulation of *fak1a* and an absence of *fak1b* expression in immotile *relaxed* mutant embryos suggesting that these genes might be linked to the mechanotransduction pathway regulating myofibril organisation. To further explore these findings we set out to determine the exact nucleic acid concentrations of *fak1a* and *fak1b* in motile controls (carriers and wildtype embryos) and in immotile *relaxed* mutant zebrafish embryos using qRTPCR. This highly sensitive technique measures PCR amplification as it occurs, rather than to collect the results once the reaction is complete as in traditional PCR, and allows to determine the starting concentration of nucleic acid in the sample. Opposite results were obtained, highlighting the unreliability and the limit of the original PCR technique.

Choosing the right negative control

In zebrafish research, heterozygote motile carriers are commonly used as negative control for the analysis of homozygous mutant lines. This practice ensures that both the mutant, in which homozygous genotype affects the phenotype, and the heterozygous carrier which present a normal unaffected phenotype (in the case of recessive mutation), are from the same batch and therefore at the exact same developmental stage (age matched). This is particularly important when considering that zebrafish have a rapid development rate, and are sensitive to environmental conditions, especially temperature. Experimental timing has to be very precise in order to capture developmental stages accurately. The gene expression levels vary throughout development with the establishment of specific tissues and structures, therefore it is particularly important to stage the embryos very accurately. However, this study shows that the heterozygous genotype is not a reliable control for molecular biology studies. When comparing the motile *relaxed* carrier genes expression levels to the wildtype and the immotile *relaxed* mutant, it appears that the carriers followed either the expression pattern of the wildtype (*foxm1*) or the one of the *relaxed* mutant (*fak1a*). Indeed, in some cases, it would have given contradictive results compared to those obtained when using the wildtype as control. It is necessary to determine the experimental priorities when dealing with *relaxed* mutant embryos, and recessive mutants in general. In some cases, a perfectly aged matched negative control might prevail, but in the case of a molecular studies, comparing the mutant recessive homozygous genotype to a wildtype homozygous genotype is crucial as it ensures that there will be no ‘residual’ effect due to a carrier heterozygous genotype. Based on the work on this thesis, the motile *relaxed* carrier is not an appropriate negative control when assessing the gene expression levels in the immotile *relaxed* mutant, and wildtypes should be used as controls.

APPENDIX C - PP2 treatment did not affect zebrafish embryos survival

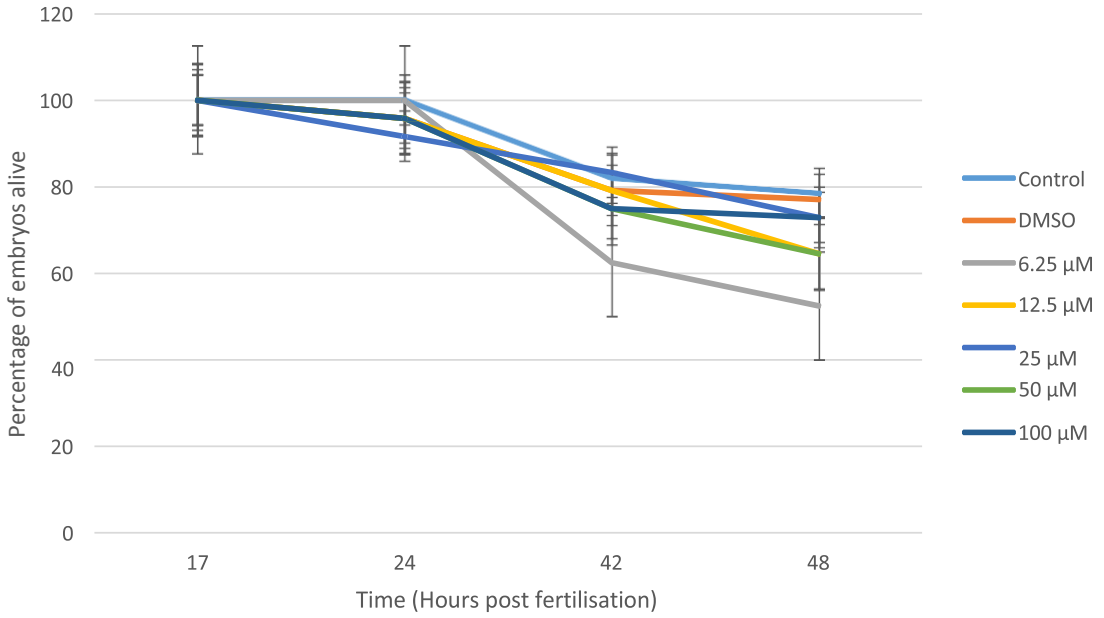

Figure C1: Survival rate of zebrafish in PP2 treatment. 17hpf embryos were incubated in their respective concentrations of PP2, and their survival was monitored at 24hpf, 42hpf and 48hpf (8 embryos/treatment, n=6). The treated embryos showed no significant change in the survival of the embryos, compared to the control embryos ($F(6,121) = 0.506$ $p = 0.803$).

Previous work showed that PP2 was an efficient Src inhibitor in zebrafish, despite a 5% increase of embryonic death at high concentrations (50-100µM) (Ashworth & Punn, personal communication). The toxicity of PP2 and its effect on survival in zebrafish embryos was determined in more detail. A maximum concentration was set at 100µM and serial dilutions were made down to a minimum concentration of 6.25µM. Incubation was started at 17hpf and at 24hpf no significant difference in embryo survival was observed. By 42hpf variation of embryo survival across the treatments was observed, although none was significant ($F(6,121) = 0.506$ $p = 0.803$). At 48hpf, survival rate in all PP2 treated embryos was comparable to controls. The reason behind the increased variance at 6.25µM remains unknown. In summary, PP2 treatments at a concentration range of 6.25-100µM administered between 17 and 24hpf does not affect zebrafish embryo survival rate. This concentration range was then used in the experiment testing of Src function in zebrafish developing skeletal muscle.

APPENDIX D - Interpretation of gene expression data at 96hpf

Evidence from this study and others (Crawford et al., 2003) has shown that there is a differential expression of the two Fak isoforms suggestive of divergences in function. Therefore, the levels of *fak* expression were analysed throughout the first four days of development to examine patterns of *fak1a* versus *fak1b* expression and whether these are affected by paralysis in motile versus non motile fish. A switch in the prevalence of fak1a and fak1b expression during development was observed and suggests that *fak1b* plays a role in early development, whereas *fak1a* might be involved in later developmental processes. At 96hpf a significant decrease in expression levels of *fak1a* was detected in carrier and *relaxed* mutant compared to wildtypes. This suggested that *fak1a* expression was affected in this mutant line. However, *foxm1* an important mitotic division and cell proliferation gene (Teh et al., 2002), displayed an expected steep decrease of its expression level in all three genotypes over the first 96hpf and also showed a significantly lower expression for the immotile *relaxed* mutant at 96hpf. This reduced mitotic division rate suggests that the metabolism of the immotile *relaxed* mutant is slowing down. These observations coincide with the arrival of embryonic death at around 120hpf. Zebrafish embryos rely on the yolk sac until 5dpf, after which they start to feed actively. Free feeding involves jaw movement and requires functional skeletal muscles, which these mutants do not have. Therefore the diminished level of *fak1a* expression observed in the *relaxed* mutants at 96hpf is probably due to the slowing down of their basal metabolism, as they are unable to feed and start to die. The low level of *fak1a* expression observed for the motile *relaxed* carrier remains however more difficult to explain. Perhaps, their survival rate is not as high as wildtype embryos, i.e. they are less robust and some are dying (which would explain the large error bars). This is supported by the fact that carriers of mutant lines are commonly known to be less healthy and to have a diminished life expectancy, compared to wildtype, even as adults.

APPENDIX E - Microarray study

Rationale

One approach that can be used to examine the expression levels of a large number of genes simultaneously is DNA microarray. This high throughput approach enables comparison of gene expression levels between treatments. Prior to the commencement of this thesis, a microarray study had been performed using *relaxed* homozygous mutants compared to control heterozygous embryos at 24hpf. Initial work in the thesis examined the microarray data in order to identify potential candidate genes that may be affected by muscle paralysis and could be important in skeletal muscle development.

Method

A total of 300 heterozygotes and 150 homozygotes zebrafish embryos aged 24hpf were pooled and snap frozen in lysis buffer, then stored at -80°C until use. The RNA extraction and microarray analysis was performed by UK Bioinformatics Ltd. mRNA was extracted from the pooled samples and its quality checked. cDNA synthesis was then performed in quadruplicates prior to conduct the microarray analysis. The Affymetrix GeneChip® Zebrafish Genome Array was used to study gene expression from over 14.900 transcripts. Analysis of the microarray data using normalisation algorithms, both MAS and RMA techniques, identified a total of 574 genes that were statistically different in the two populations (Chambers and Lumsden 2008).

Results

In order to establish which genes were of interest for this project, an initial screen of GenBank numbers was made, and selected genes were further checked on the PubMed database for structural and functional information. The initial 574 genes were narrowed down to a pool of 21 identified genes candidate, 8 down-regulated and 13 up-regulated (Table E1a and E1b). However, 170 genes remained unidentified, due to the incomplete annotation of the zebrafish genome, and further study will be necessary to complete this set of data.

GenBank Number	Annotation
AL912811	Xtriqk protein, developmental body patterning
AF487540	RICK, promote caspase-8 activation potentiated induces apoptosis
AW128322	Putative protein tyrosine phosphatase
BC045953	GIPC1 scaffolding protein regulates receptor expression and trafficking
BC045961	ARP6, actin related protein, binds nucleosomes
BC049461	CAPG, gelsolin/villin actin regulatory protein, block F-actin, controling motility in non-muscle cells
AI957700	Protein tyrosine kinase 9, binding actin monomer
BM777236	Tyrosine phosphatase, enzyme involved in cellular signal transduction, perturbation implicates many disease

Table E1a: Down-regulated potential gene candidates.

GenBank Number	Annotation
BI882775	Plectin involved in Alexander neuro-degenerative disease
BC049492	Protein involved in Bardet-Biedl syndrome, Hereditary Spastic Paraparesis
AI794329	Stimulatory factor involved in transcriptional activation and cell proliferation
BC047809	Hsp40 3A, involved in the regulation Hsp70 ATPase activity
BQ169327	Segmentation stage.
NM_175082	MAD, regulating growth and size of tissues, necessary for correct patterning
BC052476	Protein implicated in apoptosis control and Hsp regulation
BG302953	May act cooperatively with GRB10 to regulate tyrosine kinase receptor signalling.
BC044138	PAK1 cell survival and proliferation, expressed in brain, spleen and skeletal muscle
NM_131715	Embryonic nuclear C-term binding protein 2,transcriptional repressor of E-cadherin promoter
BC047184	cullin-associated & neddylation-dissociated 1, inhibiting ubiquitination in mammals
AF430842	neural cadherin required for establishment of left-right asymmetry during gastrulation
BI845700	synaptotagmin C, neurotransmitter release and hormone secretion Ca^{2+}sensors

Table E1b: Up-regulated potential gene candidates.

Differential expression was assessed at system level by classifying genes according to their tissue distribution. Using normalised data generated by both algorithms (MAS and RMA), up-regulated genes candidates were found within the ubiquitous proteins (22%), the nervous system (21%), the kidney (14%) and the retina (11%) (Figure E1A), whilst the 20 most up-regulated genes candidates were mainly found in the retina (15%), the ubiquitous proteins (10%) and the testis (10%) (Figure E1B). Down-regulated genes candidates were found within the ubiquitous proteins (36%), the kidney (14%), the ovary (13%) and the nervous system (11%) (Figure E1C), whilst the 20 most down-regulated

genes candidates were mainly found in the nervous system (20%), the kidney (20%) and the ubiquitous proteins (20%) (Figure E1D). No obvious gene candidates that could be directly attributed to skeletal muscle were identified. It is worth noting that many of the most up and down-regulated genes were still unidentified (35% and 15% respectively) (Figure E1 B, D).

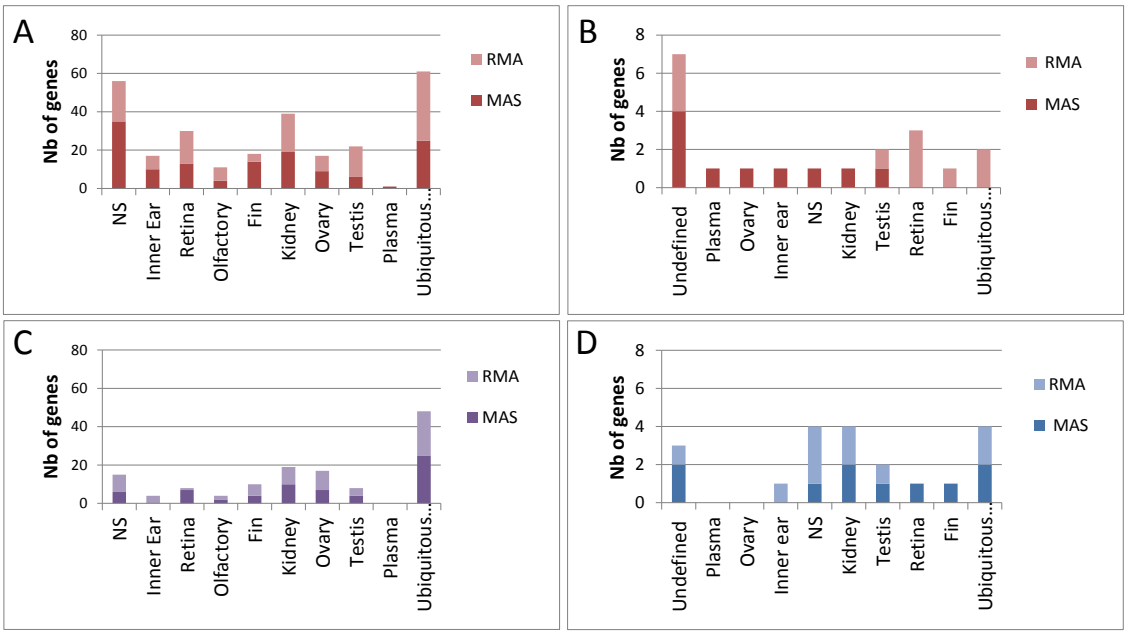

Figure E1: Deviated gene tissue distribution. [A&C] Up and down-regulated gene distribution and **[B&D]** 20 most up and down deviated genes distribution.

Analysis

Previous studies in motility mutants has revealed differential muscle specific gene expression (van der Meulen et al., 2005). However, in this study comparison of gene expression in *relaxed* homozygous compared to heterozygote embryos did not show any obvious muscle specific changes in gene expression. This result may reflect the difference in the two approaches of gene expression analysis, high throughput microarray of a wide range of preselected genes versus qRT-PCR of chosen candidates. Furthermore, given our finding in appendix C that showed that heterozygotes siblings are not the most appropriate controls for molecular studies, it would be beneficial to repeat the microarray comparing homozygous *relaxed* mutant embryos to wildtype controls.

Nonetheless a couple of gene candidates were identified, namely Alexander neurodegenerative disease and Bardet-Biedl syndrome, that have been linked to conditions associated with muscle weakness and paraparesis in humans. The two genes were not found in the group that displayed the most significant deviation in expression levels; therefore, further examination was not performed at this time. However, investigations of these genes in zebrafish could potentially inform medical studies on these human conditions.

APPENDIX F – Tricaine-BTS vs. Tricaine treatments effectiveness and survival rate

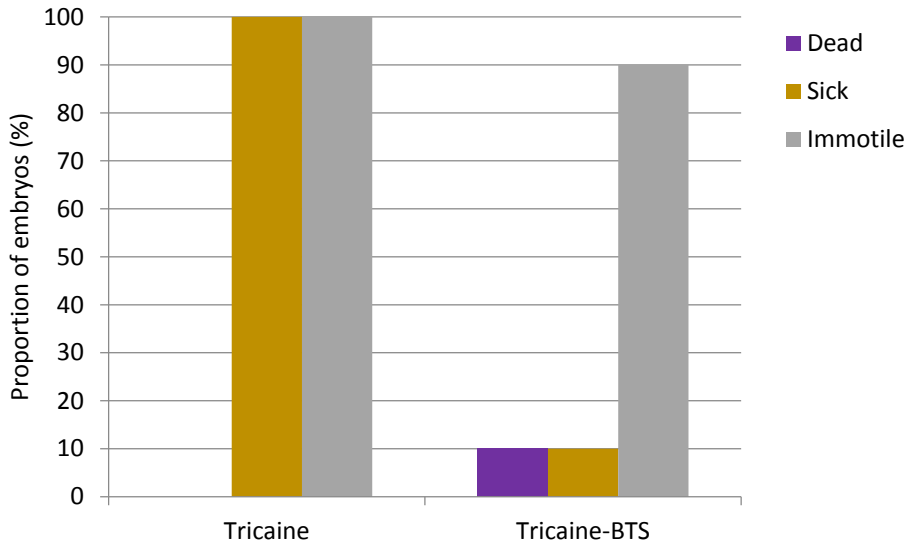

Figure F1: Tricaine-BTS and Tricaine treatments effectiveness and survival rate. Tricaine-BTS treatment, was shown to be a more effective reversible paralysing agent and to have a better survival rate (without sickness) compared to Tricaine treatment from 29hpf up to 5dpf.

Acknowledgements

I would like to thank all my colleagues and friends that supported me during my PhD, it was a journey, had more than its fair share of challenges, and I wouldn't have made it without you.

Dr. Rachel Ashworth, thank you for being my supervisor. This has been a wonderful 5 years. Through all these years, your dedication to your work and your care for fairness in everything you do was inspiring. It was challenging at times, but you showed me how to turn a difficult situation to our advantage, how to come out on top, without ever compromising your values. I am very grateful for that lesson, as well as for the expertise you shared with me and your caring guidance. I am very proud to have been your PhD student, and to have stood by you, I will do it all over again in an instant. I would also like to thank you for your understanding and support when I was struggling through my family and health issues. I have always been able to count on you. I knew that we'd get on since the moment we met, I had a feeling that this was going to be a great collaboration, I wasn't wrong. You have taught me so much, both in and out the laboratory, you really are an inspirational woman, my role model.

Pr. Maurice Elphick, thank you for chairing my advisory panel. I am grateful for our stimulating discussions, your guidance and support throughout the years.

Dr. Muy-Teck Teh, thank you for being part of my advisory panel and the helpful review of my work. Your expertise and guidance through the molecular part of my work were crucial.

Dr. Caroline Brennan, thank you for allowing me to conduct the behavioural study in your laboratory.

Dr. Matthew Parker, thank you for your help in the behavioural study and for the detailed statistical analysis.

Dr. Allistair Broke, thank you for collecting the fish for me when I was unable and for the encouraging words when it came to writing.

Pr. Anders Arner and Dr. Mei Li, thank you both for a very exciting collaboration. It was a great experience both in Stockholm and in Lund. I feel very privileged to have met you and I really hope to have the chance to work with you again in the near future.

Jugraj Singh Bassi BSc, thank you for working with me on the Src project. It was a pleasure to have you in the laboratory.

Mollie Millington, Fraser Combe, David Maley and Richard Roundtree, thank you for helping me out in the zebrafish facility.

BSc (Hons) Edward Tilsley, thank you for the wonderful illustrations and your great patience and availability.

Funding organisations: Physoc, EuFishBioMed, QMUL, thank you for funding my work and allowing me to take part in conferences and collaborations abroad.

Pr.Jon May and **Pr.Mike Watkinson,** thank you for considering my claim for an extension of my thesis submission date. You made it possible again and showed me that there is room for logical argument in British Universities.

Annie Mitchell, thank you for your support in applying for my thesis extension deadline, and for encouraging me to go and defend my case myself in front of the panel hearing, it was a major turning point for me.

Pr.John Allen and **Dr.Fanis Missirlis,** for the support that you brought to both Rachel and me. It was a pleasure to meet you and support your cause, I wish I could have been more helpful.

Stefan, I couldn't have done it without your loving support. Thank you for taking great care of me, and all your help. It is always greatly appreciated. This whirling project took us through all emotional states and I dare to believe it turned our whirlwind romance into a true loving friendship.

Maman et Papa, je vous remercie de m'avoir donné l'envie d'apprendre comme choix de vie et pour avoir cru en moi. Cela me donne la force de faire mon propre chemin et de surmonter toutes les épreuves.

Sylvain, merci pour m'avoir montré que la volonté fait tout. Ta détermination m'a toujours inspiré.

References

Ablain, J. and L. I. Zon (2013) "Of fish and men: using zebrafish to fight human diseases." Trends Cell Biol **23**(12): 584-6.

Adhikari, B. B. and P. G. Fajer (1996). "Myosin head orientation and mobility during isometric contraction: effects of osmotic compression." Biophys J **70**(4): 1872-80.

Amano, S., T. Takebayashi, et al. (2015) "Constraint-Induced Movement Therapy After Injection of Botulinum Toxin Type A for a Patient With Chronic Stroke: One-Year Follow-up Case Report." Phys Ther.

Ashworth, R., F. Zimprich, et al. (2001). "Buffering intracellular calcium disrupts motoneuron development in intact zebrafish embryos." Brain Res Dev Brain Res **129**(2): 169-79.

Azizi, E. (2014) "Locomotor function shapes the passive mechanical properties and operating lengths of muscle." Proc Biol Sci **281**(1783): 20132914.

Baker, R. E., S. Schnell, et al. (2006). "A clock and wavefront mechanism for somite formation." Dev Biol **293**(1): 116-26.

Bassett, D. and P. D. Currie (2004). "Identification of a zebrafish model of muscular dystrophy." Clin Exp Pharmacol Physiol **31**(8): 537-40.

Bassett, D. I., R. J. Bryson-Richardson, et al. (2003). "Dystrophin is required for the formation of stable muscle attachments in the zebrafish embryo." Development **130**(23): 5851-60.

Behra, M., X. Cousin, et al. (2002). "Acetylcholinesterase is required for neuronal and muscular development in the zebrafish embryo." Nat Neurosci **5**(2): 111-8.

Berger, J., S. Berger, et al. (2010) "Dystrophin-deficient zebrafish feature aspects of the Duchenne muscular dystrophy pathology." Neuromuscul Disord **20**(12): 826-32.

Bian, W., M. Juhas, et al. (2012) "Local tissue geometry determines contractile force generation of engineered muscle networks." Tissue Eng Part A **18**(9-10): 957-67.

Boonyarom, O. and K. Inui (2006). "Atrophy and hypertrophy of skeletal muscles: structural and functional aspects." Acta Physiol (Oxf) **188**(2): 77-89.

Brennan, C., M. Mangoli, et al. (2005). "Acetylcholine and calcium signalling regulates muscle fibre formation in the zebrafish embryo." J Cell Sci **118**(Pt 22): 5181-90.

Brown, M. C., L. A. Cary, et al. (2005). "Src and FAK kinases cooperate to phosphorylate paxillin kinase linker, stimulate its focal adhesion localization, and regulate cell spreading and protrusiveness." Mol Biol Cell **16**(9): 4316-28.

Burkholder, T. J. (2007). "Mechanotransduction in skeletal muscle." Front Biosci **12**: 174-91.

Casale, R., C. Damiani, et al. (2014) "Localized 100 Hz vibration improves function and reduces upper limb spasticity: a double-blind controlled study." Eur J Phys Rehabil Med **50**(5): 495-504.

Castillo, A., R. Nowak, et al. (2009). "A nebulin ruler does not dictate thin filament lengths." Biophys J **96**(5): 1856-65.

Chambers, D. and A. Lumsden (2008). "Profiling gene transcription in the developing embryo: microarray analysis on gene chips." Methods Mol Biol **461**: 631-55.

Chereau, D., M. Boczkowska, et al. (2008). "Leiomodin is an actin filament nucleator in muscle cells." Science **320**(5873): 239-43.

Cheung, A., J. A. Dantzig, et al. (2002). "A small-molecule inhibitor of skeletal muscle myosin II." Nat Cell Biol **4**(1): 83-8.

Chu, X., J. Chen, et al. (2003). "E-Tmod capping of actin filaments at the slow-growing end is required to establish mouse embryonic circulation." Am J Physiol Heart Circ Physiol **284**(5): H1827-38.

Clark, K. A., A. S. McElhinny, et al. (2002). "Striated muscle cytoarchitecture: an intricate web of form and function." Annu Rev Cell Dev Biol **18**: 637-706.

Conley, C. A. (2001). "Leiomodin and tropomodulin in smooth muscle." Am J Physiol Cell Physiol **280**(6): C1645-56.

Costa, M. L., R. Escaleira, et al. (2004). "Desmin: molecular interactions and putative functions of the muscle intermediate filament protein." Braz J Med Biol Res **37**(12): 1819-30.

Crawford, B. D., C. A. Henry, et al. (2003). "Activity and distribution of paxillin, focal adhesion kinase, and cadherin indicate cooperative roles during zebrafish morphogenesis." Mol Biol Cell **14**(8): 3065-81.

De Deyne, P. G. (2000). "Formation of sarcomeres in developing myotubes: role of mechanical stretch and contractile activation." Am J Physiol Cell Physiol **279**(6): C1801-11.

Devoto, S. H., E. Melancon, et al. (1996). "Identification of separate slow and fast muscle precursor cells in vivo, prior to somite formation." Development **122**(11): 3371-80.

Dooley, K. and L. I. Zon (2000). "Zebrafish: a model system for the study of human disease." Curr Opin Genet Dev **10**(3): 252-6.

Dou, Y., M. Andersson-Lendahl, et al. (2008). "Structure and function of skeletal muscle in zebrafish early larvae." J Gen Physiol **131**(5): 445-53.

Dundar, U., H. Toktas, et al. (2014) "A comparative study of conventional physiotherapy versus robotic training combined with physiotherapy in patients with stroke." Top Stroke Rehabil **21**(6): 453-61.

Durieux, A. C., G. D'Antona, et al. (2009). "Focal adhesion kinase is a load-dependent governor of the slow contractile and oxidative muscle phenotype." J Physiol **587**(Pt 14): 3703-17.

Durieux, A. C., D. Desplanches, et al. (2007). "Mechanotransduction in striated muscle via focal adhesion kinase." Biochem Soc Trans **35**(Pt 5): 1312-3.

Ehler, E., V. M. Fowler, et al. (2004). "Myofibrillogenesis in the developing chicken heart: role of actin isoforms and of the pointed end actin capping protein tropomodulin during thin filament assembly." Dev Dyn **229**(4): 745-55.

Eisen, J. S., P. Z. Myers, et al. (1986). "Pathway selection by growth cones of identified motoneurones in live zebra fish embryos." Nature **320**(6059): 269-71.

Ervasti, J. M. (2003). "Costameres: the Achilles' heel of Herculean muscle." J Biol Chem **278**(16): 13591-4.

Etard, C., M. Behra, et al. (2005). "Mutation in the delta-subunit of the nAChR suppresses the muscle defects caused by lack of Dystrophin." Dev Dyn **234**(4): 1016-25.

Filges, I. and J. G. Hall (2013) "Failure to identify antenatal multiple congenital contractures and fetal akinesia--proposal of guidelines to improve diagnosis." Prenat Diagn **33**(1): 61-74.

Finkel, R. S. (2010) "Read-through strategies for suppression of nonsense mutations in Duchenne/ Becker muscular dystrophy: aminoglycosides and ataluren (PTC124)." J Child Neurol **25**(9): 1158-64.

Flück, M., J. A. Carson, et al. (1999). "Focal adhesion proteins FAK and paxillin increase in hypertrophied skeletal muscle." Am J Physiol **277**(1 Pt 1): C152-62.

Flück, M., A. Ziemiecki, et al. (2002). "Fibre-type specific concentration of focal adhesion kinase at the sarcolemma: influence of fibre innervation and regeneration." J Exp Biol **205**(Pt 16): 2337-48.

Fujita, H., T. Nedachi, et al. (2007). "Accelerated de novo sarcomere assembly by electric pulse stimulation in C2C12 myotubes." Exp Cell Res **313**(9): 1853-65.

Furuta, Y., D. Ilic, et al. (1995). "Mesodermal defect in late phase of gastrulation by a targeted mutation of focal adhesion kinase, FAK." Oncogene **11**(10): 1989-95.

Garcia-Alvarez, B., J. M. de Pereda, et al. (2003). "Structural determinants of integrin recognition by talin." Mol Cell **11**(1): 49-58.

Gautel, M. (2011) "Cytoskeletal protein kinases: titin and its relations in mechanosensing." Pflugers Arch **462**(1): 119-34.

Geach, T. J., E. M. Hirst, et al. "Contractile activity is required for Z-disc sarcomere maturation in vivo." Genesis **53**(5): 299-307.

Gervasio, O. L., N. P. Whitehead, et al. (2008). "TRPC1 binds to caveolin-3 and is regulated by Src kinase - role in Duchenne muscular dystrophy." J Cell Sci **121**(Pt 13): 2246-55.

Gokhin, D. S. and V. M. Fowler. (2011). "Tropomodulin capping of actin filaments in striated muscle development and physiology." J Biomed Biotechnol **2011**: 103069.

Gokhin, D. S. and V. M. Fowler. (2013). "A two-segment model for thin filament architecture in skeletal muscle." Nat Rev Mol Cell Biol **14**(2): 113-9.

Gokhin, D. S., N. E. Kim, et al. (2012). "Thin-filament length correlates with fiber type in human skeletal muscle." Am J Physiol Cell Physiol **302**(3): C555-65.

Gokhin, D. S., R. A. Lewis, et al. (2010) "Tropomodulin isoforms regulate thin filament pointed-end capping and skeletal muscle physiology." J Cell Biol **189**(1): 95-109.

Gokhin, D. S., M. T. Tierney, et al. (2014) "Calpain-mediated proteolysis of tropomodulin isoforms leads to thin filament elongation in dystrophic skeletal muscle." Mol Biol Cell **25**(6): 852-65.

Goldspink, G. (1998). "Cellular and molecular aspects of muscle growth, adaptation and ageing." Gerodontology **15**(1): 35-43.

Gonsar, N., A. C. Schumann, et al. (2012) "An inexpensive, efficient method for regular egg collection from zebrafish in a recirculating system." Zebrafish **9**(1): 50-5.

Granato, M., F. J. van Eeden, et al. (1996). "Genes controlling and mediating locomotion behavior of the zebrafish embryo and larva." Development **123**: 399-413.

Gregorio, C. C., A. Weber, et al. (1995). "Requirement of pointed-end capping by tropomodulin to maintain actin filament length in embryonic chick cardiac myocytes." Nature **377**(6544): 83-6.

Hall, J. G., K. A. Aldinger, et al. (2014) "Amyoplasia revisited." Am J Med Genet A **164A**(3): 700-30.

Henry, C. A., B. D. Crawford, et al. (2001). "Roles for zebrafish focal adhesion kinase in notochord and somite morphogenesis." Dev Biol **240**(2): 474-87.

Hens, M. D. and D. W. DeSimone (1995). "Molecular analysis and developmental expression of the focal adhesion kinase pp125FAK in Xenopus laevis." Dev Biol **170**(2): 274-88.

Hisano, Y., S. Ota, et al. (2014). "Genome editing using artificial site-specific nucleases in zebrafish." Dev Growth Differ **56**(1): 26-33.

Howe, K., M. D. Clark, et al. (2013) "The zebrafish reference genome sequence and its relationship to the human genome." Nature **496**(7446): 498-503.

Hresko, M. C., B. D. Williams, et al. (1994). "Assembly of body wall muscle and muscle cell attachment structures in Caenorhabditis elegans." J Cell Biol **124**(4): 491-506.

Huijing, P. A. (1999). "Muscle as a collagen fiber reinforced composite: a review of force transmission in muscle and whole limb." J Biomech **32**(4): 329-45.

Huxley, H. and J. Hanson (1954). "Changes in the cross-striations of muscle during contraction and stretch and their structural interpretation." Nature **173**(4412): 973-6.

Iorga,B., Neacsu, CD. (2011). "Micromechanical function of myofibrils isolated from skeletal and cardiac muscles of the zebrafish." J Gen Physiol **137**(3):255-70.

Jaillon, O., J. M. Aury, et al. (2004). "Genome duplication in the teleost fish Tetraodon nigroviridis reveals the early vertebrate proto-karyotype." Nature **431**(7011): 946-57.

Kagawa, M., N. Sato, et al. (2006). "Effects of BTS (N-benzyl-p-toluene sulphonamide), an inhibitor for myosin-actin interaction, on myofibrillogenesis in skeletal muscle cells in culture." Zoolog Sci **23**(11): 969-75.

Karni, R., S. Mizrachi, et al. (2003). "The pp60c-Src inhibitor PP1 is non-competitive against ATP." FEBS Lett **537**(1-3): 47-52.

Kawamoto, H., H. Kandone, et al. (2014) "Development of an assist controller with robot suit HAL for hemiplegic patients using motion data on the unaffected side." Conf Proc IEEE Eng Med Biol Soc **2014**: 3077-80.

Kimmel, C. B., W. W. Ballard, et al. (1995). "Stages of embryonic development of the zebrafish." Dev Dyn **203**(3): 253-310.

Klossner, S., A. C. Durieux, et al. (2009). "Mechano-transduction to muscle protein synthesis is modulated by FAK." Eur J Appl Physiol **106**(3): 389-98.

Koegl, M., P. Zlatkine, et al. (1994). "Palmitoylation of multiple Src-family kinases at a homologous N-terminal motif." Biochem J **303 (Pt 3)**: 749-53.

Kong, K. Y. and L. Kedes (2004). "Cytoplasmic nuclear transfer of the actin-capping protein tropomodulin." J Biol Chem **279**(29): 30856-64.

Kong, K. Y. and L. Kedes (2006). "Leucine 135 of tropomodulin-1 regulates its association with tropomyosin, its cellular localization, and the integrity of sarcomeres." J Biol Chem **281**(14): 9589-99.

Kratimenos, P., I. Koutroulis, et al. (2014) "Multi-targeted molecular therapeutic approach in aggressive neuroblastoma: the effect of Focal Adhesion Kinase-Src-Paxillin system." Expert Opin Ther Targets **18**(12): 1395-406.

Kurosaki, T., M. Takata, et al. (1994). "Syk activation by the Src-family tyrosine kinase in the B cell receptor signaling." J Exp Med **179**(5): 1725-9.

Labrador, A., Y. Cerenius, et al. (2013). "The yellow mini-hutch for SAXS experiments at MAXIV." J. Phys. Conf.Ser.

Lahne, M., C. Krivcevska, et al. (2009). "A Contraction-dependent Pathway Regulates Myofibril Organisation during Skeletal Muscle Development in Vivo." Journal of General Physiology **134**(July): 4A.

Lange, S., E. Ehler, et al. (2006). "From A to Z and back? Multicompartment proteins in the sarcomere." Trends Cell Biol **16**(1): 11-8.

Li, M., M. Andersson-Lendahl, et al. (2013) "Knockdown of desmin in zebrafish larvae affects interfilament spacing and mechanical properties of skeletal muscle." J Gen Physiol **141**(3): 335-45.

Li, M., M. Andersson-Lendahl, et al. (2014) "Muscle dysfunction and structural defects of dystrophin-null sapje mutant zebrafish larvae are rescued by ataluren treatment." FASEB J **28**(4): 1593-9.

Lieschke, G. J. and P. D. Currie (2007). "Animal models of human disease: zebrafish swim into view." Nat Rev Genet **8**(5): 353-67.

Lieu, C. and S. Kopetz (2010). "The SRC family of protein tyrosine kinases: a new and promising target for colorectal cancer therapy." Clin Colorectal Cancer **9**(2): 89-94.

Lindqvist, J., H. Iwamoto, et al. (2013) "The fraction of strongly bound cross-bridges is increased in mice that carry the myopathy-linked myosin heavy chain mutation MYH4L342Q." Dis Model Mech **6**(3): 834-40.

Littlefield, R., A. Almenar-Queralt, et al. (2001). "Actin dynamics at pointed ends regulates thin filament length in striated muscle." Nat Cell Biol **3**(6): 544-51.

Littlefield, R. and V. M. Fowler (2002). "Measurement of thin filament lengths by distributed deconvolution analysis of fluorescence images." Biophys J **82**(5): 2548-64.

Littlefield, R. S. and V. M. Fowler (2008). "Thin filament length regulation in striated muscle sarcomeres: pointed-end dynamics go beyond a nebulin ruler." Semin Cell Dev Biol **19**(6): 511-9.

Luther, P. and J. Squire (1978). "Three-dimensional structure of the vertebrate muscle M-region." J Mol Biol **125**(3): 313-24.

Mardahl-Dumesnil, M. and V. M. Fowler (2001). "Thin filaments elongate from their pointed ends during myofibril assembly in Drosophila indirect flight muscle." J Cell Biol **155**(6): 1043-53.

Markwald, R. R. (1973). "Distribution and relationship of precursor Z material to organizing myofibrillar bundles in embryonic rat and hamster ventricular myocytes." J Mol Cell Cardiol **5**(4): 341-50.

Maughan, D. W. and R. E. Godt (1981). "Inhibition of force production in compressed skinned muscle fibers of the frog." Pflugers Arch **390**(2): 161-3.

Millman, B. M. (1998). "The filament lattice of striated muscle." Physiol Rev **78**(2): 359-91.

Miyamoto, S., S. K. Akiyama, et al. (1995). "Synergistic roles for receptor occupancy and aggregation in integrin transmembrane function." Science **267**(5199): 883-5.

Moerman, D. G. and B. D. Williams (2006). "Sarcomere assembly in C. elegans muscle." WormBook: 1-16.

Monti, R. J., R. R. Roy, et al. (1999). "Transmission of forces within mammalian skeletal muscles." J Biomech **32**(4): 371-80.

Moroco, J. A., M. P. Baumgartner, et al. (2014) "A Discovery Strategy for Selective Inhibitors of c-Src in Complex with the Focal Adhesion Kinase SH3/SH2-binding Region." Chem Biol Drug Des.

Murray, S. A., K. H. Ha, et al. (2015) "An assistive control approach for a lower-limb exoskeleton to facilitate recovery of walking following stroke." IEEE Trans Neural Syst Rehabil Eng **23**(3): 441-9.

Nworu, C. U., R. Kraft, et al. "Leiomodin 3 and tropomodulin 4 have overlapping functions during skeletal myofibrillogenesis." J Cell Sci **128**(2): 239-50.

Obermann, W. M., M. Gautel, et al. (1996). "The structure of the sarcomeric M band: localization of defined domains of myomesin, M-protein, and the 250-kD carboxy-terminal region of titin by immunoelectron microscopy." J Cell Biol **134**(6): 1441-53.

Ochala, J., D. S. Gokhin, et al. "Congenital myopathy-causing tropomyosin mutations induce thin filament dysfunction via distinct physiological mechanisms." Hum Mol Genet **21**(20): 4473-85.

Ochala, J., D. S. Gokhin, et al. (2014) "Pointed-end capping by tropomodulin modulates actomyosin crossbridge formation in skeletal muscle fibers." FASEB J **28**(1): 408-15.

Ono, S. (2010) "Dynamic regulation of sarcomeric actin filaments in striated muscle." Cytoskeleton (Hoboken) **67**(11): 677-92.

Pardo, J. V., J. D. Siliciano, et al. (1983). "A vinculin-containing cortical lattice in skeletal muscle: transverse lattice elements ("costameres") mark sites of attachment between myofibrils and sarcolemma." Proc Natl Acad Sci U S A **80**(4): 1008-12.

Parsons, S. J. and J. T. Parsons (2004). "Src family kinases, key regulators of signal transduction." Oncogene **23**(48): 7906-9.

Patel, T. J. and R. L. Lieber (1997). "Force transmission in skeletal muscle: from actomyosin to external tendons." Exerc Sport Sci Rev **25**: 321-63.

Peltz, S. W., M. Morsy, et al. (2013) "Ataluren as an agent for therapeutic nonsense suppression." Annu Rev Med **64**: 407-25.

Pennati, G. V., C. Da Re, et al. (2014) "How the robotic training and the botolinum toxin could be combined in chronic post stroke upper limb spasticity? A pilot study." Eur J Phys Rehabil Med.

Polte, T. R., A. J. Naftilan, et al. (1994). "Focal adhesion kinase is abundant in developing blood vessels and elevation of its phosphotyrosine content in vascular smooth muscle cells is a rapid response to angiotensin II." J Cell Biochem **55**(1): 106-19.

Ramachandran, I., M. Terry, et al. (2003). "Skeletal muscle myosin cross-bridge cycling is necessary for myofibrillogenesis." Cell Motil Cytoskeleton **55**(1): 61-72.

Reedy, M. C. and C. Beall (1993). "Ultrastructure of developing flight muscle in Drosophila. I. Assembly of myofibrils." Dev Biol **160**(2): 443-65.

Ringkob, T. P., D. R. Swartz, et al. (2004). "Light microscopy and image analysis of thin filament lengths utilizing dual probes on beef, chicken, and rabbit myofibrils." J Anim Sci **82**(5): 1445-53.

Roskoski, R., Jr. (2004). "Src protein-tyrosine kinase structure and regulation." Biochem Biophys Res Commun **324**(4): 1155-64.

Russell, B., D. Motlagh, et al. (2000). "Form follows function: how muscle shape is regulated by work." J Appl Physiol (1985) **88**(3): 1127-32.

Rybakova, I. N., J. R. Patel, et al. (2000). "The dystrophin complex forms a mechanically strong link between the sarcolemma and costameric actin." J Cell Biol **150**(5): 1209-14.

Saint-Amant, L. and P. Drapeau (1998). "Time course of the development of motor behaviors in the zebrafish embryo." J Neurobiol **37**(4): 622-32.

Sanger, J. W., S. Kang, et al. (2005). "How to build a myofibril." J Muscle Res Cell Motil **26**(6-8): 343-54.

Sanger, J. W., J. Wang, et al. (2010) "Assembly and dynamics of myofibrils." J Biomed Biotechnol **2010**: 858606.

Sanger, J. W., J. Wang, et al. (2009). "Myofibrillogenesis in skeletal muscle cells in zebrafish." Cell Motil Cytoskeleton **66**(8): 556-66.

Sato, Y., Y. Hashiguchi, et al. (2009). "Temporal pattern of loss/persistence of duplicate genes involved in signal transduction and metabolic pathways after teleost-specific genome duplication." BMC Evol Biol **9**: 127.

Schredelseker, J., A. Dayal, et al. (2009). "Proper restoration of excitation-contraction coupling in the dihydropyridine receptor beta1-null zebrafish relaxed is an exclusive function of the beta1a subunit." J Biol Chem **284**(2): 1242-51.

Schredelseker, J., V. Di Biase, et al. (2005). "The beta 1a subunit is essential for the assembly of dihydropyridine-receptor arrays in skeletal muscle." Proc Natl Acad Sci U S A **102**(47): 17219-24.

Schroter, C., S. Ares, et al. (2012) "Topology and dynamics of the zebrafish segmentation clock core circuit." PLoS Biol **10**(7): e1001364.

Schwartz, M. A. (2001). "Integrin signaling revisited." Trends Cell Biol **11**(12): 466-70.

Skwarek-Maruszewska, A., M. Boczkowska, et al. (2010) "Different localizations and cellular behaviors of leiomodin and tropomodulin in mature cardiomyocyte sarcomeres." Mol Biol Cell **21**(19): 3352-61.

Soeno, Y., Y. Shimada, et al. (1999). "BDM (2,3-butanedione monoxime), an inhibitor of myosin-actin interaction, suppresses myofibrillogenesis in skeletal muscle cells in culture." Cell Tissue Res **295**(2): 307-16.

Sonnemann, K. J., D. P. Fitzsimons, et al. (2006). "Cytoplasmic gamma-actin is not required for skeletal muscle development but its absence leads to a progressive myopathy." Dev Cell **11**(3): 387-97.

Sparrow, J. C. and F. Schöck (2009). "The initial steps of myofibril assembly: integrins pave the way." Nat Rev Mol Cell Biol **10**(4): 293-8.

Squire, J. M., C. Knupp, et al. (2008). "Zebrafish--topical, transparent, and tractable for ultrastructural studies." J Gen Physiol **131**(5): 439-43.

Stickney, H. L., M. J. Barresi, et al. (2000). "Somite development in zebrafish." Dev Dyn **219**(3): 287-303.

Streisinger, G., C. Walker, et al. (1981). "Production of clones of homozygous diploid zebra fish (Brachydanio rerio)." Nature **291**(5813): 293-6.

Teh, M. T., S. T. Wong, et al. (2002). "FOXM1 is a downstream target of Gli1 in basal cell carcinomas." Cancer Res **62**(16): 4773-80.

Trinick, J. (1994). "Titin and nebulin: protein rulers in muscle?" Trends Biochem Sci **19**(10): 405-9.

Turner, C. E. (2000). "Paxillin and focal adhesion signalling." Nat Cell Biol **2**(12): E231-6.

van der Meulen, T., H. Schipper, et al. (2005). "Effects of decreased muscle activity on developing axial musculature in nicb107 mutant zebrafish (Danio rerio)." J Exp Biol **208**(Pt 19): 3675-87.

Volff, J. N. (2005). "Genome evolution and biodiversity in teleost fish." Heredity (Edinb) **94**(3): 280-94.

Westerfield, M. (1993). The zebrafish book: A guide for the laboratory use of zebrafish (Brachydanio rerio), University of Oregon Press.

Williams, P. E. and G. Goldspink (1971). "Longitudinal growth of striated muscle fibres." J Cell Sci **9**(3): 751-67.

Williams, P. E. and G. Goldspink (1978). "Changes in sarcomere length and physiological properties in immobilized muscle." J Anat **127**(Pt 3): 459-68.

Wolfenson, H., A. Bershadsky, et al. (2011) "Actomyosin-generated tension controls the molecular kinetics of focal adhesions." J Cell Sci **124**(Pt 9): 1425-32.

Wolpert, L., C. Tickle, et al. (2015). Principles of development, OUP Oxford.

Zalk, R., O. B. Clarke, et al. (2015) "Structure of a mammalian ryanodine receptor." Nature **517**(7532): 44-9.

Zamir, E. and Geiger, B. (2001). Molecular complexity and dynamics of cell-matrix adhesions. J. Cell Sci. 114, 3583-3590.

Zhou, W., L. Saint-Amant, et al. (2006). "Non-sense mutations in the dihydropyridine receptor beta1 gene, CACNB1, paralyze zebrafish relaxed mutants." Cell Calcium **39**(3): 227-36.